Des (bio)nano-composites utilisés dans le traitement d'eaux contaminées par de l'arsenic/gentamicine ou pour des applications médicales

Jing He

UNIVERSITÉ DE GRENOBLE

THÈSE

Pour obtenir le grade de

DOCTEUR DE L'UNIVERSITÉ DE GRENOBLE

Spécialité : **Terre, Univers, Environnement**

Arrêté ministériel : 7 août 2006

Présentée par

« Jing / HE »

Thèse dirigée par **« Laurent/CHARLET »**

préparée au sein du **Institut des Sciences de la Terre**
dans **l'École Doctorale « Terre – Univers – Environnement »**

Des (bio)nano-composites utilisés dans le traitement d'eaux contaminées par de l'arsenic/gentamicine ou pour des applications médicales

Thèse soutenue publiquement le **« 02 décembre 2013 »**,
devant le jury composé de :

Professeur, David, POLYA
Fonction et lieu de la fonction, rôle (Président, Rapporteur)
Professeur, Ewen, SILVESTER
Fonction et lieu de la fonction, rôle (Rapporteur)
Professeur, Pilar, ARANDA
Fonction et lieu de la fonction, rôle (Membre)
Professeur, Rachel, AUZELY-VELTY
Fonction et lieu de la fonction, rôle (Membre)
Professeur, Laurent, CHARLET
Fonction et lieu de la fonction, rôle (Directeur de thèse, Membre)

Université Joseph Fourier / Université Pierre Mendès France /
Université Stendhal / Université de Savoie / Grenoble INP

Extended Abstract i
Résumé ix
Chapter 1 1
Arsenic as emerging contaminant in the environment 1
1.1. Occurrence of arsenic in the environment 2
1.2. Arsenic speciation and toxicity 3
1.3. High arsenic water distribution all around the world 5
1.4. Arsenic decontamination: techniques and challenges 7
1.5. Objectives - Arsenic decontamination technique and material for house-hold set-up 10
Chapter 2 12
A review of arsenic presence in China drinking water 12
2.1. Introduction 13
2.2. Source of arsenic to surface and groundwater 14
2.2.1. Minerals 14
2.2.2. Rocks, sediments, soils and air 15
2.3. Arsenic mobilization processes 20
2.3.1. Geogenic factors 20
2.3.2. Anthropogenic factors 23
2.4. High-As content in China waters - geogenic cases 23
2.4.1. Overview 23
2.4.2. Different types of geogenic high-As waters 28
2.4.3. Prediction of geogenic potential As-affected groundwater 32
2.5. High-As content in China waters - anthropogenic cases 33
2.6. Conclusions and recommendations 36
Chapter 3 39
Novel Chitosan Goethite Bionanocomposites Bead for Arsenic Remediation 39
3.1. Introduction 40
3.2. Experimental Section 42
3.2.1. Chemicals. 42
3.2.2. Synthesis of CGB 42
3.2.3. Characterization. 43

3.2.4. Batch Sorption Isotherm 45
3.2.5. Kinetic Experiment. 47
3.2.6. Effect of CGB dose on residue arsenic level 48
3.2.7. Leaching Test 49
3.2.8. Bulk XAS 49
3.2.9. μXANES and μXRF 51
3.3. Results and Discussion 51
3.3.1. Physicochemical Characteristics of CGB 51
3.3.2. As adsorption: isotherm and mechanism (EXAFS) 56
3.3.3. Effect of CGB dose 62
3.3.4. Kinetic study and diffusion pattern (μXRF and μXANES) 62
3.4. Practical applications. 70
Chapter 4 71
Antibiotics as emerging contaminants in the environment 71
4.1. Introduction 72
4.2. Sources of antibiotics contamination 74
4.2.1. Pharmaceutical manufacturing 74
4.2.2. Hospital wastewater and municipal sewage 74
4.2.3. Animal farm and aquaculture 75
4.3. Advert effects 76
4.3.1. Antibiotic resistance 76
4.3.2. Potential public health risk 77
4.3.3. Aquatic life poisoning 77
4.3. Antibiotic contamination in WWTPs and natural waters of China 78
4.4. Elimination 82
Chapter 5 84
Gentamicin adsorption on Na^+-montmorillonite and preparation of gentamicin-montmorillonite-HPMC film as burn wound dressing 84
5.1. Introduction 85
5.2. Experimental section 88
5.2.1. Materials 88
5.2.2. Methods 88

5.3. Result and Discussion 94
5.3.1. Preparation of Gt-Mt. nanohybrid and Isotherm study 94
5.3.2. Characterization, degradation and in vitro release experiment of Gt-Mt composites. 100
5.3.3. Gt-Mt-HPMC film 108
5.4. Conclusion 113
Chapter 6 114
Conclusions and perspectives 114
6.1. Conclusions 115
6.2. Further work 120
Reference 123
Acknowlegements 139
Curriculum Vitae 141
Annex1: Calculation of site density: arsenic on goethite 143

Extended Abstract

Bionanocomposites represent an emerging group of nano-structured hybrid materials. They are formed by the combination of natural polymers and inorganic solids and show at least one dimension on the nanometer scale. These hybrid materials retain the structural and functional properties of nano-structured materials. Meanwhile, the presence of biopolymer can reduce the public health and environmental risks of nano-sized materials. Properties inherent to the biopolymers, notably, biocompatibility and biodegradability, open new prospects for these hybrid materials particularly in regenerative medicine and in environmental engineering (Darder et al., 2007). Fabrication of large-sized bionanocomposites, rather than nano-sized particles, can prevent possible harmful nanoparticle (NP) intake by humans and other living things. Synergistic assembling of biopolymers with inorganic nano-sized solids leads to multifunctional bionanocomposites which can be synthesized and applied in several areas for designed purposes.

This thesis focuses on (i) the presence of toxic arsenic and antibiotics in Chinese drinking water sources; (ii) evaluation of a novel tailored bionanocompsite, namely chitosan goethite bionanocomposite (CGB), as a removal agent for inorganic arsenic species from water; (iii) using clay minerals as an adsorbent for removing gentamicin, an aminoglycoside antibiotic, from water, and assembling gentamicin-loaded clay with biopolymer hydroxypropyl methycellulose leading to a bionanocomposites film, namely gentamicin-montmorillonite-hydroxypropyl methycellulose (Gt-Mt-HPMC), to be used as a burn wound dressing.

A large number of people worldwide are exposed to elevated As concentrations in ground water – many of them in developing countries and with no available alternative water resources. Aquifer systems with high levels of arsenic, elevated by natural processes or anthropogenic activities, have been reported in different environments from all continents. Some of the best-documented and most severe cases of arsenic contaminated groundwater have been found in aquifers in Asia (e.g. parts of Bangladesh, China, India, Nepal) and South America (e.g. Argentina, Mexico) (Aureli, 2006). Estimates of the rural population exposed to unsafe As levels by drinking untreated groundwater in India, China, Myanmar, Pakistan, Vietnam, Nepal, and Cambodia has grown to over 100 million (Ravenscroft et al., 2009). Inorganic forms of arsenic: arsenite [As(III)] and arsenate [As(V)] are the two dominant species found in groundwater. Long-term drinking water exposure to arsenic may cause skin lesions (Tondel et al., 1999), peripheral vascular disease (Engel et al.,1994), hypertension (Chen et al., 1995), black-foot disease (Chen, 1990), and high risk of cancers, etc (Bates et al.,1992).

Arsenic was released to subsurface water bodies due to natural processes, such as arsenic mobilization from minerals and sediments. It is not possible to eliminate these sources. Therefore groundwater containing high level of arsenic has to be treated before use as drinking water. Common techniques for arsenic removal from water include oxidation/precipitation, coagulation, sorption, ion-exchange and membrane filtration.

In rural areas of developing nations where local population face economical – traditional – political constrains, a low-cost and practical set-up for removing arsenic from drinking water is necessary. Sorption and coagulation/precipitation are more realistic techniques than high

cost and high-tech operation techniques (i.e. ion exchanges and membrane processes). To simplify the As removal processes, a promising adsorbent which can efficiently adsorb both As(III) and As(V) is more practical than coagulation/precipitation processes, in which case pre-oxidation of drinking water for converting As(III) to As(V) is needed.

In this study, we employed a novel method to synthesize a chitosan-iron hydroxide composite, namely chitosan goethite bionanocomposites (CGB) beads. CGB beads were characterized by Mössbauer Spectroscopy and Field Emission Scanning Electron Microscopy (FE-SEM). Batch sorption and kinetic experiments were performed to assess the sorption of As(III) and As(V) onto CGB. The mechanism of As(III) and As(V) uptake onto CGB was investigated by Synchrotron Radiation X-ray Absorption Spectroscopy (SR-XAS). The diffusion of As(III) and As(V) from solution into the porous solid phase was monitored by micro X-ray fluorescence (μXRF) and micro X-ray Near Edge Spectroscopy (μXANES).

Wet Chemistry

Isotherms for the sorption of As(III)/As(V) onto CGB beads were studied at different pH values and data were found to be best described by the Freundlich and Redlich-Peterson equations. The kinetics study indicated that As(V) was adsorbed faster than As(III), and a pseudo-equilibrium was reached in both cases within 2000 min. The effect of CGB mass used in adsorption on residual As levels was studied. For 1 liter of water containing 1 mg/L of As(V) or As(III), only less than 0.5 g and around 2 g respectively of the CGB bead is needed to decontaminate the water to reach the 10 μg/L standard.

Mechanism study

The As oxidation state and binding environment were examined by synchrotron X-ray absorption spectroscopy. Results showed that As was adsorbed mainly onto goethite nanoparticles in the CGB composite material, although As can be adsorbed by chitosan as well. As(III) was partly oxidized to As(V) under an aerobic environment while As(V) species remained unchanged under both aerobic and anaerobic environments.

Diffusion pattern

As-loaded CGB samples collected from kinetics experiments at 1.5 h and 72 h were cut into 40 μm thick cross-sections. The distribution and co-localization of Fe and As in cross-sections of As-loaded CGB were studied by high resolution synchrotron radiation micro X-ray fluorescence mapping. The distribution of As reveals that, during the first 1.5 h, As(III) penetrated for 70-80 μm in the beads, while the penetration of As(V) was slightly faster, reaching 100-110 μm. After 72 h, both As(III) and As(V) diffuse in the whole CGB section, their concentration being higher at the borders and diminishing in the center of the beads in a typical U shape profile. This suggested that the arsenic adsorption took place more rapidly than the diffusion process. Effective diffusivities of arsenic were calculated: $D_{eff}(AsIII) = 6.69\times10^{-14}$ m^2/s and $D_{eff}(AsV) = 1.34\times10^{-13}$ m^2/s. The estimated effective diffusivities of As(III) and As(V) are similar. The higher estimated diffusivity of As(V) could be due to the electrostatic attraction between As(V) and the interior of the beads which accelerates the movement of As(V) towards the core of the beads.

The novel material – chitosan goethite bionanocmoposites (CGB) that this thesis presents show several outstanding properties:

(i) **High efficiency**: it can efficiently remove both the inorganic As species As(III) and As(V), without a pre-oxidation process,

(ii) **Low difficulty and cost in filtration process**: the large-scale bead (1 mm) is more easily to be removed than fine nanoparticle powders.

(iii) **Low health risk**: goethite nanoparticles are stabilized by the chitosan matrix, so there are no NPs released from the sorption process during its use. No toxic chemical was used during the fabrication of the material compared to conventional methods, in which the use of toxic cross-linking reagents is common.

(iv) **High mechanical property**: Compression mechanical property test reports the crushing strength to be 34.9 ± 6.5 N, compared to chitosan hydrogel beads (1.87 N) and that of the chitosan hydrogel beads impregnated with carbon nanotubes (7.62 N).

These properties highly reduce the cost and complexity of the water remediation process. It could be a promising material particularly for developing nations, which suffer a diversity of socio-economical-traditional constraints for water purification and sanitation.

The risk and occurrence of antibiotics in water

As with other dangerous pollutants that spread in the environment and threaten human health, there is a need for environmental scientists and engineers to help address the critical problem of antibiotics. An antibiotic is an agent that inhibits or kills bacteria. Despite decades of high usage for human medicines and veterinary purposes, the occurrence and effects of antibiotics in the environment have been little studied until very recently. Antibiotics presence has now become a focus of research efforts due to different adverse effects, especially the contribution to antibiotic resistant bacteria in the environment. The powerful killing and growth inhibitory

effects of antibiotics have reduced the numbers of susceptible strains, leading to the propagation of resistant variants (Levy, 2008). Such resistant bacteria can cause an infection both in humans and animals and may not respond to regular antibiotic treatments (Regassa et al., 2008). The presence of antibiotics, even in low dose, also potentially harm aquatic environment and pose risks to public health.

Gentamicin removal by clay mineral and synthesis of Gt-Mt-HPMC bionanocomposites film for burn wound dressing

Gentamicin (Gt.), an aminoglycoside antibiotic produced by fermentation of *Micromonospura purpurea*, is a mixture of basic, water soluble compounds containing aminocyclitol 2-deoxystreptamine and 2 additional amino sugars (MacNeil and Cuerpo, 1995). Gentamicin is used to treat many types of bacterial infections, particularly those caused by Gram-negative organisms (Moulds and Jeyasingham, 2010). The main toxic effects of the aminoglycoside antibiotics are nephrotoxicity and ototoxicity. Furthermore, fetotoxicity was observed for gentamicin (Gehring et al., 2005). Although application of Gt. in human medicine has declined, its use in veterinary and agriculture is still intense. Gentamicin can enter the environment via pharmaceutical factories, hospital waste water and animal droppings.

The sorption of Gt. onto Na^+-montmorillonite

The amino groups of the sugar rings of gentamicin exhibit variable pKa values which range from 5.6 to 9.5. Thus, gentamicin carries a net positive charge under acidic conditions when all or parts of amino groups are protonated. It offers the possibility of gentamicin intercalation in Na^+-montmorillonite by means of cationic exchange processes.

In order to investigate the adsorption isotherm, three equilibrium isotherm models were applied: the Langmuir, the Freundlich, and the Redlich-Peterson isotherms. The Langmuir and the Redlich-Peterson isotherms best fitted the data fothe adsorption of gentamicin on Na^+-montmorillonite at 294 K .

XRD results confirmed intercalation of the gentamicin in the clay interlayers, indiciated by the decrease of 2θ values. As the gentamicin/clay ratio increases, the d_{001} spacing reaches 1.4 nm when the clay reaches saturated adsorption. The increase of clay d_{001} spacing was due to the thickness of gentamicin molecule sheet. The orientation of gentamicin in the interlayer of the clay was studied.

Gentamicin-montmorillonite-HPMC film

Gentamicin-loaded montmorillonite, the solid waste from the gentamicin adsorption process, can be used to synthesize gentamicin-montmorillonite-HPMC (Hydroxyl Propyl Methyl Cellulose) (Gt-Mt-HPMC) film which can be potentially used as a burn wound dressing. The antimicrobial effect of Gt-Mt-HPMC against the skin infection-causing bacteria *Staphylococcus aureus* was examined according to ASTM E2149 (Standard test Method for determining the antimicrobial activity of immobilized antimicrobial agents under dynamic contact conditions). The reinforcing clay mineral and HPMC afford the necessary mechanical strength to the dressing, and the combined binding matrix was aimed at providing adequate moisture control and release of antibiotics to protect the wound bed from infection and to promote healing.

Gt-Mt-HPMC and Gt-HPMC showed high antimicrobial properties compared with the control tube with peptone water. The samples HPMC or/and montmorillonite which were free of

gentamicin showed no detectable antimicrobial effect. The result showed that Gt-Mt-HPMC retained the antimicrobial capability of gentamicin. The efficiency of the antimicrobial effect of the bionanocomposites was not weakened by the supporting material montmorillonite nor the HPMC.

Résumé

Les composés dits 'bionano' (bionanocomposites) apparaissent comme un nouveau groupe de matériaux hybrides nano-structurés. Ils sont issus de la combinaison de polymères naturels et de solides inorganiques et sont de l'ordre du nanomètre dans au moins une direction (Darder et al., 2007). Ces matériaux hybrides conservent les structures et les propriétés fonctionnelles des polymères et matériaux inorganiques dont ils sont composés. Parallèlement, la présence de biopolymères permet de diminuer les risques environnementaux et de santés publiques liés aux nano-matériaux. Les propriétés inhérentes aux biopolymères (biocompatibles' et biodégradables) ouvrent des perspectives intéressantes pour ces matériaux hybrides en particulier dans les domaines de la médecine regénérative et en génie de l'environnement (Darder et al., 2007). La production de bionanocomposites de taille plus importante, que les nanoparticules qu'ils renferment, permet d'éviter les effets nocifs potentiels des nanoparticules (Nps) pour les organismes vivants et plus particulièrement pour l'homme. L'association de biopolymères et de nano-solides inorganiques permet la conception de bionanocomposites multifonctionnels qui peuvent être synthétisés et utilisés pour des applications dans des domaines variés.

Cette thèse se propose d'étudier principalement (i) ma présence d'arsenic et d'antibiotiques dans les sources d'eau potable en Chine; (ii) l'évaluation d'un nouveau bionanocomposites, à savoir le CGB (chitosan goethite bionanocomposite), dans la décontamination des eaux contenant des espèces inorganiques d'arsenic; (iii) l'évaluation d'argiles comme adsorbants de

décontamination de la gentamicine (un antibiotique aminoglycoside) présent dans l'eau de même que celle de bionanocomposés fait d'argiles riches en gentamicine de polymères de methycelluloses hydroxypropyles Gt-Mt-HPMC (gentamicin-montmorillonite- hydroxypropyl methycellulose) utilisés comme pansement contre les infections qui ont lieu suite à des brûlures.

Une part importante de la population mondiale est exposée à des concentrations élevées d'arsenic à travers les ressources en eau présentes dans le sous-sol – principalement dans les pays en développement où il n'existe pas de sources d'eaux alternatives. Les systèmes aquifères présentant des concentrations en arsenic élevées résultant de processus naturels ou de l'activité humaine ont été observés sur l'ensemble des continents et dans différents environnements. C'est en Asie (e.g. Bangladesh, Chine, Inde, Népal) et en Amérique du Sud (e.g. Argentine, Mexique) que les cas les plus spectaculaires de contamination à l'arsenic via les aquifères ont été répertoriés (Aureli, 2006). On estime que le nombre de personnes exposé à un taux d'arsenic posant des problèmes sanitaires dans les régions rurales d'Inde, de Chine, du Pakistan, du Vietnam, du Népal et du Cambodge dépasse aujourd'hui 100 millions (Ravenscroft et al., 2009). Les formes inorganique d'arsenic majoritairement présentent dans les aquifères sont l'arsenite [As(III)] et l'arséniate [As(V)]. La consommation prolongée d'eau contaminée à l'arsenic peut conduire entre autres à des lésions cutanées (Tondeal et al., 1999), à de l'artériopathie oblitérante des membres inférieurs (Chen, 1990; Engel et al., 1994), à de l'hypertension (Chen et al., 1995) et à des cancers du poumon, de la peau et du foie (Bates et al., 1992).

L'arsenic dans les aquifères provient des minéraux présents dans les sédiments suite à des mécanismes biogéochimiques de mobilisation. Il n'est pas possible d'éliminer ces sources naturelles. L'eau issue des aquifères doit donc être traitée avant d'être consommée. On peut citer parmi les techniques couramment employées l'oxydation/précipitation, la coagulation, la sorption, l'échange d'ions et la filtration par membrane.

Les contextes sociaux-économiques des zones rurales des pays en voie de développement nécessitent le développement de méthodes de décontamination peu onéreuses et faciles à mettre en place. Les techniques basées sur les mécanismes de sorption ou de coagulation/précipitation apparaissent comme plus réalisables au contraire des techniques plus avancées et plus cher comme l'ozonation, les échanges d'ions ou la filtration par membrane. Dans l'optique de simplifier les techniques de décontamination, il est probablement plus intéressant d'envisager un composé capable d'absorber à la fois l'arsenite et l'arséniate que de développer les mécanismes de coagulation/précipitation où une opération de pré-oxydation de l'eau est nécessaire afin de convertir As(III) en As(V).

Dans l'étude présentée, nous décrivons une nouvelle méthode permettant de synthétiser des billes d'hydroxide fer-chitosan, le CGB (Chitosan Goethite Bionanocomposites). Ces billes de CGB ont été caractérisés à l'aide de la spectrométrie Mössbauer et de la microscopie électronique à balayage (FE-SEM). Des expériences de sorption et de leur cinétique ont été conduites afin d'estimer la diffusion et l'immobilisation de As(III) et As(V) sur les billes de CGB. Le processus de fixation de As(III) et As(V) a été étudié à l'aide de la spectroscopie d'absorption des rayons X au Synchrotron (SR-XAS) et la diffusion de As(III) et As(V) dans

les billes de CGB a été suivies en utilisant la micro spectrométrie de fluorescence X (μXRF) et la micro spectroscopie proche bord des rayons X (μXANES).

Chimie des solutions

L'étude de la sorption de As(III)/As(V) sur les billes de CGB a été effectuée pour différentes valeurs de pH et les données on été interprétées à l'aide des équations de Freundlich et Redlich-Peterson. L'étude cinétique a montré que As(V) était adsorbé plus rapidement que As(III) et que le pseudo-équilibre était atteint pour les deux espèces en moins de 2000min. L'impact de la quantité de billes CGB utilisés pour l'adsorption des résidus d'arsenic a également été étudié. Respectivement moins de 0.5g et 2g de billes de CGB dans un litre d'eau contaminée à 1mg/L de As(V) ou As(III) est nécessaire pour obtenir une eau avec moins de 10 μg/L d'arsenic.

Etude des mécanismes

L'état d'oxydation et les interactions de l'arsenic ont été examinés en utilisant la spectroscopie d'absorption des rayons X. Les résultats montrent que l'arsenic est principalement adsorbé sur les nanoparticules d'oxyhydroxyde de fer composant les billes de CGB bien que l'arsenic puisse également être adsorbé par la matrice de chitosan. As(III) est partiellement oxydé en As(V) dans un environnement anaérobique alors que As(V) reste inchangé dans un environnement aérobique ou anaérobique.

Diffusion

Des sections de 40μm d'épaisseur de billes de CGB soumises aux expériences d'adsoprtion ont été étudiées après 1.5h et 72h d'exposition. La distribution et la co-localisation du fer et de

l'arsenic sur ces sections ont été analysés en utilisant la micro spectrométrie de fluorescence X. La distribution d'arsenic a mis en évidence qu'en 1.5h, As(III) pénètre de 70-80 μm dans les billes alors que As(V) pénètre de 100-110 μm. Après 72h, les deux espèces ont diffusés dans la totalité de la bille avec un gradient de concentration tel que la concentration au cœur des billes est moindre que sur les bords. Les résultats indiquent que le temps caractéristique de l'adsorption est plus court que celui de la diffusion. Les coefficients de diffusion effectifs des deux espèces ont été calculé et les valeurs obtenues sont du même ordre de grandeur pour les deux degrés d'oxydation de l'arsenic = 6.69×10^{-14} m^2/s et = 1.34×10^{-13} m^2/s. La valeur plus élevée pour le coefficient de diffusion de As(V) peut être expliquer par l'attraction électrostatique qui a lieu entre As(V) et l'intérieur des billes (chitosan négativement chargé) accélérant ainsi la migration de As(V) vers le cœur des billes.

Le nouveau matériaux (CGB) étudié présente donc des propriétés remarquables:

(i) Efficacité : il permet d'absorbé les espèces d'arsenic As(III) et As(V) sans oxydation au préalable.

(ii) Facilité de mise en place et peu onéreux: les billes de CGB étant de taille importante (1mm), il est plus faciles de les récupérer que les poudres à base de nanoparticules.

(iii) Pas de risque sanitaire : les nanoparticules de goethites sont stabilisés via la matrice de chitosan prévenant ainsi la présence de Nps lors de l'utilisation du procédé. De plus il faut noter que la synthèse des billes de CGB ne nécessite pas l'utilisation de produit toxique contrairement aux méthodes conventionnelles qui utilisent par exemple le glutaraldéhyde.

(iv) Propriétés mécaniques : Les tests sous les contraintes de compression ont indiqués des ruptures à 34.9 ± 6.5 N. Ces résultats sont à comparer avec 1.87 N obtenu avec les

billes d'hydrogel de chitosan et 7.62 N obtenu avec des billes d'hydrogel de chitosan contenant des nanotubes de carbone.

Ces propriétés réduisent considérablement les coûts et la complexité des techniques de décontamination. Ce matériaux offre donc des perspectives intéressantes pour les pays en voie de développement qui souffrent de problèmes sociaux-économiques récurrents qui limitent les possibilités de purification et de traitement des eaux.

Les antibiotiques et l'eau : état des lieux et risques

La présence d'antibiotiques dans le milieu naturels nécessite la mobilisation des scientifiques et ingénieurs comme cela se fait pour les autres polluants qui posent des problèmes sanitaires. Les antibiotiques sont des agents qui inhibent ou tuent les bactéries. Pendant des décennies, alors qu'une quantité importante été utilisé dans la médecine pour l'homme ou les animaux, leur distribution et leur impact sur l'environnement étaient peu étudiés et ce jusqu'à récemment. La répartition des antibiotiques dans les environnements naturels a fait l'objet d'études importantes suite à la découverte d'effets indésirables comme la résistance accrue aux antibiotiques de certaines bactéries dans l'environnement et nous avons passé en revue les données sur la Chine. L'utilisation massives des antibiotiques a réduit le nombre de souches en favorisant les souches résistantes (Levy, 2008). Ces bactéries peuvent être responsables d'infection chez l'homme ou l'animal que les traitements classiques ne peuvent régler (Regassa et al., 2008). La présence d'antibiotique, même à faible dose, peut également endommager les milieux aquatiques voir poser des problèmes de santé publiques.

Epuration de la gentamicine à l'aide d'argile et synthèse de pansements contre les brûlures à base de films de bionanocomposites Gt-Mt-HPMC

La gentamicine (Gt), un antibiotique de la famille des aminoglycosides issue de la fermentation de *Micromonospura purpurea*, est composé d'éléments solubles dans l'eau dont l'aminocyclitol 2-deoxystreptamine et deux sucres amino (MacNeil et Cuerpo, 1995). La gentamicine est utilisée dans le traitement de nombreuses infections bactériennes, et plsu particulièrement celles causées par des organismes à Gram négatifs (Moulds et Jeyasingham, 2010). Les principaux effets toxiques observés avec les antibiotiques de la famille des aminoglycosides sont des effets nephrotoxiques et ototoxiques. En outre, des effets fetotoxiques ont été rapportés lors de l'utilisation de la gentamicine (Gehring et al., 2005). Bien que l'utilisation de la gentamicine en médecine ait diminué, son utilisation en médecine vétérinaire et en agriculture est encore importante. La gentamicine peut être introduite dans l'environnement via les lieux de productions ou via les les eaux usées des hôpitaux et les rejets de fermes d'élevage.

Sorption de la gentamicine sur Na^+-montmorillonite

Les groupes amino des anneaux de sucres de la gentamicine présentent des valeurs de pKa quie varient entre 5.6 et 9.5. De ce fait, la gentamicine possède une charge positive nette dans des conditions acides quand l'ensemble des groupes amino sont protonés ce qui offre la possibilité à la gentamicine de s'intercaler dans Na^+-montmorillonite au travers de mécanismes d'échanges de cations. Afin d'étudier l'adsorption isotherme, trois modèles d'équilibre isotherme ont été utilisés : le modèle de Langmuir, le modèle de Freundlich et le modèle de Redlich-Peterson. Les modèles de Langmuir et de Redlich-Peterson ont permis de

modéliser au mieux l'adsorption de la gentamicine sur la montmorillonite saturée en Na+ à 294 K (r^2=0.978).

Les résultats issus de DRX montrent l'inclusion de la gentamicine dans les inter-couches d'argile avec la diminution des valeurs 2θ lors de l'augmentation du ratio gentamicine/argile et l'espacement d_{001} atteint 1.4 mm dans l'argile saturée à la gentamicine. L'augmentation de l'espacement d_{001} est dû à l'épaisseur des molécules de gentamicine. L'orientation de la gentamicine dans les inter-couches d'argile a également été étudié.

Films de Gentamicin-montmorillonite-HPMC

La phase solide, la montmorillonite contenant de la gentamicine, résultant de l'adsorption de gentamicine peut être utilisée afin de synthétiser les films de gentamicin-montmorillonite-HPMC (Hydroxyl Propyl Methyl Cellulose) qui peuvent potentiellement être appliqués comme pansements suite à brûlures. Les propriétés anti-bactériennes de Gt-Mt-HPM pour contrer les infections cutanées de *Staphylococcus aureus* ont été étudiées suivant le protocole ASTM E2149 (test standard pour déterminer l'activité anti-bactérienne d'agents immobiles anti-bactériens sous contraintes dynamiques). L'argile et HPMC agissent alors comme une structure ayant les propriétés mécaniques nécessaires pour le pansement en même temps qu'une matrice capable de fournir un environnement humide et capable de délivrer lentement l'antibiotique protégeant ainsi la blessure d'une infection.

Gt-Mt-HPMC et Gt-HPMC ont démontrés leurs propriétés anti-bactériennes avec un tube de contrôle d'eau peptonée. Les échantillons HPMC et/ou montmorillonite sans gentamicine n'ont montré aucune efficacité anti-bactérienne. Les résultats montrent que Gt-Mt-HPMC conserve l'ensemble des capacités anti-bactériennes de la gentamicine sans que le support montmorillonite et HPMC n'en diminue ses effets.

Chapter 1

Arsenic as an emerging contaminant in the environment

Jing He，Laurent Charlet

1.1. Occurrence of arsenic in the environment

Arsenic-bearing minerals including arsenic-rich pyrite, arsenopyrite, orpiment, realgar and As-associated metal sulfides can release large amounts of arsenic when the chemical environment has been changed. O_2-enriched environments leads to oxidation of these minerals followed by As mobilization. Insoluble As-bearing minerals are rapidly oxidized by exposure to the atmosphere and then the released soluble As(III) is carried by runoff and groundwater flow into surface and ground waters.

Major natural processes responsible for observed concentrations of arsenic in surface and ground water include: mineral precipitation/dissolution, adsorption/desorption, chemical transformation, ion exchange, and biologic activity (Welch et al., 1988; Smedley and Kinniburgh, 2002). Ordinary solid phases containing arsenic at around the crustal abundance can give rise to high dissolved arsenic (0.05 mg/L) (Nordstorm, 2002).

Adsorption and desorption reactions between arsenic and Fe/Mn/Al oxides and hydroxides surfaces are particularly important controlling reactions because these oxides are widespread in the hydrogeologic environment and arsenate adsorbs strongly to oxides and hydroxides surfaces in acidic and near-neutral-pH water (Dzombak and Morel, 1990; Waychunas et al., 1993). However, arsenate adsorption rapidly decreases in basic media (Mamindy-Pajany et al., 2011). pH value plays an important role in the desorption of arsenic because of its effects on the species distribution of anions, the surface charge of the arsenic-bearing oxides and hydroxides, and subsequent electrostatic forces between arsenate and solids (Xu et al., 2012).

Anaerobic microbial respiration, utilizing either sedimentary or surface-derived organic carbon, is one important process contributing to the mobilization of arsenic from host minerals, notably hydrous iron oxides (Charlet and Polya, 2006). Many studies have given evidence of arsenic release under reducing environments in the presence of Fe-reducing bacteria. Burial of fresh organic matter, infiltration of fresh DOC and the slow diffusion of O_2 through the sediment lead to reducing conditions just below the sediment-water interface in lakes or in superficial groundwaters as abundantly described in SE Asia deltas (Charlet and Polya, 2006; Fendorf et al., 2010). This encourages the reduction of As(V) and desorption from Fe and Mn oxides, as well as the reductive dissolution of As-rich Fe oxyhydroxides.

1.2. Arsenic speciation and toxicity

Arsenic speciation is controlled by redox potential (Eh) and pH values. Arsenic can occur in the environment in several oxidation states (-3, 0, +3 and +5), being organic compounds or inorganic forms. In natural waters, arsenic is mostly present in its inorganic form as oxyanions of trivalent arsenite [As(III)] or pentavalent arsenate [As(V)] (Figure 1.1). Under oxidising conditions, arsenate occurs as anionic forms: $H_2AsO_4^-$ is dominant pHs less than about 6.9, while $HAsO_4^{2-}$ becomes dominant at higher pH values. Under reducing conditions, the uncharged arsenite species $H_3AsO_3^0$ is dominant at pH $\leq$9.2 (Smedley and Kinniburgh, 2002). An overview of arsenic species depending on the pH and Eh in the aqueous phase is given in the pH-Eh diagram (Fig. 1.2).

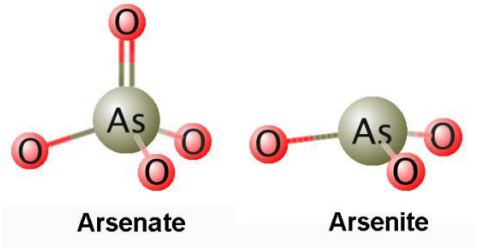

Figure 1.1: Molecule structures of arsenate and arsenite (Hydrogen atoms are omitted).

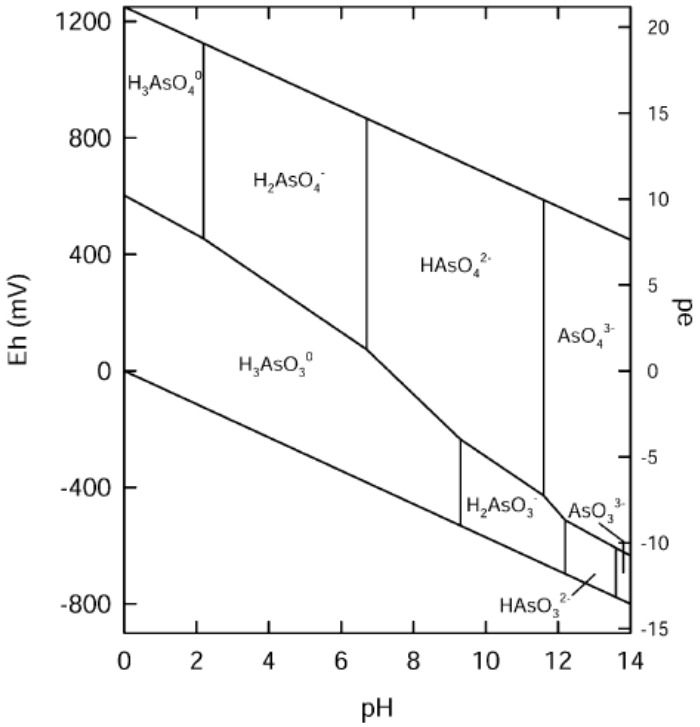

Figure 1.2: Eh-pH diagram of arsenic species in the aqueous phase at 25°C and 1 bar total pressure (Smedley and Kinniburgh, 2002).

Inorganic As species are significantly more harmful than organic As species. In short, we only discuss the toxicity of inorganic forms of arsenic: arsenite and arsenate. Acute arsenic poisoning is associated initially with nausea, vomiting, abdominal pain, and severe diarrhea (Ratnaike, 2003). Long-term drinking water exposure of arsenic may cause skin lesions (Tondel et al., 1999), peripheral vascular disease (Engel et al.,1994), hypertension (Chen et al., 1995), black-foot disease (Chen, 1990), and high risk of cancers (Bates et al.,1992). High drinking water As concentration was found to elevate late fetal mortality and neonatal/postneonatal mortality (Hopenhayn-Rich et al., 2000). As exposure was also observed to impair cognitive development in school children and lead to children DNA

damage and immunodeficiency (Yanez et al., 2003; Vega et al., 2008). Some research findings from Chile link in utero and early life As exposure to cardiovascular, respiratory and lung cancer later in adult life (Smith et al., 2006; Yuan et al., 2007).

WHO's recommendations for drinking-water quality go back to 1958. The International Standards for Drinking-Water established the maximum allowable level of arsenic in drinking water as 0.20 mg/L. In 1963 the standard was re-evaluated and reduced to 0.05 mg/L. The guideline value was provisionally reduced in 1993 from 0.05 mg/L to 0.01 mg/L. Many countries, including China, have kept the old guideline value of 0.05 mg/L as their water quality standard for several years, even up until now.

1.3. High arsenic water distribution all around the world

A large number of people worldwide are exposed to elevated As concentrations in ground water – many of them in developing countries and with no available alternative water resources. Aquifer systems with high levels of arsenic, elevated by natural processes or anthropogenic activities, have been reported in different environments from all continents. Some of the best-documented and most severe cases of arsenic contaminated groundwater have been found in aquifers in Asia (e.g. parts of Bangladesh, China, India, Nepal) and South America (e.g. Argentina, Mexico) (Aureli, 2006). Estimates of the rural population exposed to unsafe As levels by drinking untreated groundwater in India, China, Myanmar, Pakistan, Vietnam, Nepal, and Cambodia has grown to over 100 million (Ravenscroft et al., 2009). Bhattacharya et al. (2002) reported As concentrations of up to 3700 μg/L in groundwater in the Bengal Delta Plain, Bangladesh; High arsenic concentrations up to 11,000 μg/L were found in some areas of Ontario, Quebec, New Brunswick, Nova Scotia and British Columbia (Health Surveillance, Alberta Health and Wellness, 2000); Arsenic concentrations up to

12,000 µg/L were measured in groundwater from an aquifer in the Fox River valley in eastern Wisconcin, USA (Schreiber et al., 2003); High arsenic levels in drinking water have been measured throughout the province of Cordoba, located in the centre of Argentina, often above 100 µg/L and reaching levels of over 2000 µg/L (Hopenhayn-Rich et al., 1998). Most of the contaminated aquifers are related to sediments of Quaternary age (Acharyya, 2005). Also known for As-enriched waters are geothermal areas, such as the Yellowstone National Park in the West of the United States, the Donargarh rift belt of Central India (Mukherjee, 2009), the Guide Basin of China (Shi et al., 2010) and Central Italy (Angelone, 2009). A comparison of occurrences in the Ganges–Brahmaputra, Mekong, and Red River basins shows that common geological characteristics include river drainage from the rapidly weathering Himalayas, rapidly buried organic bearing and relatively young (ca. Holocene) sediments, and very low, basin-wide hydraulic gradients (Charlet and Polya, 2006). Statistical models based on the statistical relationship of As concentrations and relevant explanatory variables such as geology, climate or topography have recently been developed (Amini et al., 2008; Rodriguez-Lado et al., 2008; Winkel et al., 2008). Amini et al. (2008) used a large database of measured arsenic concentration in groundwaters from around the world as well as digital maps of physical characteristics such as soil, geology, climate, and elevation to model probability maps of global arsenic contamination. Maps of modeled global probability of geogenic arsenic contamination in groundwater for reducing and high-pH/oxidizing conditions were delineated (Fig. 1.3).

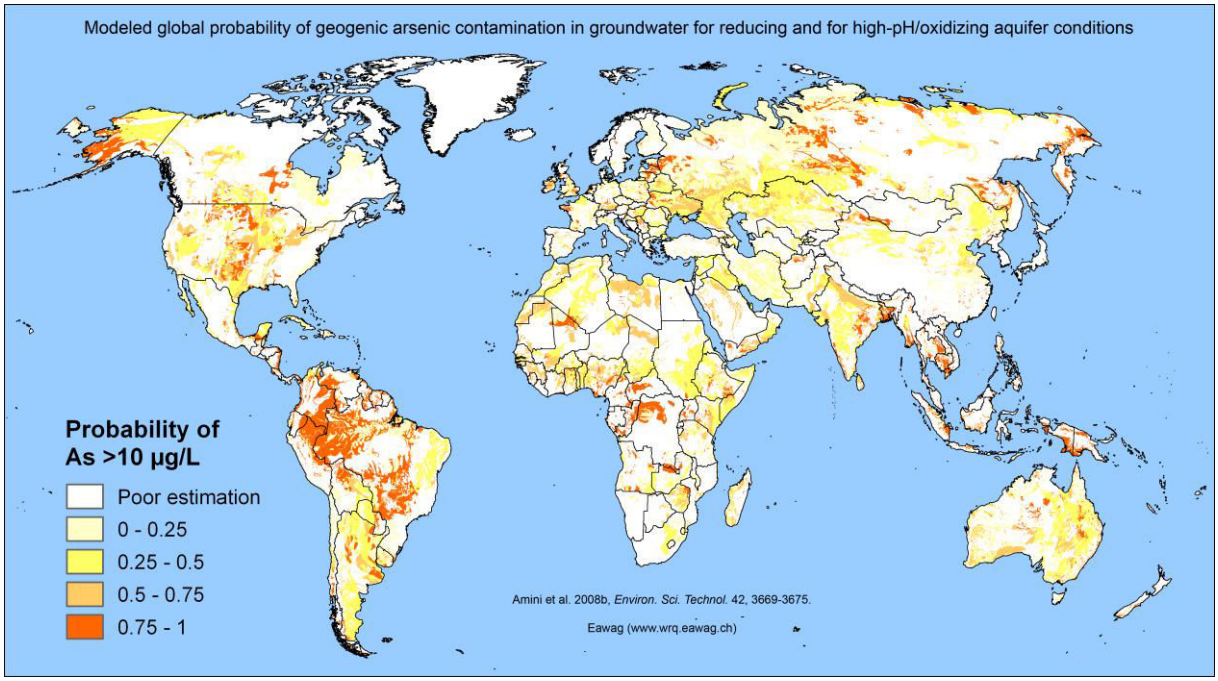

Figure 1.3: Modeled global probability of geogenic arsenic contamination of reducing and for high-pH/oxidizing aquifer conditions (Amini et al., 2008).

1.4. Arsenic decontamination: techniques and challenges

With limited alternative drinking water resources, millions of people are affected by groundwater with elevated arsenic concentration. Arsenic was released to subsurface water bodies due to natural processes, such as arsenic mobilization from minerals and sediments. It is not possible to eliminate these sources. Therefore groundwater containing high level of arsenic has to be treated before used as drinking water. Table 1.1 summarized advantages and disadvantages of common techniques for arsenic removal from water.

Table 1.1: Arsenic removal techonologies

Techonology		Advantages	Disadvantages
Oxidation/ precipitation	Air oxidation	Relatively simple, Low-cost, in situ As removal,	Slow process,
	Chemical oxidation	Rapid process, kill microbes at the same time	pH control is needed
Coagulation		Relatively low–cost, Common chemicals are available, wider range of pH	Toxic sludge, Low removal of As, Pre-oxidation may be required, Sedimentation, filtration needed, pH readjustment needed,
Sorption		Wide range of sorbents can be chosen, easy set up	Regeneration, replacement, toxic solid waste
Ion-exchange		High capacity, pH independent	High cost, high-tech operation and maintenance.
Membrane filtration		Green, less chemical consumption, several contaminants can be removed at once	High cost, high energy consumption

Oxidation

The purpose of oxidation is to convert soluble As(III) to As(V), which is followed by precipitation or sorption of As(V). As(V) is more easily adsorbed onto solid surface than neutral As (III) over a wide range of pH condition, thus oxidation of As(III) to As(V) is considered to be helpful for further treatment. Oxidation is essential for anoxic groundwater, since As(III) is the predominant form at near neutral pH (Masscheleyn et al., 1991).

Coagulation and Precipitation

By adding a coagulant to the contaminated water, flocs form and arsenic co-precipates with or adsorbs on the surface of the coagulant, followed by settling of the aggregate or removal by filtration. Generally the best removal is achieved at the pH at which the precipitated species is

least soluble. The nature and size of the flocs are important as they adsorb the soluble As from water and finally transform it into an insoluble product. Among the various chemical coagulants used for As removal, Fe and Al based coagulants are mostly used (McNeill and Edwards, 1995).

Adsorption

Adsorption takes place on the surface of solid adsorbents. High abrasion resistance, high thermal stability and high exposed surface area are important properties of adsorbents for being practical and efficient in the removal of contaminants. Several adsorbents have been used to remove As from aqueous solution. Among all the adsorbents, iron oxides, oxyhydroxides and hydroxides, including amorphous hydrous ferric oxide, goethite and hematite, are the most promising adsorbents for removing both As(III) and As(V) from water. Most iron oxides are fine powders that are difficult to separate from the solution after treatment. Therefore, the EPA has proposed iron oxide-coated sand filtration as an emerging technology for arsenic removal at small water facilities (EPA, 2000; Thirunavukkarasu et al., 2003).

Ion exchange

By electrostatic attachment, many contaminants can effectively be removed from aqueous and solutions. Solid polymeric or mineralic ion exchangers, either cation exchangers or anion exchangers, are chosen depending on the contaminant and the chemistry of water. The resins need to be regenerated by rinsing with a solution of high resin-ion concentration after all the ions on the surface of the resin are exchanged with the contaminant ions. Arsenate is

predominantly removed by ion exchange techniques, whereas these are not effective for the uncharged arsenite species.

Membrane processes

Membranes are a selective barrier, allowing some constituents to pass while blocking the passage of others. The movement of constituents across a membrane requires a driving force (i.e. a potential difference between the two sides of the membrane) including pressure, concentration, electrical potential, or temperature. Pressure-driven membranes are frequently used for contaminant removal. Based on the pore size of the membrane, pressure-driven membranes are often classified into four categories: microfiltration (MF), ultrafiltration (UF), nanofiltration (NF), and reverse osmosis (RO). High-pressure processes (i.e., NF and RO) have a relatively small pore size compared to low-pressure processes (i.e., MF and UF) (EPA, 2000). Although high pressure processes can remove a broader range of contaminants than low pressure processes, the high energy consumption requirement of this technique constrains its use.

1.5. Objectives - Arsenic decontamination technique and material for house-hold set-up

In rural areas of developing nations where local population face economical – traditional – political constrains, a low-cost and practical set-up for removing arsenic from drinking water is necessary. Sorption and coagulation/precipitation are more realistic techniques than high cost and high-tech operation technique (i.e. ion exchanges and membrane processes). To simplify the As removal processes, a promising adsorbent which can efficiently adsorb both As(III) and As(V) is more practical than coagulation/precipitation processes, in which case pre-oxidation of drinking water for converting As(III) to As(V) is needed. Nanomaterials

which have high surface-to-volume ratio give hope for higher arsenic removal capacities than with convention materials (Theron et al., 2008). However, the high reactivity and small size of nanoparticles also come with higher potential risks due to a better uptake and interaction with biota (Auffan et al., 2009). Many metal nanoparticles have been found to cause chromosomal aberrations, DNA strand breaks, oxidative DNA damage, and mutations (Xie et al., 2011). The difficulty nanoparticles bring to filtration processes due to their nano-size constrains their application in water treatment as well. The goals of this work are to (i) design a novel nano-material which can efficiently remove inorganic As species As(III) and As(V), (ii) minimize the difficulty and cost in filtration process by the new properties of the material, (iii) lower the health risks of the material, and (iv) examine the mechanism of arsenic adsorption on to the material.

Chapter 2

A review of arsenic presence in China drinking water

Jing He，Laurent Charlet

Journal of Hydrology 492 (2013) 79–88

2.1. Introduction

WHO's norms for drinking-water quality go back to 1958. The International Standards for Drinking-Water established allowable level arsenic in drinking water as 0.20 mg/L. In 1963 the standard was re-evaluated and reduced to 0.05 mg/L. The guideline value was provisionally reduced in 1993 from 0.05 mg/L to 0.01 mg/L. Many countries including China had kept the old guideline value 0.05 mg/L as water quality standard for several years. In 2006, Ministry of Health PRC gave a revision of the *Standards of drinking water quality* with allowable arsenic concentration as 0.01 mg/L instead of 0.05 mg/L, as used in the past decades (Ministry of Health of China and Standardization Administration of China, 2006).

Chronic endemic arsenicosis was found in Taiwan in 1968 and reported in Xinjiang Province in Mainland China in the 1970s. In the 1980s, more areas were reported to be affected by arsenicosis via drinking water. Up to year 2012, endemic arsenicosis distributed over 45 counties in 9 provinces, while 19 provinces had the problem that arsenic concentration in drinking water exceeded water standard level (0.05 mg/L). Even though China government has been working on building up water supply plants to ensure safe drinking water, the population at risk is still large: about 1.85 million according to the recent official data from Ministry of Health PRC et al. (2012) is drinking water with As level above 0.05 mg/L. Population exposed to drinking water with As level 0.01 mg/L - 0.05 mg/L was not included in that survey.

One goal of the present study is to draw a picture on arsenic sources of China and to know how the respective importance of each type of source is for elevating As concentration in drinking water. Secondly, we discuss some major documented hotspots that were well-known as As-affected areas. An additional goal is to summarize the features of environment where

different types of natural high-As waters and the reasons why acute poisoning incidents happen.

2.2. Source of arsenic to surface and groundwater

2.2.1. Minerals

Arsenic is a metalloid which exists in earth crust and ranks 14th in element abundance order. The background concentration varies from 1.8 mg/kg to 2.1 mg/kg according to different reviews. Arsenic occurs as a major constituent in more than 200 minerals, including elemental As, arsenides, sulphides, oxides, arsenates and arsenites (Smedley and Kinniburgh, 2002). However, most of those arsenic containing minerals are rare in nature and generally found as sulfides associated with Au, Cu, Pb, Zn, Sn, Ni, and Co in ore zones. The most dominant minerals exist in environment are arsenopyrite (FeAsS), realgar (AsS) and orpiment (As_2S_3).

China has large amount of arsenic reserves: The known arsenic reserves were reported to be 3977 kt, and 2796 kt preserved reserves, of which 87.1% existed in paragenetic or associated ores up to the end of 2003 (Xiao et al., 2008). In 2011, China was the top producer of white arsenic with almost 50% world share, followed by Chile, Peru, and Morocco. (U.S. Geological Survey, 2012). Xiao et al., (2008) reported the distribution of arsenic deposits in China (Figure 2.1). Documented arsenic ore reserves, as demonstrated in Fig. 2.1, are mostly located in southern and western regions of China. The sum of arsenic reserves locating in Guangxi, Yunnan and Hunan Province represents more than 60 percent of the total arsenic reserves explored in China. As reported, up to 87 percent of reserves are believed to be present in sulphide ores which are paragenetic or associated with transition metals ores.

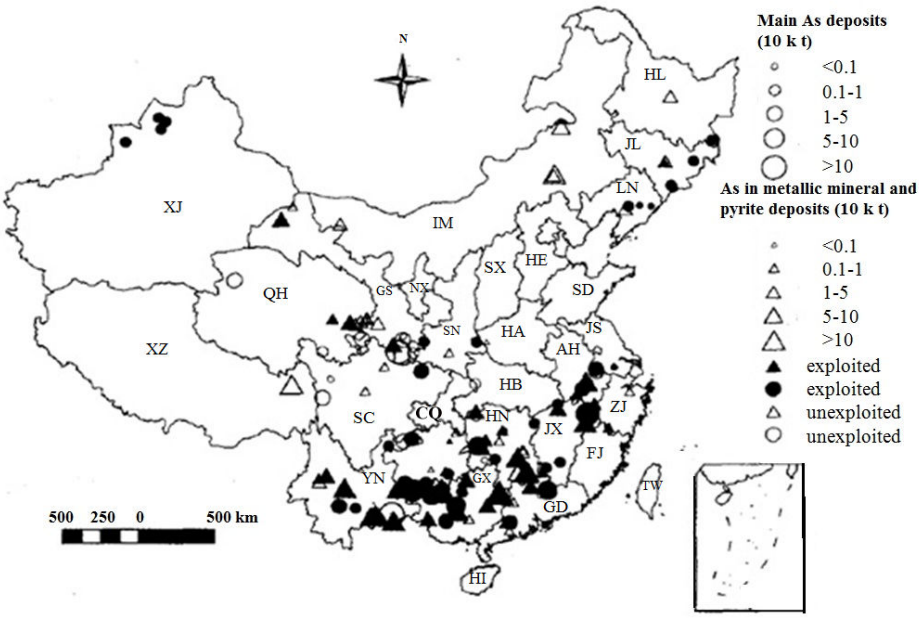

Figure 2.1: Distribution of arsenic deposits in China (See abbreviations in Table 2.2) (from Xiao et al., 2008, revised).

2.2.2. Rocks, sediments, soils and air

2.2.2.1. Rocks

The arsenic abundance of China's continental lithosphere (CCL) has been reported to average 1.2 mg/kg (Li and Ni, 1997). Compositions of rocks in eastern China were with higher arsenic levels, particularly in clastic rock (5.0 mg/kg), pelite (7.8 mg/kg) and carbonatite (3.2 mg/kg) (Yan et al., 1997).

Concentrations in coals are variable depending on the area. Wang et al. (2005) sampled and analyzed 297 coal samples and found that 16 percent of the samples have arsenic concentrations higher than 8 mg/kg, while concentration ranged from 0.24 to 70.83 mg/kg.

Other research reported much higher arsenic concentrations up to 32,000 mg/kg arsenic in coal sample (Ren et al.,1999). Guizhou province is well-known for its large amount of coal reserves, and these contain high arsenic concentration. In southwest of Guizhou, Emeishan basaltic rocks, which is believed to have close relationship with the forming of high-arsenic coal, contain 11 - 113 mg/kg of arsenic (Xie and Nie, 2007), although the basaltic rocks in earth crust are considered having low average arsenic concentration, around 2 mg/kg according to research of Turekian and Wedepohl (1961).

2.2.2.1. River and aquifer sediments.

Average As concentrations for sediments of water system in China is 9.1 mg/kg (Luo et al., 2010). This value is notably higher than world average river sediments which is 5 mg/kg (Martin and Whitfield, 1983). Changjiang River (Yangzte River) is the 3rd longest river in the world. The Changjiang River Basin drains an area of 1.8 million square km, 18.8% of China's land area (CWRC, 2005-2013). Zhang et al., (1995) investigated 260 sediment samples from Changjiang River Basin and the average As concentration of raw sediments appears to be 7.6 mg/kg, while the fine grained parts (< 63μm) tends to be higher as 9.0 mg/kg. Huai River, another main river of China, has been reported to have an average As concentration in sediments of 12.6 mg/kg (9 - 21.8 mg/kg) (Luo et al., 2010). Studies carried out on the Yellow River have reported high arsenic abundance and notable cases of arsenic poisoning in various areas along the river. Fan et al. (2008) reported that As sediments concentrations in Shanyin (in Datong Basin area), Shanxi Province ranged from 3.09 to 26.25 mg/kg with the highest concentration found at depth of 28 - 34 m. Also within the Datong Basin, along Huangshui River and Sanggan River, Xie et al. (2008) collected aquifer sediment samples retrieved from 0 m to 50 m depths below ground level, and arsenic contents ranged from 4.9 to 118.2 mg/kg with mean value of 18.6 mg/kg. Hetao Plain located in the Great Bend of

Yellow River in Inner Mongolia is one of the representative arseniasis-affected areas in China. In Hangjinhouqi County, northwest of Hetao Basin, sediments contained As concentrations ranging from 6.8 to 58.5 mg/kg, reported by Deng et al. (2009). The As concentrations of sediments from the Huhhot Basin which locates close to Hetao Plain lie in the range 3 - 29 mg/kg (Smedley et al., 2003).

2.2.2.2. Soils and atmospheric input

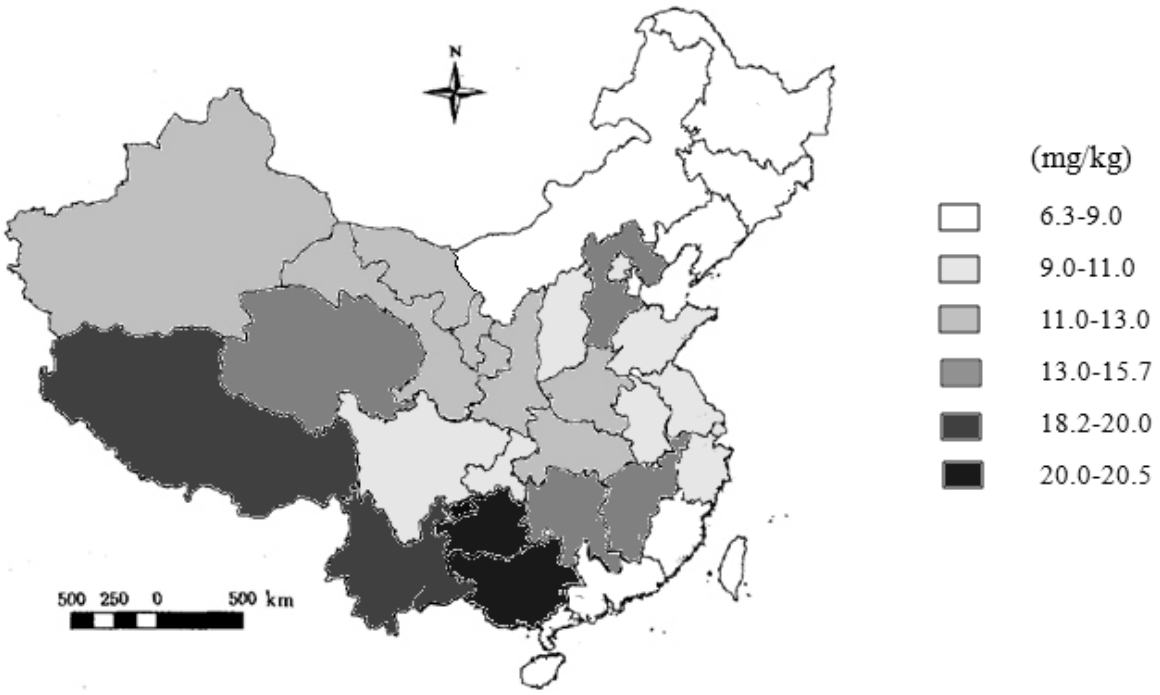

Figure 2.2: Content distribution of arsenic in topsoil of Mainland China (from Weng et al. 2000, revised).

Baseline concentrations of As in soils are generally of the order of 5 - 10 mg/kg (Smedley and Kinniburgh, 2002). An average geochemical background level in world soils was set as 7.2 mg/kg by Boyle and Jonasson (1973). By analyzing 4095 soil samples from all over mainland China, Wei et al. (1991) investigated this geochemical background level for 61 elements. Table 2.1 shows As results in China compared with the As background levels for some other countries. Soil content for 95% of total samples was in the range of 2.5 - 33.5 mg/kg. Among different types of soil of China, regosol and mountain soils have relatively high As concentrations (around 16 mg/kg) and unsaturated siallitic soils have the lowest arsenic content 4 mg/kg. Based on the same dataset, Weng et al. (2000) studied the content distribution of As in Chinese topsoil (Figure 2.2). Arsenic content in soils tended to associate with calcium content in the north and with iron content in the south of China. While As correlation with Fe is well recognized due to the high affinity of secondary iron oxyhydroxides for arsenic oxyanion (Charlet and Poly, 2006; Charlet et al., 2011), the correlation with calcium is less frequent and could be linked to the substitution of As(III) in calcite (Roman-Ross et al., 2006; Bardelli et al., 2011). Compare Fig. 2.2 with Fig. 2.1, we found the content of distribution to be positively correlated to ore deposits.

The deposition of atmosphereic arsenic may increase the arsenic content in aqueous system and soils slightly. Volcanic activities and eolian erosion of arsenic-containing minerals are natural processes which can release arsenic into the atmosphere. However, human activities are believed to play a more important role as source of arsenic air pollution. Fossil-fuel combustion for energy generation, mining and agricultural operations, such as biomass waste combustion, cause national wide problem both in urban and countryside areas. Combustion of coal is the principle source of China's outdoor air pollution (Sheldon et al., 1992). China

relies on coal for 70% to 75% of its energy needs, consuming 1.9 billion tons of coal each year (Millman et al., 2008). Tian and Qu (2009) estimated atmospheric arsenic emission from coal combustion reached 1500 tons by China for year 2005. Atmospheric particles (PM2.5 and PM10) were analyzed for As concentration in some cities. As concentration in the air was 43.36 ng/m^3 (11.98 - 82.55 ng/m^3) in Taiyuan, 24.4 ng/m^3 in Guangzhou and 0.32 ± 0.17 mg/m^3 (0.07 - 0.79 mg/m^3) in Beijing (Xie et al., 2006; Huang et al., 2007; Yang et al., 2012).

Table 2.1: Comparison between background concentrations of arsenic in soils in Mainland China and some other countries (Wei et al., 1991).

Country	Range (mg/kg)	AM[a]	GM[b]
Mainland China	0.01-626	11.2	9.2
USA	<0.1-97	7.2	5.2
Japan	-	9.02	-
UK	-	11.3	-

a: AM-Arithmetic mean

b: GM-geometric mean

2.3. Arsenic mobilization processes

2.3.1. Geogenic factors

Major processes responsible for observed concentrations of arsenic in surface and ground water include: mineral precipitation/dissolution, adsorption/desorption, chemical transformation, ion exchange, and biologic activity (Welch et al., 1988; Smedley and Kinniburgh, 2002). Ordinary solid phases containing arsenic around crustal abundance can give rise to high dissolved arsenic (0.05 mg/L) (Nordstorm, 2002).

Evaporation

In arid or semi-arid areas, use of groundwater is widespread due to lack of surface water. Extensive use of groundwater combined with high evaporation rate and low recharge rate leads to concentration of arsenic in groundwater, especially in low-lying places and closed basin where arsenic can hardly be flushed away by water flow. Studies on arsenic uptake by calcite and gypsum demonstrated that arsenic can be kept by accumulated salt contents (calcite and gypsum) in soil in saline area (Roman-Ross et al., 2006; Fernandez-Martinez et al., 2007). Rainfall or irrigation can release arsenic from those salts and then carry arsenic down into the subsoil and groundwater.

High pH

Adsorption and desorption reactions between arsenic and Fe, Mn and Al oxides and oxides and hydroxides surfaces are particularly important controlling reactions because those oxides are widespread in the hydrogeologic environment and arsenate adsorbs strongly to oxides and hydroxides surfaces in acidic and near-neutral-pH water (Dzombak and Morel, 1990; Waychunas et al., 1993). However, arsenate adsorption rapidly decreases in basic medium

(Mamindy-Pajany et al., 2011). pH value plays an important role in the desorption of arsenic, because of its effects on the species distribution of anions, surface charge of the arsenic-bearing oxides and hydroxides, and subsequent electrostatic forces between arsenate and solids (Xu et al., 2012). The study of Bhattacharya et al. (2006) suggested the volcanic ash as the probable source of groundwater As. Locally, elevated pH values linked to carbonate dissolution, cation exchange, and dissolution of silicates promote release of adsorbed As. In high pH zones As remains dissolved in groundwater. Some studies also reported arsenic release from different iron-bearing minerals, soils and sediments by desorption process as pH values become alkaline (Appelo et al., 2002; Smedley and Kinniburgh, 2002; Breit and Guo, 2012).

Geothermal

The release of arsenic from geothermal systems into surface and ground waters have been reported from several parts of the world. Arsenic concentrations in geothermal well fluids generally range from <0.1 mg/kg to 10 mg/kg. However, As concentrations of >20 mg/kg are not uncommon, at the other extreme. Most reservoir fluids are undersaturated with respect to arsenopyrite and other arsenic minerals (Ballantyne and Moore, 1988) and hence As leaching, rather than As precipitation, is predicted to occur in the reservoir. Hot springs, geysers and steam features with high As contents drain unimpeded into the nearest catchment system and contaminate shallow aquifer systems by natural upward movement of geothermal fluid and some other anthropogenic activities (Webster and Nordstrom, 2003; Aksoy et al., 2009). Dissolution of As oxide and orpiment, relevant to pH value, redox condition and fluid temperature, plays an important role in regulating arsenic mobility. Secondary minerals that form after the dissolution of Fe-As sulphides such as Fe-hydroxides exert a greater influence

on the mobility of arsenic in the geothermal environment (Pascua et al., 2006). Study of Winkel et al. (2013) reveal that where Fe-(hydr)oxides are not sufficiently abundant to act as major scavengers for arsenic, arsenic can be closely associated with calcite matrix in a CO_2-enriched environment.

Sulfide Oxidation

Arsenic-bearing minerals including arsenic-rich pyrite, arsenopyrite, orpiment, realgar and As-associated metal sulfides can release great amount of arsenic when the chemical environment has been changed. O_2-enriched environment leads to oxidation of these minerals followed by As mobilization. Insoluble As-bearing minerals are rapidly oxidized by exposure to atmosphere and then released soluble As(III) is carried by runoff and groundwater flow into surface and ground waters.

Reductive dissolution

Anaerobic microbial respiration, utilizing either sedimentary or suface-derived organic carbon, is one important process contributing to the mobilization of arsenic from host minerals, notably hydrous iron oxides (Charlet and Polya, 2006). Many studies have given evidences of arsenic release under reducing environments in presence of Fe-reducing bacteria. Burial of fresh organic matter, infiltration of fresh DOC and the slow diffusion of O_2 through the sediment lead to reducing conditions just below the sediment-water interface in lakes or in superficial groundwaters as abundantly described in SE Asia delta (Charlet and Polya, 2006; Fendorf et al., 2010). This encourages the reduction of As(V) and desorption from Fe and Mn oxides, as well as the reductive dissolution of As-rich Fe oxyhydroxides.

2.3.2. Anthropogenic factors

As a by-product of some human activities, arsenic can be added to natural waters by chemical industry, mining operations, and agriculture. Arsenical pesticide, industrial sewage/sludge and mining tailing have been reported as sources of arsenic and had contaminated groundwater and surface water via natural processes (e.g. oxidation of mine waste) or direct human manipulations, such as rainwater infiltration, irrigation, runoffs and sewage discharge. In addition to the chemical conditions of the As sources, the composition and states of the primary materials, treatment methods, storage design are influential as well (Breit and Guo, 2012).

2.4. High-As content in China waters - geogenic cases

2.4.1. Overview

One of the most pervasive problem afflicting people in rural area in China is inadequate access to clean water. By the end of 2010, the rural population with safe drinking water was 670 million, and only 54.7% of rural population had tap water (Ministry of Water Resources, PRC, 2011). Before 1962, residents mainly relied on shallow well water and surface water (Sun, 2004). Deeper wells were drilled after shallow well water was discovered to induce fluorosis and after surface water was shown to be polluted. Since chronic endemic arsenicosis was found in Taiwan in 1968 and reported in Xinjiang Province in Mainland China in the 1970s, more areas have been identified to be affected by arsenicosis via drinking water. Up to year 2012, endemic arsenicosis distributed over 45 counties in 9 provinces, while 19 provinces had the problem that arsenic concentration in drinking water exceeded water standard level (0.05 mg/L). In total, the recent official data from Ministry of Health PRC et al.

(2012) showed the population at risk reached to 1.85 million, less than 2.34 million which was reported by Xia and Liu (2004). Moreover, a systemic research was carried out on endemic arsenicosis affected and suspicious areas by China government during 2004 and 2010. There were 12,835 villages with a total population of around 1.25 billion under investigation. The result showed 844 villages with 697,000 people were exposed to high-arsenic drinking water (>0.05 mg/L) (Sun, 2011). Sun also gave the distribution of villages with high-arsenic drinking water (Table 2.2). Although in 2006, Ministry of Health PRC gave a revision of *Standards of drinking water quality* with permitted arsenic concentration as 0.01 mg/L instead of 0.05 mg/L as used in the past decades, it was considered as target rather than requirement (Ministry of Health of China and Standardization Administration of China, 2006). However, the new standards started to be subject to enforcement in July of 2012, which means more population would be taken into account if they have been exposed to drinking water with As concentration of 0.01 - 0.05 mg/L. Summary of documented cases of geogenic high-As groundwaters of China is shown in Table 2.3. Figure 2.3 shows documented areas with groundwaters containing high-As content above 0.05 mg/L. As shown in the Fig. 2.3, high-As groundwaters mainly appear in Zone I- i.e. in the north of China under arid or semi-arid climate.

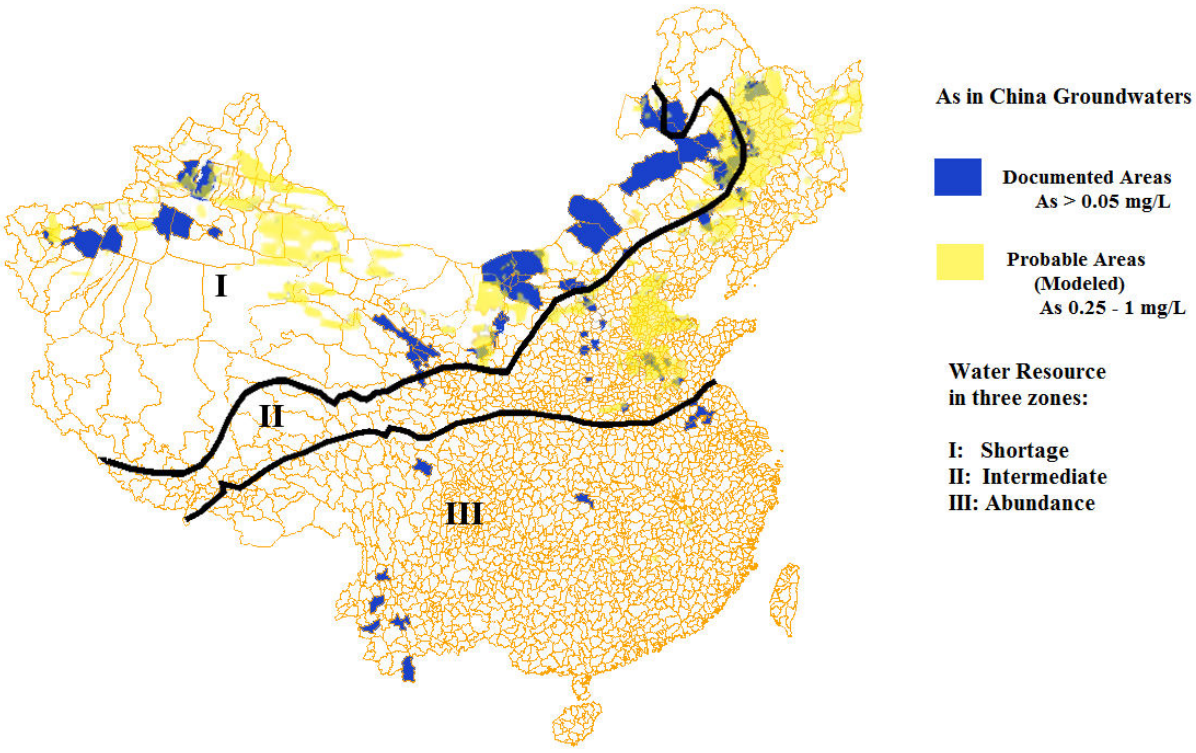

Figure 2.3: Water resource distribution in China and comparison of map of documented high-As groundwaters and modeled map of probability of geogenic high-As groundwater (See abbreviations in Table 2.2.) (from Shen et al., 2005; Yu et al., 2007; Amini et al. 2008 ; Courrier International, 2009; Zhang et al., 2010).

Table 2.2: The distribution of villages with high-arsenic drinking water in rural areas of China (from Sun, 2011, revised).

As content / Provinces (abbreviation)	0.05-0.1 mg/L		0.1-0.15 mg/L		0.15-0.5 mg/L		>0.5 mg/L	
	Village number	Population	Village number	Population	Village number	Population	Village number	Population
Xinjiang (XJ)	184	164,040	33	36,200	16	15,462	2	2114
Inner Mongolia (IM)	137	11,544	29	3165	36	2748	4	575
Bintuan, Xinjiang	61	62,723	7	4667	6	4741	2	12,125
Shanxi (SX)	48	73,994	22	22,139	4	8334	2	1675
Jilin (JL)	46	16,153	8	2604	17	5772	-	-
Shandong (SD)	26	30,642	5	7489	1	916	-	-
Anhui (AH)	24	32,390	9	16,952	18	32,686	4	7229
Henan (HA)	20	27,612	2	1893	4	5994	-	-
Shaanxi (SN)	10	12,826	1	1100	-	-	1	987
Yunnan (YN)	8	10,048	5	13,488	1	440	1	6201
Qinghai (QH)	6	4166	2	538	2	3470	6	1989
Gansu (GS)	6	4756	4	4501	1	146	2	3170
Hubei (HB)	4	5940	2	3202	1	983	1	1342
Jiangsu (JS)	1	1500	-	-	1	300	-	-
Heilongjiang (HL)	1	1713	-	-	-	-	-	-
Sichuan (SC)	-	-	-	-	-	-	-	-
Total	582	46,047	129	117,938	108	81,992	25	37,407

Table 2.3: Summary of documented cases of geogenic high-As groundwaters of China.

Province/Region	Concentration ranges (μg/L)	Aquifer type	Groundwater conditions	reference
Inner Mongolia (Including Hetao Plain and Hubao Plain)	Up to 1740	Holocen alluvial and lacustrine sediments	Strongly reducing conditions, neutral pH, high alkalinity.	Deng et al., 2008; Deng, 2009
Xinjiang (Tianshan Plain)	40-750	Holocene alluvial plain	Reducing, deep wells (up to 660m) are artesian	Wang and Huang, 1994
Shanxi (Datong Basin)	105-1932	Quaternary sedimentary basin	Reducing, high pH (8.09), high concentration of phosphate and organic matters	Guo et al., 2003; Guo and Wang, 2005
Jilin and Heilongjiang (Songnen Plain)	Up to 152.4	Quaternary sedimentary basin	Reducing, high pH(8.0-9.3), high concentration of organic matters	Zhang et al., 2010
Ningxia (Yinchuang Plain)	<10-177	Holocene alluvial and lacustrine sediments	Reducing and oxidizing , highest As level exists in reducing environment, pH (7.18-8.58)	Han et al., 2010
Kuitun, Xinjiang	Up to 880	Quaternary alluvial and lacustrine sediments	Reducing and oxidizing. Some tubewells water contain mainly As(V).	Wang et al., 2004; Luo et al., 2007
Qinghai (Guide Basin)	<112-318	Artesian aquifer, metamorphic rocks and volcanic	Geothermal water (18.5-34.6 °C), high pH (>8).	Shi et al., 2010

While high-arsenic content in drinking water is widespread problem, it occurs only under special natural circumstances relating to geochemical environment and hydrological features. At least, two conditions are necessary: i) Abundant source of arsenic and ii) Arsenic transportation from the source to water and accumulation. Not all the areas which locate near the arsenic-contained minerals or rocks have arsenic contaminated problem. It is quite usual that one village is discovered to be with high-As content in water from wells at the same time the neighboring village has extreme safe water. Below, we will discuss some examples which exist in different areas of China and the main characteristics of them.

2.4.2. Different types of geogenic high-As waters

2.4.2.1. Oasis-like reducing/oxidizing water

Xinjiang Province is a very arid region and it is the place where arsenicosis was first reported in Mainland China. Kuitun, one of the arsenicosis affected cities, has annual rainfall of 160 - 185 mm while annual evaporation of 1800 mm (Wang et al., 1985). The affected areas in Xinjiang involve Dzungaria Basin on the north side of Tianshan Mountains in the west to Mamas River in the east, a stretch of ca. 250 km (Wang and Huang, 1994). According to a recent report (Sun, 2011) and to the map given by Shen et al. (2005), the south side of Southern Tianshan Mountains and the south side of Altai Mountains were areas exposed to high-As drinking water. Wang (1984) found As concentrations up to 1.2 mg/L in groundwaters from this province. Most of arsenicosis areas in Xinjiang are low-lying lands with relatively low altitude. Although some researches believed in that the high-As groundwater was under reducing environment in Xinjiang, one research did analysis water samples which had As level above 0.6 mg/L and found only As(V) in these ground waters (Wang et al., 2004).

2.4.2.2. Geothermal waters.

Hot springs with elevated As concentration have been reported in several parts of China, including geothermal zones of Guide County of Qinghai Province, Rehai and Ruidian of Yunnan Province, Tibet and Taiwan.

Guide County of Qinghai is one of the areas which are suffering serious endemic diseases. Both fluosis and arsenicosis exist in Guide County, affecting around 590,000 population. Geothermal water (18.5 - 34.6 ℃) contains 0.32 - 4.57 mg/L fluoride and 0.112 - 0.318 mg/L arsenic. It's considered that the sources of arsenic are metamorphic as well as volcanic rocks in the north part of Guide Basin. The concentrations of arsenic were found to be positive associated with water depth and temperature of thermal water. The distributions of high-As and high-F groundwater had the same pattern as the abnormal geothermal regions (Shi et al., 2010).

Several water samples from hot springs in Rehe and Ruihai region of Yunnan were investigated. Almost all the hot springs water had pH value above 7.9 except one spring which had a pH of 3.5. The alkaline thermal waters contain arsenic ranging from 0.083 mg/L to 687 mg/L while the single acidic spring water had only 0.0436 mg/L of arsenic. Only inorganic arsenic had been found in those samples. The environment of those hot springs could be oxidizing and reducing as well. Four of eleven springs had As(V) as the dominant specie and other samples had considerable concentration of As(III) with the highest ratio up to 91% for As(III)/Total As (Liu et al., 2009).

2.4.2.3. Natural mineral waters

The arsenic contamination of mineral water in Hexigten Banner was first discovered in 1979, when more than 20 student campers who had done their intern exploration in the area ended

up getting sick because of toxic spring water they had drunk in mountain area. After they were diagnosed as acute arsenic poisoning cases, local disease control and prevention centers carried out sampling and analysis in surrounding areas. Arsenic concentrations up to 2.43 mg/L were found in mountain spring water and arsenic content in groundwater ranged from 19.8 to 82.2 μg/L. Most of arsenicosis-endemic villages were located within this mountain area in valleys. Arsenic was derived from large outcrops of FeAsS, Zn and Pb ores distributed throughout the mountains where large mine tailings were frequently found (Ministry of Health of Inner Mongolia, 2009; Zhang et al., 2010).

2.4.2.4. Reducing environments

Irrigated Hetao Plain and Hubao Plain in Inner Mongolia

The Hetao Plain with an area of 13,000 km^2 is located in the western region of Inner Mongolia, bounded by the Yin Mountain in the north, by the Yellow River in the south, by Ulan Buh (Wulanbuhe) desert in the west, and by Ulansuhai Nur Lake (Wuliangsuhai) in the east. In the late Jurassic, a fault basin located in the northwest of the Hetao plain was formed. Lacustrine sediments with highly reducing conditions were formed in the closed basin. This region has groundwaters with high dissolved concentrations of arsenic (Yang et al., 2008). Concentrations up to 1.74 mg/L have been found in the groundwater in Hangjinhouqi, a county locating in the west part of Hetao Plain (Deng, 2008). Deng et al. (2009) reported results on arsenic concentrations and speciation in water samples collected in Hangjinhouqi, with an arsenic concentration ranging from 0.076 mg/L to 1.09 mg/L and speciation dominated by As(III): the As(III) to the total soluble As ratio ranging from 84% to 99%.

Hubao Plain lays in the east side of Hetao Plain and has similar geological structure. 74 groundwater samples were collected from chronic endemic arsenic poisoning areas around

Hubao Plain in 1998 and 1999 respectively for water quality analysis. The results showed that high arsenic samples (>0.05 mg/L, As(III)/Total As = 82%) had low average levels of dissolved oxygen (0.0 mg/L) and low Eh value (39 mV) (Zhang et al., 2002). Lin and Tang (1999) also reported As-rich groundwater samples (As content: 0.42 mg/L), with 100% As(III) to total As ratio.

Datong Basin-Shanxi

Arsenicosis was revealed in early 1990s in Shanxi Province after local residents started to use water from deep wells (20 - 50m). The geochemical features of Datong Basin are close to those found in Hetao Plain. The analysis of 66 groundwater samples collected from Shanyin area of Shanxi Province showed that 23 of them had high-As content (0.105 - 1.932 mg/L) and they have relative high As(III) to total As ratio ranging from 50% to 80.4% (Guo et al., 2003). Xie et al. (2011) identified the sources of arsenic in the shallow aquifers of Datong Basin through a thorough mineralogical, geochemical and zircon U–Pb dating study. Instead of pyrite which had arsenic content <1 mg/kg, Fe oxides (with up to 2000 mg/kg of arsenic) were shown to be the major mineral phases of arsenic enrichment in Datong bedrocks. The sedimentary rocks including coals were the most probable sources of arsenic in aquifer sediments according to zircon ages and geochemical data. The same group (Xie et al., 2008) reported that the aqueous arsenic levels were strongly depth-dependent in the Datong Basin and that the high arsenic concentrations were found at depths between 15 m and 60 m, with a maximum concentration equal to 1.82 mg/L. The hydrochemical characteristics of high arsenic groundwater from the study area indicated that the mobilization of arsenic was related to reductive dissolution of Fe oxides/oxyhydroxides and/or desorption from the Fe oxides/oxyhydroxides at high pH (above 8.0).

2.4.3. Prediction of geogenic potential As-affected groundwater

Statistical models based on the statistical relationship between As concentrations and relevant explanatory variables such as geology, climate, topography or soil organic matter content have recently been developed (Amini et al., 2008; Rodríguez-Lado et al., 2008; Winkel et al., 2008). Some researchers started to use logistic regression to assess the probability that As concentrations exceed a pre-defined threshold (Lee et al., 2009; Twarakavi and Kaluarachchi, 2006; Winkel et al., 2011). Amini et al. (2008) used a large databank of groundwater arsenic concentration from around the world as well as digital maps of physical characteristics such as soil, geology, climate, and elevation to model probability maps of global arsenic contamination. The relative significance of the variables in the arsenic model showed: The occurrence of arsenic under reducing aqueous conditions was most closely correlated to climatic, geological, and drainage parameters while under high-pH/oxidizing aqueous conditions it was most closely correlated to soil parameters (clay and silt), and drainage condition. Maps of modeled global probability of geogenic arsenic contamination in groundwater for reducing and high-pH/oxidizing conditions were delineated respectively. Nearly all the areas with high probability of arsenic occurrence in China groundwater were found in oxidizing conditions. The China part of their maps is compared with published and documented As-affected area in Figure 2.3. Modeled map agreed well with the already established high As contaminated areas. However, documented high As regions such as Hetao Plain and Datong Basin were actually found to be under reducing conditions rather than predicted oxidizing conditions. Despite the moderate accuracy on the groundwater types, the map could still be used as a reference to investigate unknown areas, in order to prevent mass intoxication via groundwater with elevated As concentration.

Targeting the Shanxi Province, Zhang et al. (2012) applied stepwise logistic regression to analyze the statistical relationships of a dataset of As concentrations in groundwaters with some environmental explanatory parameters, where most of As investigations in this province focused on the Datong and Taiyuan Basins. They identified some environmental parameters are closely related to the distribution of high As concentrations, namely i) Holocene sediments; ii) Topographic Wetness Index; iii) hydrological characteristics; iv) Gravity and (v) Remote sensing information.

2.5. High-As content in China waters - anthropogenic cases

Table 2.4 gives a list of incidents of drinking waters polluted by industry in China in the last decade and three case studies were discussed below.

Table 2.4: Cases of drinking water source polluted by human activities in China.

Province/Region	Polluted water type	Time	Contamination source	As level in polluted water (mg/L)	Notes	Reference
Dushan, Guizhou	Duliu River	2007	Sulfuric acid plant	Up to 14.2	65 poisoned	Chen et al., 2010
Chenxi, Hunan	Ground Water	2008	Sulfuric acid plant	Up to 19.5	17 poisoned	Chen et al., 2010
Hechi, Guangxi	Ground Water	2008	Smelter		15 poisoned	Chen et al., 2010
Yunan	Yangzonghai Lake, freshwater lake	2008	Chemical plants	> 0.1	26,000 threatened	Liu, 2009; EPA, Yunnan, 2008-2010; Wang et al., 2010
Henan	Dasha River,	2008	Sulfuric acid	Up to 2.56	Plant	Peoples Court of

	Minsheng River		plant		discharge with As level up to 445mg/L	Minquan County, 2010
Xichang, Sichuan	Well water	2006	Copper Smelter	-	17 poisoned	Chen et al., 2010
Yingde, Guangdong	Water channel	2005	Mining industry	-	34 poisoned	Chen et al., 2010
Jiangsu and Shangdong	Picang flood-diversion channel	2009	Chemical plants	Up to 1.987	500,000 threatened	Ling et al., 2009

Mining and smelting activities

Arsenic is present in sulfide minerals associated with Au, Cu, Pb, Zn, Sn, Ni, and Co mineral ores and can be released in the water during the slow oxidation of As- rich pyrite waste tailings, or in the air during the smelting process. Up to 70% of total arsenic is abandoned as tailing by mine selections process.. Only 10% of total arsenic is recovered while the remaining part is kept in intermediate material or found in solid waste residue and wastewaters (Wei and Zhou, 1992).

Acute poisoning has often occurred in China because of mine tailings. For example, in 1961, 308 people were poisoned and 6 were killed in Xinhua, Hunan Province. Arsenic-containing (5% - 13%) tailings from antimony mine were disposed close to drinking water tube well and contaminated the water (Yang, 1992). More recently, i.e. in the latest decade, this type of disaster happened quite often as a result of booming mining and smelting activities. In Hechi, Guangxi Province, arsenic acute poisoning happened at least 3 times between 2001 and 2008, with an increasing number of smelters being built in this region, famous as a non-ferrous

metal-rich-area. The contamination was usually triggered by heavy rains or floods which flushed the waste water from smelter treatment tanks directly into surface waters. On the other hands, too many plants have been running without or under poor supervision from government. The lack of waste treatment system led to several problems as well.

Pesticide use

Inorganic arsenicals, such as lead, calcium, magnesium and zinc arsenate, zinc/sodium arsenite, Paris green (acetoarsenite) or organic arsenicals have been used extensively as agricultural chemicals. Those chemicals are used as herbicides, desiccants, antiseptics, toxic rat poisons, oncomelania hupensis poisons and so on. Because of their highly toxicity, many pesticides including arsenical products have been banned by China government. Although arsenical pesticides mainly draw some concerns related to soil pollution, it could also affect the quality of drinking water directly. It was reported that well water had been contaminated by pesticide and the concentration of As was around 1.15 mg/L in Yangshan, Anhui Province (Li et al., 2006).

Zhang and Xiao (1993) revealed that arsenic concentration measured in tube well waters was positively related to rainfall. The tube well was believed that have been contaminated by pesticide waste disposed around the well. Tube well water samples contained 0.008 - 0.044 mg/L arsenic in dry seasons and 0.03 - 2.00 mg/L of arsenic in rainy seasons. Arsenic concentration in soils and vegetables were studied as well. Soils contain 2.5 - 49.5 mg/kg at 40 cm depth and 7 - 97.5 mg/kg at 80 cm depth. The highest level of arsenic (5 mg/kg) was found in roots of vegetables.

Chemical Industries

Sulfuric acid is produced by oxidation of sulfur rich ores. The use of As-bearing sulfide minerals as raw material in sulfuric acid manufactures is all-pervading in China chemical industries. Illegal use of low-class mineral ores that contain large amounts of arsenic, lack of safe waste treatment system and illegal discharge of waste waters into surface water made pollution incidents inevitable to happen. In the single year 2008, Heishui River of Guizhou, Groundwater of Chenxi, Hunan and Yangzonghai Lake of Yunnan were all polluted by sulfuric acid production plants. The Yangzonghai Lake is an exemplary case. Its waters had arsenic concentration less than 0.006 mg/L prior to September 2007. A contamination was noticed in April 2008 and resulted in arsenic concentration of lake water above 0.1 mg/L, according to analysis results of samples collected in July, September and October 2008 (Liu, 2009; EPA, Yunnan, 2008-2010; Wang et al., 2010).

2.6. Conclusions and recommendations

This review has attempted to list the current available information on the occurrence and distribution of As contamination in China drinking water. The current facts related to drinking water contamination by arsenic in China appear alarming: i) the problem is widespread throughout China; ii) a large population has been exposed to drinking water with high level of geogenic As; iii) an increasing number of sudden and accidental As pollution events is taking place due to human activities.

Geogenic high As water are mostly found in arid or semi arid North of China. It results from: i) use of groundwater as water supply is more common in the north, where As-rich groundwaters are more likely to be discovered, than in the south, and ii) climate, geochemical and hydrological conditions are favorable for formation of high-As water. Although natural

arsenic resource is abundant and high-As in drinking water is widespread in China, the problem only occurs when certain geochemical and hydrological conditions are met. There are some common features among those cases. High-As spring or groundwater are found in closed basins where As is hard to be flushed away or be diluted. Affected areas are usually low-lying zones with high pH value (≈8.5), which is favorable for As being released and exchanged from minerals or rocks (Charlet and Polya, 2006). Reducing type As-rich groundwater bodies are mainly found in the north of China, under arid or semi-arid climate.

In contrast, in south of China, arsenic existence in drinking water is mainly due to human activities. Large amount of As ore reserves and As-containing mineral mines are located in the south where extensive mining activities and chemical industries increase the likelihood of As pollution accidents. Surface water in the south are contaminated by industrial discharge or runoff containing high As content from industries, triggered by heavy rains and floods in those subtropical or tropical zones.

Almost all arsenic-contamination cases were discovered thanks to poisoning accidents. It can be foreseen that under the current situation of water scarcity people will exploit more and more natural water for drinking or other uses. In order to ensure water safety as well as to prevent further environmental disasters, the government needs to conduct effective water quality monitoring and management. For those areas which have been identified as As-affected, continuous water quality test should be carried out on-site. Arsenic level as well as arsenic speciation should be examined.

Previous investigations of a number of affected sites in China have given people a better understanding of the As-contamination problem. However, research focused mainly on heavily contaminated water bodies with water As concentrations above 0.05 mg/L, and areas

of groundwater with lower concentrations (0.01 - 0.05 mg/L) of arsenic will call out for government and researchers attention in the near future. Low concentration of arsenic could be dangerous if there's a high ratio of As(III) to total As. Knowledge on the speciation of arsenic is gaining increasing importance because toxicological effects of arsenic are connected to its chemical form and oxidation states. To have a better view of the danger of As-containing water and to give more comprehensive information to the exposed public, the analyses should not be restricted on the determination of total As. Arsenic speciation is also important and necessary to be measured.

Besides, more researches should focus on understanding the occurrence, origin and distribution of arsenic. Government should pay more attention to industrial and agricultural activities which lead to As pollution. More technical supports should be given to mining or chemical plants to deal with sewage and sludge storage and waste treatment. Supervision departments should increase the frequency of sampling and analyzing of the discharge from industrial plants.

Chapter 3

Novel Chitosan Goethite Bionanocomposites Bead for Arsenic Remediation

Jing He, Fabrizio Bardelli, Antoine Gehin, and Laurent Charlet

Under submission to Environmental Science & Technology

3.1. Introduction

One of the most pervasive problems afflicting people throughout the world - water scarcity - has increased people's dependence on groundwater resources in many parts of the world. During the past two decades, arsenic poisoning via groundwater has become a worldwide issue (Nordstrom, 2002). Some of the best-documented and most severe cases of arsenic contaminated aquifers have been found in Asia (e.g. parts of Bangladesh, China, India, Nepal) and South America (e.g. Argentina, Mexico) (Aureli, 2006; He and Charlet, 2013; Ravenscroft et al., 2009). Among common possible oxidation states (-3, 0, +3 and +5) inorganic arsenate (As(V)) and arsenite (As(III)) pose the greatest threat to human health, since they are the main species occurring in natural waters and are the most toxic forms. In particular, arsenite is more toxic than arsenate, due to a higher mobility in the environment and possible passive cell uptake via aquaporins. To address this public health threatening problem, numerous methods have been developed focusing on As-rich water decontamination (Charlet and Polya, 2006; Mohan and Pittman, 2007).

Iron hydroxides have a high sorption affinity toward both As(V) and As(III) over a wide range of pH values (Dixit and Hering, 2003). They are important constituents of soils and sediments therefore they play an important role in regulating arsenic concentrations in natural waters. Consequently, many water treatment industries use iron oxides/hydroxides adsorbents. However, most reactive iron oxides/hydroxides are fine powders, and are difficult to separate from solution after completion of the adsorption process. To overcome this limitation, plenty of research has studied polymer - iron oxide/hydroxide hybrid compounds (Rorrer et al., 1993; Wang et al., 2009; Zou et al., 2012). The hybrid materials have macroscopically larger sizes so that it is less difficult to separate them by filtration procedures in water treatment

manipulation. Also, polymeric coating may stabilize the iron oxide/hydroxide by increasing repulsive forces to balance the magnetic and van der Waals attractive forces acting on the nanoparticles (Wu et al., 2008). Chitosan, being a low-cost, biodegradable and non toxic biopolymer, has been used as one of possible coating polymers for fabricating iron oxide/hydroxide-polymer composites (Ngah et al., 2011). Besides the contribution of iron oxide/hydroxide, chitosan can function as arsenic adsorbent independently. The intrinsic pK of chitosan amine groups are close to 6.5, favoring their protonation and resulting in an enhanced affinity to arsenic anions in acidic solutions (Chassary et al., 2004). However, since the low "porosity" of chitosan polymer contributing to low ion diffusivities constrains the diffusion process of arsenic anions, most studies have made use of chitosan synthesized from the gel bead method, which allows an expansion of the polymer network, enhancing anion diffusion and improving access to the internal sorption sites (Guibal et al., 1998; Jin and Bai, 2002). To fabricate composite beads, some investigations treated chitosan beads with $FeCl_3 \cdot 6H_2O$ solutions or hydrated ferric oxides suspensions, or conversely started with dispersing iron oxides into chitosan solution, followed by the bead formation step (Dias et al., 2011; Guo and Chen, 2005; Qiu et al., 2012; Rorrer et al., 1993). Chemical cross-linking of chitosan with glutaraldehyde is usually employed to enhance the mechanical properties of the polymer beads by exploiting a Shiff's reaction between aldehyde and the amine groups (Nedelko et al., 2006).

In this study, we employed a novel method to synthesize a chitosan-iron hydroxide composite, namely chitosan goethite bionanocomposites (CGB) beads, making no use of toxic glutaraldehyde. Goethite nanoparticles and chitosan gel-beads were prepared simultaneously, leading to a homogenous distribution of goethite nanoparticles in the chitosan network.

Goethite and chitosan develop cross-links providing enhanced mechanical property in term of compressive strength, without need of further treatments by toxic chemical compounds. CGB beads were characterized by Mössbauer Spectroscopy and Field Emission Scanning Electron Microscopy (FE-SEM). Batch sorption and kinetic experiments were performed to assess the sorption of As(III) and As(V) onto CGB. The mechanism of As(III) and As(V) uptake onto CGB was investigated by Synchrotron Radiation X-ray Absorption Spectroscopy (SR-XAS). The diffusion of As(III) and As(V) from solution into the porous solid phase was monitored by micro X-ray fluorescence (μXRF) and micro X-ray Near Edge Spectroscopy (μXANES).

3.2. Experimental Section

3.2.1. Chemicals.

All solutions were prepared with Milli-Q water (resistivity: 18.2 Ω cm). High molecular weight chitosan (average MW: 342500 $g \cdot mol^{-1}$), sodium meta-arsenite ($NaAsO_2$, 99%), sodium arsenate ($Na_2HAsO_4 \cdot 7H_2O$, 98.5%), iron(III)-chloride hexahydrate ($FeCl_3 \cdot 6H_2O$), sodium hydroxide (NaOH, 98%) and hydrochloric acid (HCl, 37%) were purchased from Sigma-Aldrich. Acetic acid (100%) was from Merck.

3.2.2. Synthesis of CGB.

Chitosan acetic acid solution, was prepared by adding 30 g of high molecular weight chitosan into 1L of acetic acid (1%, v/v). The solution was constantly stirred at 50 °C until chitosan powder was completely dissolved and then cooled down to room temperature. Ferric solution was prepared by dissolving 25.2 g of $FeCl_3 \cdot 6H_2O$ into 200 mL of acetic acid (1%, v/v). A ferric acetic acid mixture (200 ml) ($c[FeCl_3] = 0.466$ mol L^{-1}, 1% (v/v) of acetic acid) was gently poured into the chitosan solution, and the mixture was stirred until it became

homogenous. The resulting solution was pumped through a fixed pipette tip (1 ml) drop by drop into a chitosan casting bath containing 0.5 mol/L NaOH (Figure 3.1). The gel ferric chitosan beads were kept for 24 h in the NaOH bath and then washed with Milli-Q water until the residual water reached a neutral pH. Finally beads were separated from solution and air dried at 25 °C.

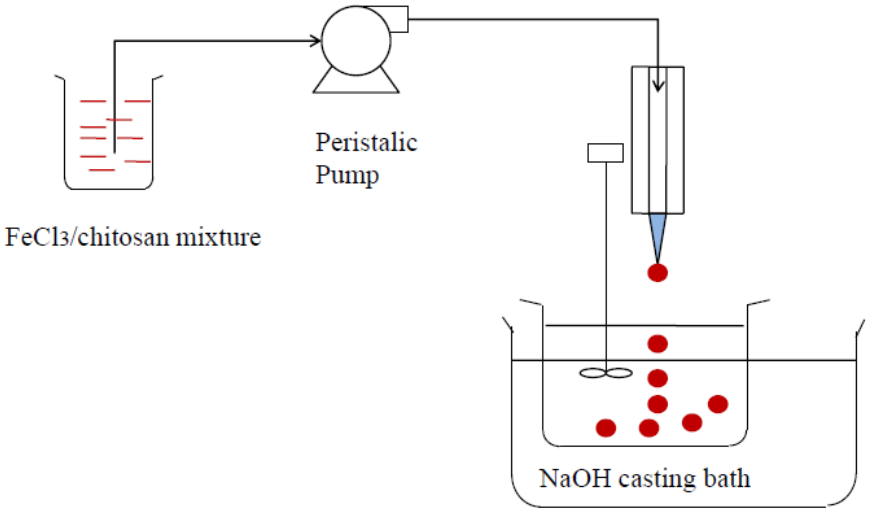

Figure 3.1: Apparatus for casting CGB beads.

3.2.3. Characterization.

The CGB beads size distribution was measured by a Mastersizer - 2000 (Malvern) and the pore volume was tested by mercury intrusion using PoreMaster® Series Porosimeters - Automatic Pore Size Analyzers. CGB mechanical properties were investigated with an 'Adamel Lhomargy' with a 500 N load cell. During the test procedure one CGB sample was placed between the specimen stage and upper punch and loaded at a constant rate of 1 µm/s until failure (Fig. 3.2). The force (crushing strength, FC) and the CGB deformation (DdC) were recorded until failure happened.

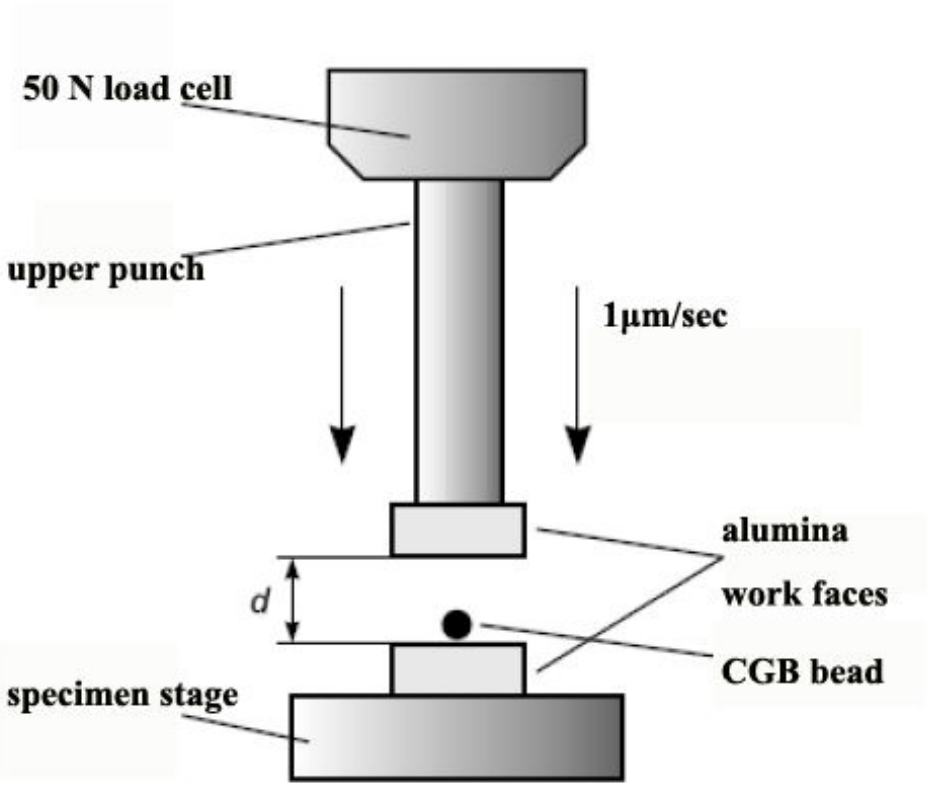

Figure 3.2: Experimental scheme of mechanical property test.

CGB iron (nano)particles were investigated (i) by zero-field ^{57}Fe Mössbauer measurements at room temperature (RT, 300 K) and liquid nitrogen temperature (LNT, 77 K) using a bath cryostat in transmission mode with a constant acceleration driving unit using a ^{57}Co/Rh γ–ray source. The spectrometer was calibrated using a standard Fe foil and the isomer shift values were expressed with respect to this standard at 300 K. The fitting of the spectra was performed using the MOSFIT program (MOSFIT: Teillet and Varret, unpublished program). This fitting model used a discrete number of independent quadrupolar doublets of Lorentzian lines where the full width at half maximum Γ (mm.s^{-1}), the isomer shift δ (mm.s^{-1}) and the quadrupole splitting ΔE_Q (mm.s^{-1}) were refined using a least-squares fitting procedure. The

relative uncertainty of the hyperfine parameters was assumed to be near 5 %. The proportions of the different Fe species were estimated from the relative respective absorption area, assuming thus the same values of *f* Lamb Mössbauer recoilless factors; and (ii) by Field Emission Scanning Electron Microscopy (Nova^{TM} NanoSEM 230) using an accelerating beam at a voltage of 5 kV (magnification: 80000×).

CGB solid samples (10.9 mg) were digested by 4 ml of HNO_3 and HCl (1:3) (aqua regia) in teflon digestion tube at 70 ºC for 500 min in Mid Temperature Graphite Digestion Blocks, DigiPREP Block Digestion Systems (SCP SCIENCE, Canada). After digestion, the residue was diluted to 30 ml by Milli-Q water. The resulting solution was filtered through a 0.45 μm microporous membrane into a plastic bottle ready for ICP-OES analysis.

3.2.4. Batch Sorption Isotherm

CGB beads were added to (i) two arsenate solutions (prepared with Na_2HAsO_4) at pH 5 and pH 9 with initial As concentrations ranging from 0.069 to 0.84 mmol/L, and (ii) arsenite solutions ($NaAsO_2$) at pH 5 and pH 9 with initial As concentrations ranging from 0.093 to 1.2 mmol/L (2.5 g/L, CGB adsorbent to arsenic adsorbate ratio). The adsorption studies were performed at 298 K under a constant 200 rpm shaking for 120 h. Supernatants were collected by pipette prior to analysis. Three equilibrium isotherms, namely Langmuir, Freundlich, and Redlich-Peterson, were used to model the experimental data.

The theoretical Langmuir isotherm is often used to describe adsorption of a solute from a liquid solution onto a single type of surface site as (Ho et al., 2002; Langmuir, 1918)

$$q_e = \frac{q_m K_a C_e}{1 + K_a C_e} \quad ; \tag{3.1}$$

where q_e is the equilibrium adsorption capacity (mmol/g), C_e is the equilibrium liquid phase concentration (mmol/L), q_m is the maximum adsorption capacity (mmol/g), K_a is adsorption equilibrium constant (L/mmol). The Freundlich isotherm (Freundlich, 1906) is an empirical isotherm that can be used to model the adsorption from dilute solutions and can be thought of as the result of a log-normal distribution of Langmuir parameters, K_a (Sposito, 1984). The ordinary adsorption isotherm is expressed by the "Freundlich" equation:

$$q_e = K_F C_e^{1/n} \quad ; \tag{3.2}$$

where C_e is the equilibrium concentration in the solution, (mmol/L), q_e is the equilibrium adsorption capacity, (mmol/g), K_F and $1/n$ are empirical constants. K_F is the adsorption value, the amount adsorbed at unit concentration (1 mmol/L). It is a characteristic of both the adsorbent and the adsobate. The Redlich-Peterson isotherm contains three parameters and incorporates the features of both the Langmuir and the Freundlich isotherms (Redlich and Peterson, 1959). It is parameterized as follows:

$$q_e = \frac{AC_e}{1 + BC_e^g}; \tag{3.3}$$

It has three isotherm constants, namely A, B, and g with ($0 < g < 1$).

Due to the inherent bias resulting from linearization, alternative isotherm parameter sets were determined by non-linear regression. This provides a mathematically rigorous method for determining the isotherm parameters using the original form of the isotherm equation (Ho, 2004; Seidel and Gelbin, 1988). To compare the three isotherms, a trial-and-error procedure was applied to obtain the isotherm parameters. We used an optimization routine to maximize

the coefficient of determination r^2 between the experimental data and isotherms (Ho, 2006; Ho and Ofomaja, 2005).

The coefficient of determination r^2 is defined by:

$$r^2 = \frac{\sum\left(q_m - \overline{q_e}\right)^2}{\sum\left(q_m - \overline{q_e}\right)^2 + \sum\left(q_m - q_e\right)^2}; \quad (3.4)$$

where q_m is the equilibrium capacity obtained from the isotherm model, q_e is the equilibrium capacity obtained from experiment, and $\overline{q_e}$ is the average of q_e.

3.2.5. Kinetic Experiment.

For each experiment, 0.2 g of CGB beads were added into 0.1 L arsenate solution (Na_2HAsO_4, 0.066 mmol/L, pH=7) for 0 to 3000 min or into 0.1 L arsenite solution ($NaAsO_2$, 0.082 mmol/L, pH=7) for 0 to 10080 min, both at 298 K. At fixed time intervals, 2 ml of solution was collected using a syringe attached with a 0.2 μm pore size filter. Kinetics data from our experiments were fitted with a pseudo-second-order kinetic model to estimate the rate constants, initial sorption rates, and arsenic sorption capacities on CGB (Ho and McKay, 1999; Ho and McKay, 2000).

All the supernatant samples were analyzed by Inductively Coupled Plasma Optical Emission Spectrometers (ICP-OES) (Varian 720-ES, Varian, Inc.) to determine the arsenic and iron concentrations and evaluate the release of iron during the sorption process, respectively (detection limit: As: 1 μg/L; Fe: 0.1 μg/L). Further filtration by 0.45 μm microporous membrane or centrifugation did not induce changes in the total aqueous concentrations

Second-order kinetics

The sorption was represented by the equation:

$$\frac{dq_t}{dt} = k(q_e - q_t)^2; \tag{3.5}$$

where k is the pseudo-second-order rate constant. For boundary conditions $t = 0$ to $t = t$, and $q_t = q_t$, where q_e and q_t are the sorption capacity at equilibrium and at time t, respectively (mmol/g). The integrated form of the equation is:

$$\frac{1}{q_e - q_t} = \frac{1}{q_e} + kt; \tag{3.6}$$

which can also be written as:

$$q_t = \frac{t}{(1/kq_e^2) + (t/q_e)}; \tag{3.7}$$

or in the linear form:

$$\frac{t}{q_t} = \frac{1}{h} + \frac{1}{q_e}t; \tag{3.8}$$

where $h=kq_e^2$ can be regarded as the initial sorption rate as t approaches 0.

3.2.6. Effect of CGB dose on residue arsenic level

Different doses of CGB beads (0.5 g – 5.5g CGB/ 1L arsenic solution) were added to arsenate and arsenite solutions at pH 7 with two initial As concentrations 5 mg/L and 1 mg/L (0.067 mmol/L, 0.013 mmol/L), respectively. The adsorption processes were performed at 298 K under a constant 200 rpm shaking for 120 h. Supernatants were collected by pipette prior to analysis.

3.2.7. Leaching Test

Arsenic and iron concentration of all the aqueous samples (initial and final solutions) from the isotherm and kinetic study were measured by ICP-OES. All the calibration and sample solutions were prepared with 2% HNO_3. After the adsorption, no iron could be detected in the samples. The result shows that no iron/goethite was released into the solution during the adsorption.

3.2.8. Bulk XAS

Arsenic-loaded CGB samples for XAS measurements were prepared by introducing 1g CGB beads into 40 ml arsenic solution (7 mmol/L arsenate or 5.6 mmol/L arsenite solution at pH = 5 and pH = 9). After 72h of sorption process at 298K in an anaerobic glove box, the beads were separated from the solutions. The supernants of all solution were measured by ICP-OES to evaluate the adsorbed quantities of As onto CGB. The adsorbed quantities of the arsenate-adsorbed beads were 0.113 mmol/g, at pH=5 and 0.052 mmol/g, at pH=9, and that of the arsenite-adsorbed beads were 0.151 mmol/g, at pH=5 and 0.156 mmol/g, at pH=9. The As-loaded samples were dried and ground in the glove box, and were kept in liquid nitrogen until the measurements at the synchrotron facility. XAS measurements at the As K-edge (11.867 keV) were performed at the European Radiation Synchrotron Facility (ESRF, Grenoble, France) using the bending magnet French absorption spectroscopy beamline (FAME-BM30B) (Proux et al., 2005; Proux et al., 2006). An As(III) reference (As_2O_3) was placed behind the samples and measured along each energy scan for accurate energy calibration.

The XAS spectra were recorded in fluorescence mode using a high-throughput 30-elements solid state germanium detector (Canberra, St Quentin Yvelines, France). The spectra of the As reference compounds were acquired in transmission mode using two ionization chambers to measure the incoming and transmitted photons. The storage ring was operated with a ~200 mA current. Two Rh-coated mirrors for efficient harmonics rejection, collimation, and vertical focusing of the beam are located up and down stream the monochromator with respect to the beam direction. The beam energy was selected using a Si (220) double-crystal monochromator. A sagittal focusing system provided a beam intensity of 10^{10} photons·s^{-1} at 12 keV, and a beam size on the sample of approximately 300 × 200 μm (H × V). At the working energy and conditions, the resolution, which was equal to the energy sampling, was of ~0.5 eV. XANES spectra were background subtracted, normalized, and then the absorption edge energy of each 'internal' As(III) reference spectrum was shifted to match the As_2O_3 absorption edge.

Structural parameters were obtained from shell fitting following standard procedures for data reduction and analysis (Lee et al., 1981). The FitEXA code (Meneghini et al., 2012; Monesi et al., 2005) was used for least square minimization. Fits were performed in the wave vector space up to k = 12 $Å^{-1}$, without Fourier filtering. Atomic clusters of the reference compound structures centered on the absorber atoms were calculated using the ATOMS code (Ravel, 2001), and were used as starting points for refinements. The FEFF8 code (Ankudinov et al., 1998) was used to calculate EXAFS theoretical amplitude and phase photoelectron scattering functions. Uncertainties on refined parameters were calculated using the MINOS subroutine from the MINUIT package (James and Roos, 1975), which takes into account the correlation between free parameters.

3.2.9. µXANES and µXRF

As-loaded CGB samples collected from kinetics experiments at 1.5h and 72h were cut into 40 µm thick cross-sections using a cryo-microtome (Shandon Cryotome^{TM} SME Cryostat, Thermo Scientific). µXRF analyses were performed at the DiffAbs beamline at the Soleil synchrotron radiation facility (France). An excitation energy of 12.0 keV was selected using a Si (311) double crystal monochromator, and a beam spot size of 10×10 µm^2 was achieved using a Kirkpatrick-Baez mirror system. The X-ray fluorescence spectra were recorded with a Si (Li) detector. The µXRF maps were processed with PyMCA 4.4.6 software (Sole et al., 2007). Based on the distribution of As and Fe, points of interest were selected for µXANES analysis at the As K-edge in the 11.8-12.0 keV range with 3s integration time per energy point. $NaAsO_2$ and $Na_2HAsO_4 \cdot 7H_2O$ (Alfa Aesar) were also measured and used as As(III) and As(V) references. Background subtraction and normalization of the XAS spectra were performed using the IFEFFIT package (Ravel and Newville, 2005).

3.3. Results and Discussion

3.3.1. Physicochemical Characteristics of CGB.

The dark red chitosan goethite bionanocomposites beads (Fig. 3.3) have an average diameter of 1018 ± 241 µm and a density of 1.447 g/cm^3. The total pore volume is 0.024 cm^3/g according to Mercury porosimetry test and thus a porosity ϕ of 3.5 %.

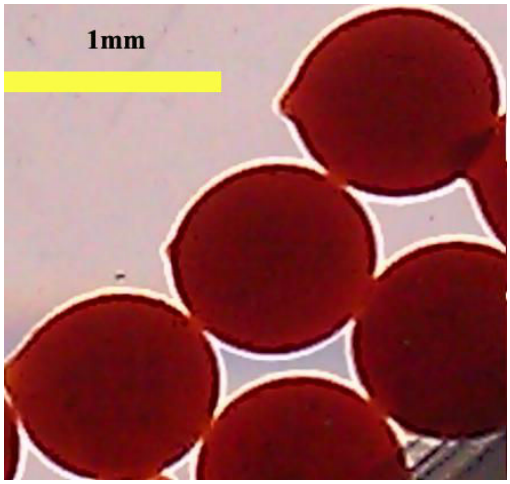

Figure 3.3: Picture of CGB.

CGB were characterized by combining two techniques FE-SEM and Mössbauer spectroscopy. The results indicate the presence of goethite nanoparticles in chitosan matrix. CGB consists of 20.33 wt.% of goethite particle and 79.67 wt.% of chitosan according to result of ICP-OES measurement of digested CGB by strong acids. To elucidate the size and morphology of the mineral/chitosan phases, we used FE-SEM (Fig. 3.4). The image shows that the CGBs are composed of goethite lath-like particles (average size: ~200-300 nm in length, ~50 nm in width, and ~10 nm in thickness) surrounded by chitosan network. Compression mechanical property test reports an average value for the crushing strength and deformation of CGB of 34.9 ± 6.5 N and 12.6 ± 4.6 %, respectively. The maximum endurable force is significantly higher than the breaking down forces of the chitosan hydrogel beads (1.87 N) and that of the chitosan hydrogel beads impregnated with carbon nanotubes (7.62 N) reported by (Chatterjee et al., 2009). The result proves that by impregnating 20.33 wt.% goethite into the chitosan matrix, the mechanical property of the gel bead was greatly improved. Therefore, CGB

material can be easily transported and used for water purification by water treatment plant or household set-up.

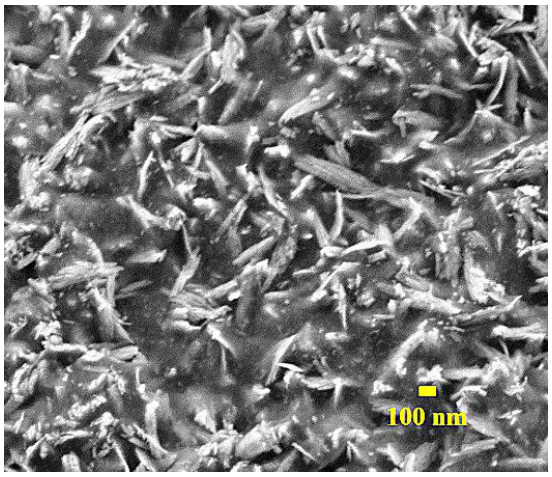

Figure 3.4: FE-SEM photomicrograph of CGB at 80,000 X.

CGB Mössbauer spectra performed at RT and LNT are shown in Fig. 3.5a and Fig. 3.5b. The result of the fitting and the relative areas (RA) are summarized in Table 3.1. Both RT and LNT spectra display hyperfine magnetic and paramagnetic components characteristic of trivalent iron. There is a distribution of hyperfine magnetic field, $S_{distribution}$, at RT whereas only one sextet (S) is present at LNT. Paramagnetic components (D_{77} and D_{300}) are also present. The magnetic and paramagnetic components have the same RA (within one percent) whatever the temperature, indicating two different iron environments: #1 and #2. For iron #1, fitting line shapes of the magnetic components, $S_{distribution}$ and S, differ at RT and LNT. Hyperfine magnetic fields (290kOe at RT, and 495kOe at LTN, Table 3.1) are those of a stoichiometrically composed and well crystallized α-FeOOH goethite. The presence of sextets is due to Fe antiferromagnetic order in goethite (T_{Neel} = 400K, for goethite bulk). This component could correspond to the goethite lath particles observed by FE-SEM. For iron #2, the paramagnetic doublets (D_{300} and D_{77}) are characteristic of trivalent iron. That doublets RA

does not change with the temperature indicates these doublets are characteristic of the same iron environment, i.e. the same kind of particles. The doublets width tends to be larger at lower temperature (0.58 $mm.s^{-1}$ at RT and 0.90 $mm.s^{-1}$ at LNT, Table 3.1), which may indicate the beginning of the paramagnetic state to the ordered state magnetic transformation. This behavior is typically characteristic of nano-particles, whose size and shape influence the temperature of ordered magnetic state. Nano-ferrihydrite and nano-goethite both give rise to a paramagnetic doublet with very close hyperfine parameters, preventing determining their relative amount from Mössbauer measurements.

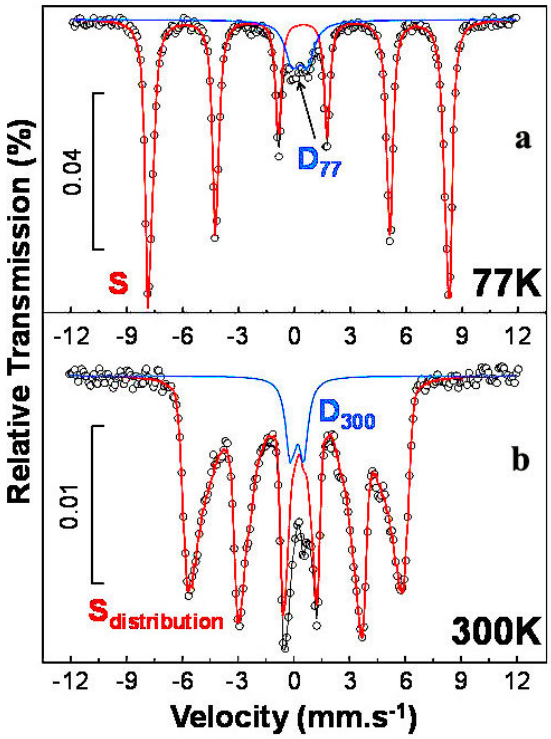

Figure 3.5: (a) 57Fe Mössbauer spectra of CGB at liquid nitrogen temperature (LNT = 77K); (b) room temperature (RT = 300K). Experimental values are shown as marked grey points; solid lines are fitted spectra components: $S_{distribution}$ and S is respectively for a sextet distribution and one single sextet. D_{77} and D_{300} are paramagnetic doublets. The corresponding hyperfine parameters are given in Table 3.1.

Table 3.1: Mössbauer spectroscopy hyperfine parameters of CGB spectra at LNT (77 K) and at room temperature (RT = 300K), displayed in Fig 3.5a and 3.5b. Values in angle brackets are average values.

Temperature of analysis	Component	δ ($mm \cdot s^{-1}$) ± 0.01	Γ ($mm \cdot s^{-1}$) ± 0.01	ΔE_Q ($mm \cdot s^{-1}$) ± 0.01	2ε ($mm \cdot s^{-1}$) ± 0.01	H (T) ± 0.2	RA (%) ± 2
LNT	S	0.48	0.38	—	-0.22	49.5	88
	D_{77}	0.42	0.90	0.74	—	—	12
RT	$S_{distribution}$	⟨0.38⟩	0.30	—	⟨−0.25⟩	⟨29.0⟩	87
	D_{300}	0.32	0.58	0.64	—	—	13

$\delta (mm.s^{-1})$: Isomer shift;

Γ $(mm.s^{-1})$: Linewidth at half height;

ΔE_Q $(mm.s^{-1})$: Quadrupole splitting;

2ε $(mm.s^{-1})$: Quadrupole shift;

H (T): Hyperfine field;

RA (%): Relative area.

The formation of goethite chitosan bionanocomposites could occur through the following steps: (i) precipitation of Fe(III) occurs at low pH by formation of precursor particles in the Fe(III)-chitosan acetic acid mixture; (ii) when the drop of Fe(III)-chitosan acetic acid mixture reaches the NaOH casting bath, pH increases sharply and goethite forms by an adsorption of free Fe^{3+} onto the already formed Fe(III) colloids (Charlet, 1994). At the mean time, the reaction of the acetic acid solvent with the non-solvent NaOH solution causes the chitosan to precipitate, forming the gel beads (Rorrer et al., 1993). The homogeneous distribution of

chitosan inside the ferric-chitosan acetic acid mixture offers the reaction support for the growth of the goethite nanoparticles, and prevents their aggregation during the beads casting procedure.

3.3.2. As adsorption: isotherm and mechanism (EXAFS)

The theoretical plots of each model are shown in Fig. 3.6a and 3.6b for As(V) and As(III) (panels a and b, respectively), together with the experimental data (obtained at pH 5 and pH 9) for adsorption of As(V) and As(III) on CGB at 298K. The graphs are plotted in the form of As(V) and As(III) adsorbed per unit mass of CGB, q_e (mmol/g), against the concentration of As(V) and As(III) remaining in solution, C_e (mmol/L). q_m. The maximum adsorption quantity at higher pH value (pH = 9) for adsorption of As(V) onto CGB is lower than the one at lower pH value (pH = 5); while the adsorption quantities of As(III) at pH 5 and at pH 9 are close to each other.

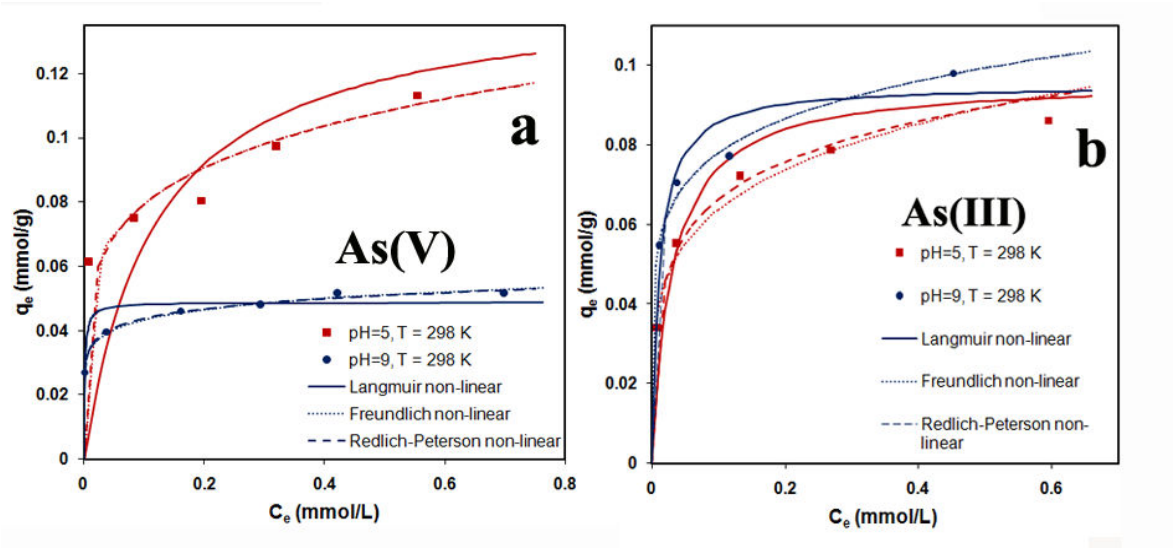

Figure 3.6: Isotherms of arsenate (a) and arsenite (b) adsorption onto CGB at 298 K, at pH=5, 9.

A comparison of coefficient of determination for three isotherms has been made and listed in Table 3.2. The Redlich-Peterson isotherm is found to be the most suitable model for describing both the adsorption equilibrium of As(V) and As(III) onto CGB. Comparing the Langmuir and the Freundlich isotherm, the Freundlich model better reproduces the sorption of As(V) and As(III) on CGB.

Table 3.2:.Isotherm parameters obtained using the non-linear method for the adsorption of arsenate and arsenite onto CGB at 298K at pH 5 and pH 9.

Isotherm		As(V)		As(III)	
		pH=5	pH=9	pH=5	pH=9
Langmuir	q_m. *mmol/g*	0.146	0.0488	0.0964	0.0951
	K_a. *L/mmol*	8.43	689	33.6	91.7
	r^2	0.768	0.852	0.903	0.863
Freundlich	*1/n*	0.193	0.104	0.209	0.150
	K_F. *(mmol/g)(L/mmol)*$^{1/n}$	0.124	0.055	0.103	0.110
	r^2	0.933	0.989	0.972	0.980
Redlich-Peterson	*g*	0.807	0.907	0.832	0.850
	B. (L/mmol)^g	138293	5053.4	173	172504
	A. L/g	17111	275	17.5	19011
	r^2	0.933	0.992	0.981	0.980

At pH 5, the maximum amount of adsorbed As(V) and As(III) equals to 0.151 mmol/g and 0.113 mmol/g, respectively, corresponding to a site density of 12.8 μmol/m^2 and 9.57 μmol/m^2.

Those values are higher than the theoretical maximum arsenic sorption capacity calculated from the site density of goethite (2.0 sites/nm^2, i.e. 3.33 μmol/m^2) reported by Dixit and Hering (Dixit and Hering, 2003). This could be due to the size effect of goethite nanoparticles in CGB. The high surface area to volume ratio of nanoparticles provides more active edges for binding As. The estimated site density could be slightly higher than the true value since we have neglected the insignificant contribution of chitosan in As adsorption. The goethite particle cuboid geometrical assumption which is used to simplify calculation could cause error as well.

The adsorption mechanism of As on CGB is investigated by studying the As local environment by means of extended X-ray absorption fine structure (EXAFS) spectroscopy and compared with that of pure chitosan (batch experiments with As(V) and As(III) and pure chitosan were made at pH 5). The X-ray absorption near-edge spectroscopy (XANES) spectra on bulk samples (see Fig. 3.7a), indicate that the oxidation state of As is maintained after reaction with both pure chitosan and CGB. This is expected, because the samples were kept in an O_2-free glove box until measurement, brought to the synchrotron facility in liquid nitrogen, and measured at low temperature (20K) in helium atmosphere.

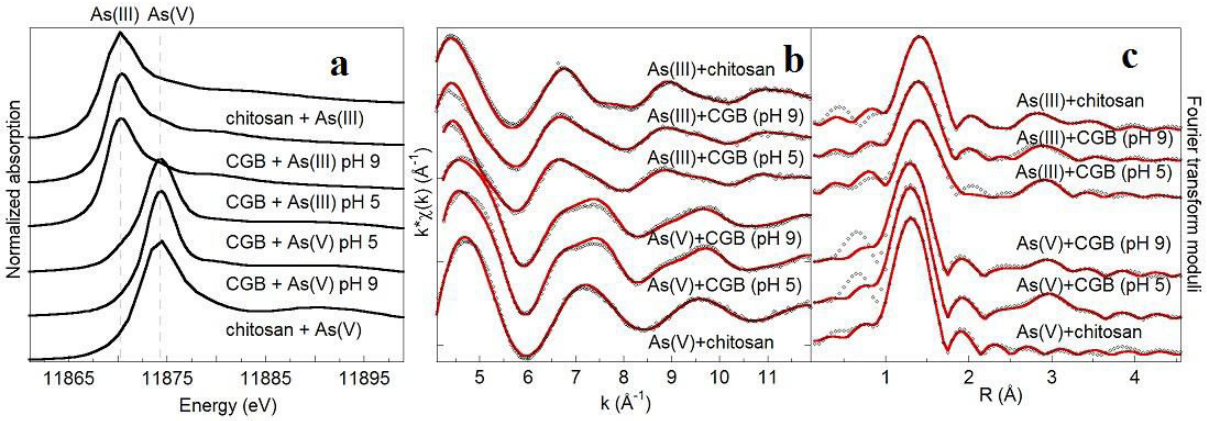

Figure 3.7: (a) XANES spectra of As(III)- and As(V)-loaded CGB and pure chitosan reacted at pH 5 and 9. The vertical lines indicate the position of the main adsorption peak of the As(III) and As(V) references; (b) Experimental EXAFS signal (points) and the fit curves (thick red lines); (c) Fourier Transforms (experimental = points, fit curves = thick red lines) of CGB and pure chitosan reacted with As(III) and As(V) at pH 5 and 9 (the FT are not corrected for the phase shift).

The Fourier transforms and fit curves of the EXAFS signals of As(III/V)-loaded CGB and As(III/V)-loaded pure chitosan are shown in Fig. 3.7c (the EXAFS signals are reported in Fig. 3.7b). As(V)-loaded CGB: the lack of coordination shells higher than the first (Table 3.3) indicates that As(V) is adsorbed as an outer-sphere complex on pure chitosan. On the other hand, the presence of As-Fe contributions in As-loaded CGB suggests that As is adsorbed mainly on the goethite phase, as inner-sphere complex (Fig. 3.8). The structural refinement of the As local environment reveal that CGB can adsorb both As(V) and As(III). This was expected, considering the high affinity of goethite, as well of Fe-oxides and oxyhydroxides in general, with As. As(III)-loaded CGB: structural refinements of As(III)-loaded pure chitosan reveal that, when in the 3+ oxidation state, As forms inner-sphere complexes on the chitosan

molecule. A possible sorption site for arsenite compatible with the EXAFS refinements is shown in Fig. 3.9. Conversely, in As(III)-loaded CGB, again As(III) is preferentially adsorbed onto the goethite phase as inner-sphere complex, as suggested the presence of an As-Fe contribution (Table 3.3).

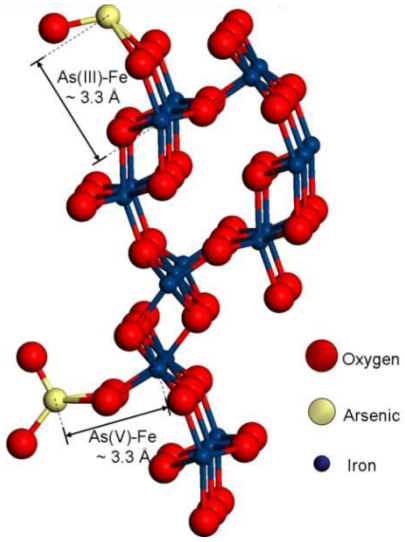

Figure 3.8: Structural diagram of bidentate binuclear As(III)/As(V) surface complexes on the (110) plane of goethite (α-FeOOH) showing (a) the protonated bidentate surface species at 3.3 Å. Only the bidentate binuclear complex was used in surface complexation modeling.

Figure 3.9: 3D atomistic model of a possible sorption site of As(III) on pure chitosan (black: As atom; light grey: oxygen atoms; grey: carbon atoms; blue: nitrogen atoms). Hydrogen atoms have been omitted for clarity.

TABLE 3.3: Refined structural parameters of pure chitosan and CGB reacted with As(III) and As(V). The numbers within parenthesis represent the error on the last digit.

	1st shell			2nd shells				
	CN	R (Å)	σ^2 ($Å^2 \cdot 10^3$)	CN	R (Å)	σ^2 ($Å^2 \cdot 10^3$)	S_0^2	χ_v^2
As(V)								
Chitosan	4 O	1.690(3)	2.2(4)	-	-	-	1.0(1)	1.0
CGB (pH 5)	4 O	1.686(6)	3.1(5)	2.0(5) Fe	3.28(2)	8(3)	1.0(1)	1.0
				9.9(5) O	3.52(5)	21(9)		
CGB (pH 9)	4 O	1.688(3)	2.8(4)	2.0(5) Fe	3.28(2)	8(3)	1.0(1)	1.0
				8.0(5) O	3.52(5)	21(9)		
As(III)								
Chitosan	3 O	1.792(5)	2.0(6)	2 C	2.91(4)	8(9)	1.0(1)	1.0
				4 C	3.32(4)	7(9)		
				2 C	3.66(4)	7(9)		
CGB (pH 5)	3 O	1.780(6)	2.4(6)	2.0(5) Fe	3.33(2)	8(3)	0.9(1)	1.0
				1.0(5) O	3.55(5)	11(5)		
CGB (pH 9)	3 O	1.787(6)	3.9(4)	0.8(7) Fe	3.34(1)	4(4)	1.0(1)	1.3
				1.3(8) O	3.54(3)	12(6)		

CN: Coordination Number;

R: distance from the absorber;

σ^2: Debye-Waller factor

3.3.3. Effect of CGB dose

Figure 3.10 shows the residual arsenic concentration after adsorption treatment of different dose of CGB beads at 298 K. Reacting with high initial concentration (5 mg/L) of arsenic solution, 3.5 g of CGB beads are needed to decontaminate the solution in order to reduce arsenate/arsenite level to meet the 50 μg/L water standard. The residual arsenic level is decreasing with the increasing amount of CGB bead. For lower initial concentration (1 mg/L) of arsenic solution, the 10 μg/L water standard level can be reached by using 0.5g and 2.5 g of CGB as adsorbent, respectively. CGB bead shows higher efficiency on removing As(V) than on As(III).

3.3.4. Kinetic study and diffusion pattern (μXRF and μXANES)

The results of kinetic experiments reveal that the sorption of As(III) and As(V) by CGB took less than 2000 min (33h) to reach equilibrium (Fig. 3.11). The adsorption of arsenate was more rapid than that of arsenite. The initial sorption rate usually increases with an increase in the initial concentration. However, the initial sorption rate of arsenate is higher than that of arsenite, although the initial concentration of arsenite was lower than that of arsenate. At 1.5h, 50.19% of the total amount of As(V) was removed from the solution, while 35.49% of the total As(III) was removed at the same time. Most of arsenic molecules were trapped by CGB in the first 24h (88.60% of arsenite and 97.64% of arsenate), and after this time, adsorption of As(V) and As(III) onto CGB tend to a plateau. A widely used parameter to compare reaction rate is the half-life, $t_{1/2}$, the time within which half of the initial concentration of arsenic has disappeared, that is C/C_0=0.5. In our experiments, half-life of As(V) and As(III) were 94 min and 166 min, respectively.

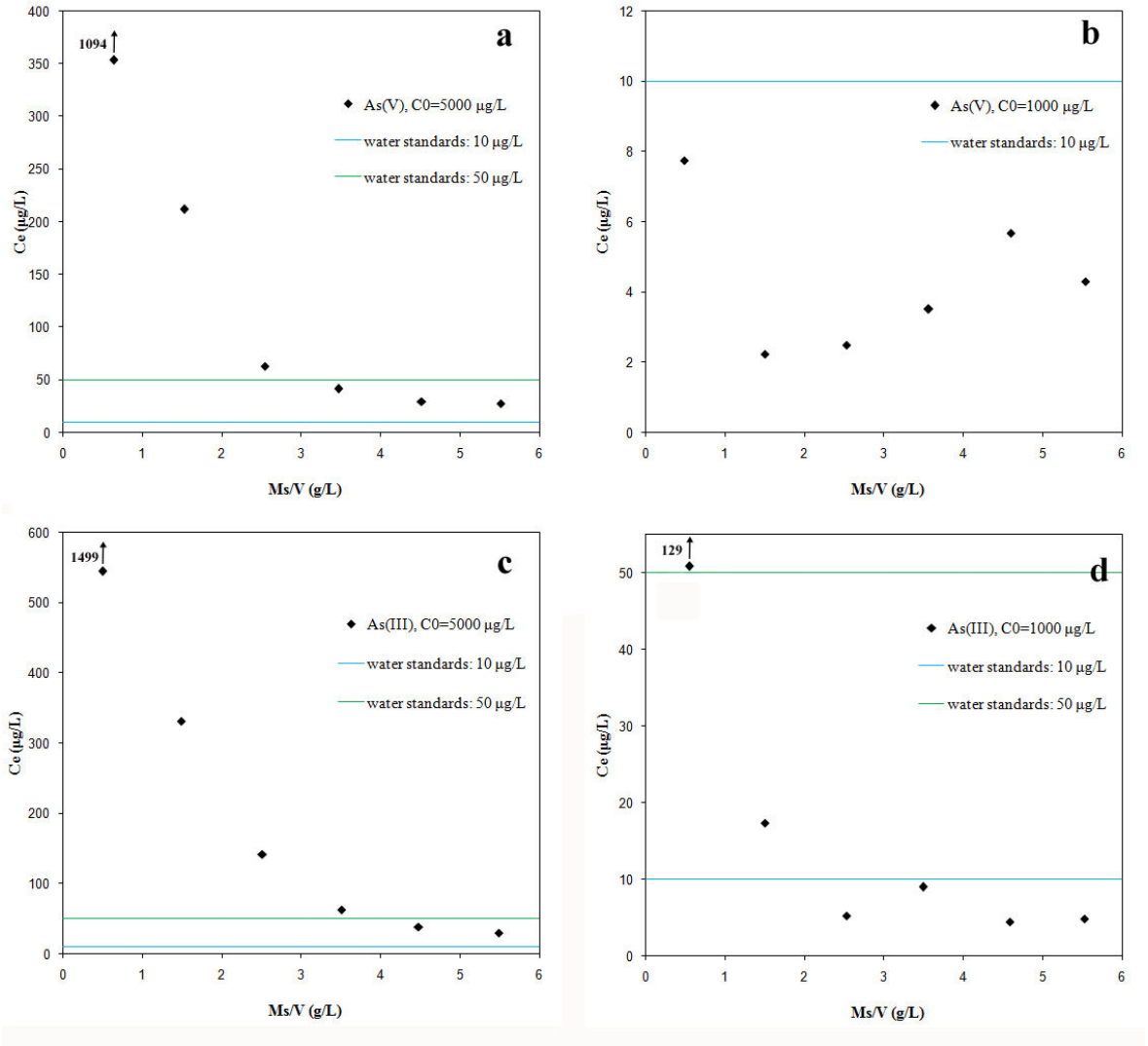

Figure 3.10: Effect of CGB dose on residual arsenic concentration (initial As concentration 5000 µg/L and 1000 µg/L, at pH 7, 298K).

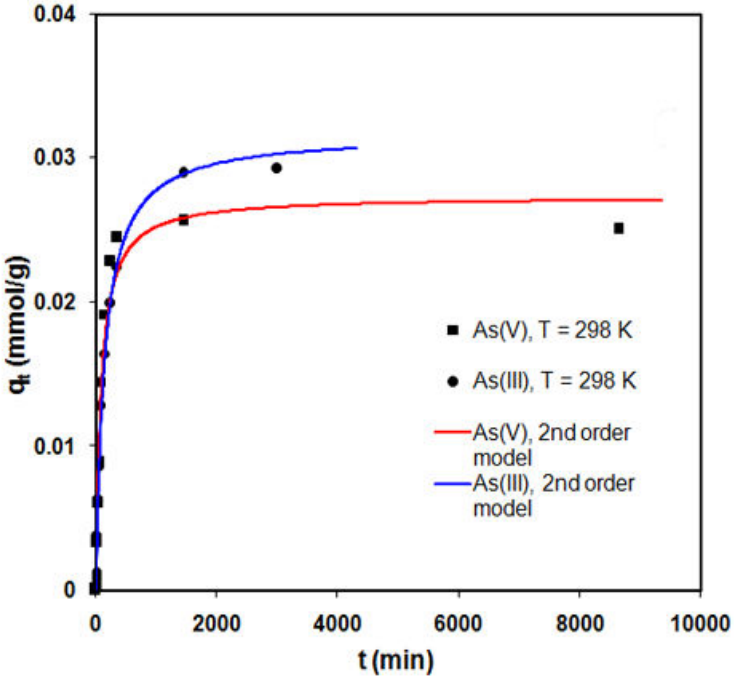

Figure 3.11: Kinetics study of arsenite and arsenate adsorption onto CGB at 298 K, at pH=7.

Table 3.4: Kinetic parameters for the sorption of As(III) and As(V) on CGB at pH 7, at 298 K.

Kinetic		As(III)	As(V)
pseudo-second order	C_0. *mmol/L*	0.0817	0.0657
	q_e. *mmol/g*	0.0317	0.0274
	k. g/mmol min	0.224	0.438
	h. mmol/g min	$2.25 \cdot 10^{-4}$	$3.26 \cdot 10^{-4}$
	r^2	0.998	0.971
arsenic removal ratio	*t=1.5 h (90 min)*	35.5%	50.2%
	t=24 h (1440 min)	88.6%	97.6%
	$t_{1/2}$. *min*	166	94

C_0, initial arsenic concentration; *k*, rate constant; *qe*, equilibrium sorption quantity; *h*, initial sorption rate; *r2*, coefficients of determination.; *t1/2*, half-life of arsenic in solution.

Selected distribution maps of As and Fe of As(V) and As(III)-loaded CGB cross-sections (at 1.5h and 72h reaction time of kinetic experiment) are shown in Fig. 3.12. The distribution of Fe reveals the vacuolar nature of the CGB, which consists of spheres tending to be hollow or with uneven distribution of material at their inside. The hollow areas of CGB at 72h reaction time were larger than that of samples at 1.5h. This could be due to chitosan polymer swelling in solutions occurring during the experiment. The distribution of As reveals that, during the first 1.5h, As(III) penetrated for 70-80 μm in the beads, while the penetration of As(V) was slightly faster, reaching 100-110 μm. These value are consistent with the results of kinetics study data which show that As(V) adsorption onto CGB is faster than that of As(III). The profile distribution plots (Fig. 3.12) of As(III) and As(V) at 1.5 h indicate that the diffusion front is limited to a well defined ring at the beads surface, suggesting that the As adsorption is primary due to the formation of surface complexes.

μXANES spectra collected at the points of interest, highlighted in Fig. 3.12 by white numbered circles, are reported in Fig. 3.13. Spectra 1-4 indicate that As is mainly (or only), in the 5+ oxidation state, while spectra 5-8 indicate mixed (3+ and 5+) As oxidation states. The results reveal that arsenic remained in 5+ oxidation state in all As(V)-loaded beads, while in the As(III)-loaded beads, it was partly oxidized to As(V). Since the μXANES and μXRF measurements were conducted in air and at room temperature, the oxidation of As from the 3+ to the 5+ state is most probably due to the exposition to oxygen (bulk XANES performed in anaerobic environment and at low temperatures show no change in the oxidation state).

After 72h, both As(III) and As(V) diffuse in the whole CGB section, their concentration being higher at the borders and diminishing moving to the center of the beads in a typical U shape

profile. This suggests that the arsenic adsorption takes place more rapidly than diffusion process. At the beginning of the reaction, arsenic concentration in the bath drops sharply due to the rapid adsorption on the surface and rim of the CGB bead. Once the arsenic ions enter the porous CGB, local micro-scale adsorption occurs between the porous aqueous phase containing arsenic solution and solid goethite/chitosan phase. With the transport of arsenic from bath solution into CGB, part of arsenic ions are preferentially adsorbed on the goethite/chitosan, and the rest could diffuse further to the core of bead. The diffusion and sorption reaches equilibrium when the As concentration in all pores of the beads equals to the As concentration in bath solution. The distribution of As in As-loaded CGB at the equilibrium (Fig. 3.12b, 3.12d) shows shell-to-centre arsenic concentration gradients.

The observed inhomogeneous arsenic distribution can be ascribed to the decreasing concentration of the bulk solution. The kinetic experiments were performed in the finite bath sorption regime; i.e. the initial concentration in the solution outside the bead was not constant during sorptive equilibration process between the bath solution surrounding the beads and CGB particles themselves. The finite bath regime can be characterized by the nondimensional number (Schwarzenbach et al., 2005):

$$\gamma = K_d^{'} S_t \tag{3.9}$$

where $K_d^{'}$ is the microscopic distribution coefficient that applies within the beads and S_t is the solid concentration per total volume. γ corresponds to the final ratio of the mass adsorbed on the solid to the mass dissolved in the solution when sorption equilibrium is reached. The solute concentration inside the aggregate pores, $C_w^{'}$, is always at equilibrium with the local adsorbed phase, $C_s^{'}$, which satisfies the condition:

$$C_s^{'} = K_d^{'} C_w^{'} \tag{3.10}$$

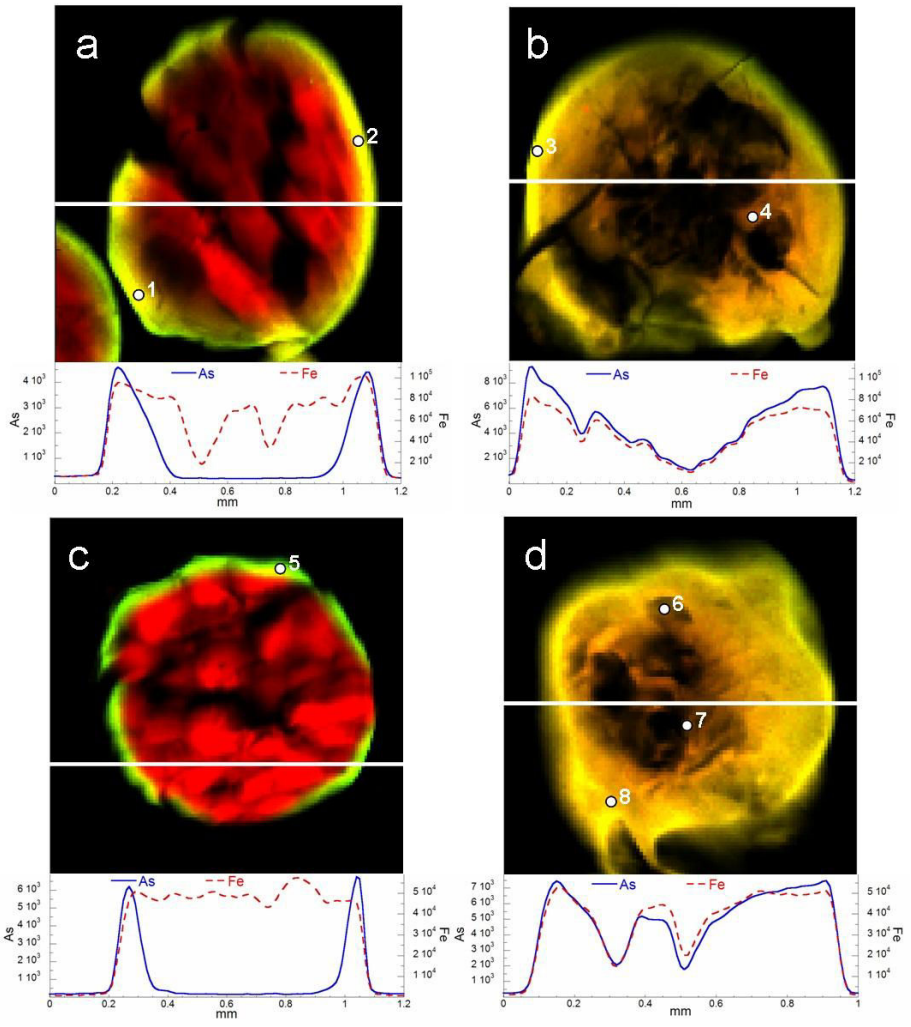

Figure 3.12: Distribution maps of As (green color) and Fe (red color). The pixel size is 10 x 10 μm^2. The yellow to orange colors indicate the co-presence of As and Fe. The distribution of As(V) and Fe is reported in panels (a), after 1.5h reaction time, and (b), after 72h reaction time. Panels (c) and (d) show the distribution of As(III) and Fe, respectively after 1.5h and 72h reaction time. The plots below the distribution maps show the As and Fe concentration profiles calculated along the white thick lines superimposed with the distribution maps. The numbered white circles indicate the points where the μXANES spectra were acquired (Fig. 3.13).

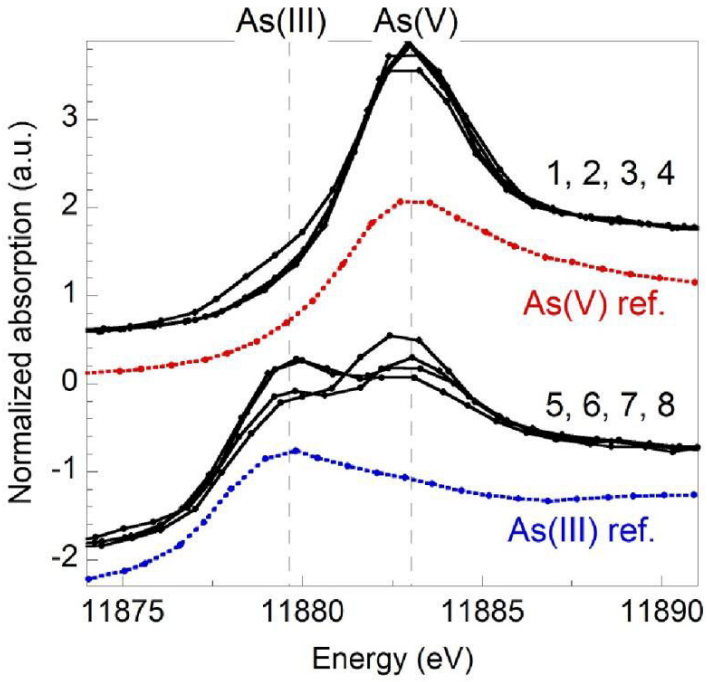

Figure 3.13: μXANES spectra acquired at the points of interest shown in Fig. 3.12.

According to Wu and Gschwend (Wu and Gschwend, 1988), for different values of γ, sorption proceeds as a function of the nondimensional time t^*.

$$t^* = \frac{D_{eff} t}{r_o^2} = \frac{D_{pm} t}{(1 + K_d^{'} r_{sw}) r_o^2}, \tag{3.11}$$

where,

D_{eff} is the effective intraparticle diffusivity;

D_{pm} is the diffusivity in the porous matter which is due to tortuosity or the Renkin effect;

$$r_{sw} = \rho_s \frac{1-\phi}{\phi}, \tag{3.12}$$

where r_{sw} is the solid-to-water-phase ratio of the particle aggregate, ρ_s is the density of dry solid and ϕ is the porosity of the particle;

r_o is the radius of the bead (m), and

t is the exposed time (s).

The non dimensional number γ can be calculated by kinetics parameters and in our case ($\gamma_{As(III)}\approx3.5$, and $\gamma_{As(V)}\approx5$), the nondimensional time, t^*, required to reach 50% equilibration ($M_t/M_\infty=0.5$), is about 0.00153 for As(III) and 0.00262 for As(V), which are obtained from the first-order sorption model and radial diffusion model at half-equilibration time for finite bath system according to Wu and Gschwend (Wu and Gschwend, 1988).

Hence,

for As(III) and As(V), we have, respectively:

$$t_{0.5}(\gamma=3.5)= 0.00153 \times \frac{r_o^2}{D_{eff}(AsIII)}; \quad (3.13)$$

$$t_{0.5}(\gamma=5)= 0.00262 \times \frac{r_o^2}{D_{eff}(AsV)}; \quad (3.14)$$

From the kinetics experiments we have: $t_{0.5}$ (AsIII)≈140.8 min and $t_{0.5}$ (AsV)≈83.9 min and r_o = 5.09×10^{-4} m, so we can calculate $D_{eff}(AsIII)$ = 6.69×10^{-14} m^2/s and $D_{eff}(AsV)$ = 1.34×10^{-13} m^2/s. The estimated effective diffusivities of As(III) and As(V) are similar. The higher estimated diffusivity of As(V) could be due to the electrostatic attraction between As(V) and the inner surface of the beads which accelerates the movement of As(V) towards the beads.

3.4. Practical applications.

This study demonstrate that CGB remove both As(III) and As(V) from water efficiently. Hence, manipulation of pre-oxidation of As(III)-contained water for enhancing As removal rate is not necessary. For 1 liter of high-arsenate/arsenite water (1 mg/L), 0.5g and 2.5g CGB beads, respectively, can eliminate arsenic level to meet the 10 µg/L water standard. The results of leaching test prove that little extra iron was released from CGB during adsorption process, which demonstrates that CGB doesn't pose potential health risk by releasing nanoparticle or toxic element in application (compared other adsorbents like Mn/Al oxides or NPs). The mechanical property test shows that the material is very rigid and stable so that it can be easily stored, transported and used. The size and density of CGB beads allow for water decontamination without complicated or energy-consuming separation procedure, since those beads would precipitate at the bottom of the water container after their use for As removal or could be kept in permeable porous textile or plastic bags during the procedure. These properties highly reduce the cost and complexity of water remediation process. It could be a promising material particularly to developing nations, which suffer a diversity of socio-economical-traditional constraints for water purification and sanitation.

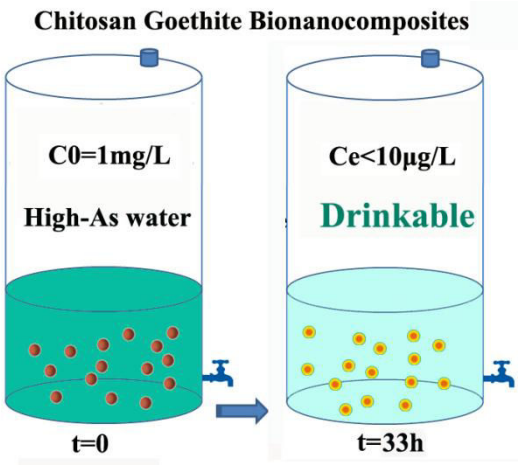

Figure 3.14: Proposed application of CGB in households for arsenic remediation.

Chapter 4

Antibiotics as emerging contaminants in the environment

Jing He and Laurent Charlet

4.1. Introduction

An antibiotic is an agent that inhibits or kills bacteria. Its discovery is considered as one of greatest inventions of the 20th century since humankind could start to treat many bacteria-caused diseases which were often fatal. An overview of the most important classes and groups of antibiotics are listed in Table 4.1. Despite decades of the large rate of use for human and veterinary medicines, the occurrence and effects of antibiotics in the environment have been little studied until very recent times when it began to receive more notice and concern. Two reviews on antibiotics and related environmental issues published by Sarmah et al. (2006) and Kümmerer (2009) have highlighted the worldwide occurrence of antibiotics. Human and animal faeces, hospital effluents, pharmaceutical industries and municipal sewage influent that contain antibiotics result in antibiotic residues in surface water and ground water (Figure 4.1). The presence of antibiotics, even in low doses, gives rise to public concern due to a series of adverse effects to aquatic environment and potential risks to public health.

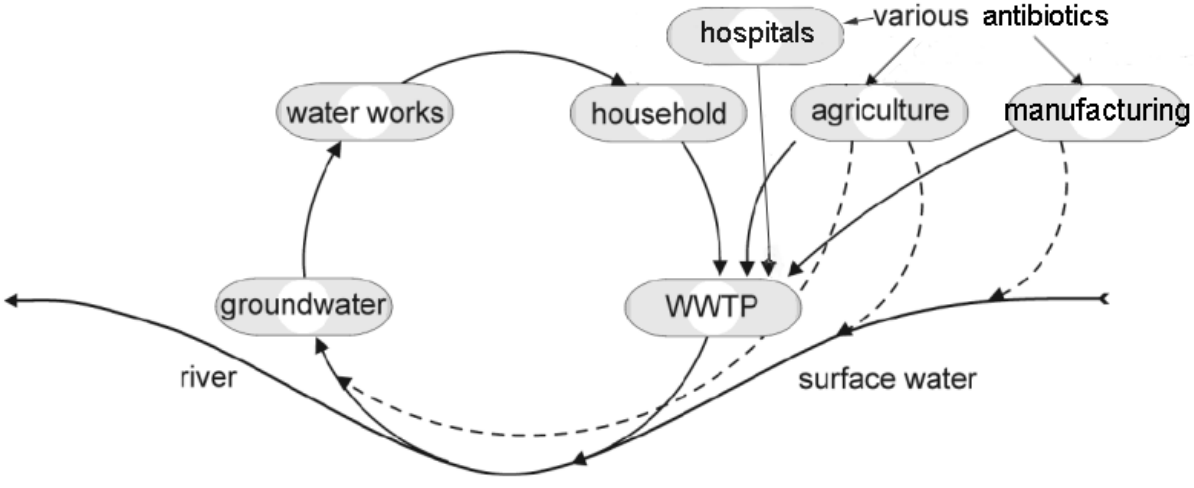

Figure 4.1: Antibiotics in the water cycle.

Table 4.1: Important classes and groups of antibiotic compounds (Kümmerer, 2009).

Class	Group	Subgroup	Example
β-lactams	Penicillins	Benzyl- Penicillins	Phenoxypenicillin
		Isoxazolylpenicillins	Oxacillin
		Aminopenicillins	Amoxicillin
		Carboxypenicillins	Carbenicillin
		Acylaminopenicillins	Piperacillin
	Cephalosporins	Cefazolin group	Cefazolin
		Cefuroxim group	Cefuroxim
		Cefotaxim group	Cefotaxim
		Cefalexin group	Cefprozil
	Carbpenems		Meropenem
Tetracyclines			Doxycycline
Aminoglycosides			Gentamicin 1c
Macrolides			Erythro-mycin A
Glycopeptides			Vancomycin
Sulfonamides			Sulfamethoxazole
Quinolones			Ciprofloxacin

4.2. Sources of antibiotics contamination

4.2.1. Pharmaceutical manufacturing

Discharge from basic drug manufacturing facilities (BDMF) and drug formulation facilities (DFF) have been considered of minor importance but recent studies have shown that they can be substantial point sources with levels much higher than any other route (Khan et al., 2013). Larsson et al. (2007) reported high levels of antibiotics found from effluent of drug manufacturers in Patancheru, India, with the concentration of ciprofloxacin, the most abundant drug found downstream the plant, reaching 31 mg/L. Several antibiotics (highest concentrations range from 1100-49000 ng/L for different drug residues) were detected from water samples near one drug formulation facility in Pakistan (Khan et al., 2013).

4.2.2. Hospital wastewater and municipal sewage

Another possible route for antibiotic agents entering into the environment is hospital wastewater. Due to the heavy use of antibiotics in hospitals, their concentrations are usually higher than those in domestic wastewater. About 0.7–124.5 mg/L of ciprofloxacin and 20–80 mg/L of β-lactams were found in effluents of a German hospital (Kümmerer 2003). Wastewater samples collected from a hospital in Girona, Spain were found to contain Ofloxacin and Ciprofloxacin at concentrations up to 10368 ng/L and 7494 ng/L, respectively (Gros et al., 2013). Elmanama et al. (2006) discussed the contribution of hospital wastewater to the spread of antibiotic resistance.

The presence and fate of antibiotics in municipal wastewater treatment plants (WWTPs) are becoming an emerging research topic in recent years. Extensive researches on antibiotics

occurrence have been reported mainly in East Asia, North America, Europe, and Australia, according to Zhang and Li (2011), who report the occurrence, transformation, and fate of antibiotics in WWTPs. This review summarized much literature work published over the previous 8 years and concluded that many antibiotics cannot be removed completely in wastewater treatment processes and would enter into environment via effluent and sludge (Zhang and Li, 2011). Hospitals are considered as major sources of pharmaceutical residues discharged to municipal wastewater (Reinthaler et al., 2003; Garciaetal., 2007), but some new research showed that the contribution of hospitals to the loads of selected, quantifiable pharmaceuticals in sewage treatment plant influents was limited (Guardabassi et al., 2002; Le Corre et al., 2013). The overall impact of discharging untreated hospital effluents into the sewer system is still under debate (Le Corre et al., 2013).

4.2.3. Animal farms and aquaculture

Animal farms are recognized as a major contributor to environmental pollution with antibiotic resistance genes. Although in the European Union, as well as in some other countries such as Switzerland, the use of antibiotics as growth promoters in animal farms has been banned, other countries still extensively use antibiotics in livestock. Over 84% of the antibiotics produced in the USA are still used in agriculture, with non-therapeutic livestock usage accounting for 70% of the total antimicrobial use (Mellon et al. 2001). China is the world's biggest producer and consumer of antibiotics in the world. Antibiotics consumption on animal farms was estimated to be more than 970 kt per year in China, accounting for more than 46% of the total annual production of antibiotics (CAST, 2007, The Conversation, 2013). Antibiotics (antimicrobials at large) are extensively used in animal farming as well as

aquaculture for preventing/treating infections and promoting growth (Holmstrom et al., 2003; Smith et al., 2002). Many kinds of drugs with remarkable concentrations were ubiquitous in animal farms and aquafarms (Le and Munekage, 2004; Miranda et al., 2009). Several studies have revealed the veterinary/aquaculture antimicrobial compounds can lead to the contamination to the environment via animal feces or aquaculture discharge (Karci and Balcioglu, 2009; Hoa et al., 2011; Barkovskii and Bridges, 2012; Zhou et al., 2013).

4.3. Advert effects

4.3.1. Antibiotic resistance

Over the past five decades the increasing use of antibiotics, not only for people, but also for animals and in agriculture, has delivered a selection unprecedented in the history of evolution (Levy, 1992). The powerful killing and growth inhibitory effects of antibiotics have reduced the numbers of susceptible strains, leading to the propagation of resistant variants (Levy, 2008). Such resistant bacteria can cause an infection both in humans and animals and may not respond to regular antibiotic treatments (Regassa et al., 2008). Antibiotic resistant bacteria have been found in many hospital wastewaters and municipal sewage all around the world (Akter et al., 2012; Huang et al., 2012; Novo et al., 2013; Korzeniewska et al., 2013). In natural waters, antibiotic resistant bacteria were also detected worldwide (Hoa et al., 2011; Khan et al., 2013; Skariyachan et al., 2013; Coleman et al., 2013). Microbes circulate everywhere - resistance determinants and resistant bacteria can spread locally and globally, selected by widespread use of the same antibiotics in people, animal husbandry and agriculture (Levy, 2008).

4.3.2. Potential public health risks

The potential presence of antibiotics in drinking water sources is of concern due to the unknown health effects of chronic low-level exposure to antibiotics over a lifetime if the antibiotics survive drinking water treatment and are present in consumers' drinking water (Ye et al., 2007). Pomati et al. (2006) reported that a complex mixture of therapeutic drugs (including four antibiotics) at environmentally relevant concentrations inhibits proliferation of human embryonic cells. (Kim and Aga, 2007). Chen et al. (2012) studied the potential toxicity of sulfanilamide antibiotic to human health. Results suggested the microenvironment and conformation of human serum albumin (HAS) were changed in the presence of sulfamethazine (SMZ). Hence, the abuse of antibiotics or excess ingestion of SMZ would affect the normal biological function of proteins, and cause potential human health risks.

4.3.3. Aquatic life poisoning

Thibaut et al. (2006) provided evidence of inhibitory effects of low levels of pharmaceuticals on the catalytic activities of different xenobiotic metabolizing enzymes in carp liver. Those pharmaceuticals might potentially impact aquatic life as well according to the study of Pomati et al. (2006). Doramectin (DOR), metronidazole (MET), florfenicol (FLO), and oxytetracycline (OXT), the four most widely used veterinary drugs in animal husbandry or in aquaculture, were have been investigated as to their aquatic toxicity to marine bacteria (*Vibrio fischeri*), green algae (*Scenedesmus vacuolatus*), duckweed (*Lemna minor*) and crustaceans (*Daphnia magna*). It was found that OXT and FLO have a stronger adverse effect on duckweed and green algae (Kolodziejska et al., 2013). Toxicities of amoxicillin, erythromycin,

levofloxacin, norfloxacin and tetracycline to cyanobacterium Anabaena CPB4337 and the green alga *Pseudokirchneriella subcapitata* have been examined. Results showed that erythromycin was highly toxic for both organisms; tetracycline was more toxic to the green algae whereas the quinolones levofloxacin and norfloxacin were more toxic to the cyanobacterium than to the green alga. Amoxicillin also displayed toxicity to the cyanobacterium but showed no toxicity to the green alga (Gonzalez-Pleiter et al., 2013).

4.3. Antibiotic contamination in WWTPs and natural waters of China

After being used, antibiotics are excreted into effluent and reach wastewater treatment plants or reach the environment directly. In this process, antibiotics can be partially metabolized. Since WWTPs can only eliminatantibiotics partially, the residual parts pass though WWTPs and then end up in the environment – surface water, ground water, sea water, soil or sediment.

As China is the largest producer and consumer of antibiotics in the world, it's not surprising that antibiotics have been found to be widespread in WWTPs and the environment. Table 4.2 lists reports of the presence of antibiotics throughout China, in WWTPs, surface waters, ground waters, etc. A variety of antibiotics have been reported with considerable concentrations especially in some surface waters. Obviously, densely populated areas are particularly prone to antibiotics contamination. In some water bodies, the levels of antibiotics are in the same range as those in WWTPs. The level of antibiotics in tap water reached 697 ng/L in Macau and Guangzhou (Wang et al., 2010).

Table 4.2: Presence of antibiotics in WWTPs and natural waters of China.

Sample type: wastewater treatment plant	**Antibiotic**	**Level (ng/L) (influent)**	**Level (effluent)**	**Location**	**Reference**
	erythromycin-H_2O, etc (chloramphenicol, fluoroquinolone, sulfonamide and macrolide groups)	Up to1978	Up to 2054	Pearl River Delta	Xu et al., 2007
	Cefalexin, etc; Cefotaxim, etc	Up to 2900; Up to 1100	Up to 1800	Hong Kong	Gulkowska et al., 2008.
	Ofloxacin etc; (eight fluoroquinolones, nine sulfonamides and five macrolides)	Up to 3100	Up to 1200	8 STPs in Beijing	Gao et al., 2012
	Quinolones, etc; (eight quinolones, nine sulfonamides, and five macrolides)	Up to 4916	Up to 123	Beijing	Li et al., 2013
	Sulfamethoxazole, etc; (sulfadiazine, ofloxacin and chloramphenicol)	Up to 7910		2 STPs in Guangzhou	Peng et al., 2006

	Clotrimazole Fluconazole, econazole, ketoconazole, and miconazole	Up to 1834		Guangzhou	Peng et al., 2012
	Cefalexin, ofloxacin and etc.	Up to 5640 and 7900, respectively	Up to 5070, 7870, respectively	Hong Kong	Leung et al., 2012
Sample type :Natural Waters/Water supply	**Antibiotic**	**Level (ng/L)**		**Location**	**Reference**
	14 sulfonamides, 2 chloramphenicols and 4 tetracyclines	Up to 9.23		Seawater, Dalian	Na et al., 2013
	eight quinolones, nine sulfonamides and five macrolides	Up to 1563		Baiyangdian Lake	Li et al., 2012
	sulfonamides, fluoroquinolone, tetracycline and chloramphenicol	8.6, 11.6 in groundwater and in lake water (summer); 7.3, 11.7 in groundwater and in lake water (winter)		Groundwater, lake water near pig farm, Hubei Province	Tong et al., 2009
	4 tetracyclines, 3 chloramphenicols, 2 macrolides, 6	Up to 623.27		Huangpu River, Shanghai	Jiang et al., 2011

	fluoroquinolones, 6 sulfonamides and trimethoprim			
	Sulfamethazine, etc	Up to 218	Pearl River Estuary	Liang et al., 2013
	dehydration erythromycin, sulfamethoxazole and trimethoprim	Up to 50.4 and 663, in sea water and fresh water, respectively	Coast of Yellow Sea and river close to the sea	Zhang et al., 2013
	Erythromycine-H_2O, sulfamethoxazole and trimethoprim	Up to 50.9	Beibu Gulf	Zheng et al., 2012
	fluoroquinolones, macrolides, sulfonamides and trimethoprim	Up to 13,600 for trimethoprim	LaizhouBay	Zhang et al., 2012
	sulfonamides, macrolides, and trimethoprim	Up to 1336	Tributaries of YongjiangRiver	Xue et al., 2013
	Erythromycin-H_2O concentrations	Up to 460	Victoria Harbour of Hong Kong and the Pearl River at Guangzhou	Xu et al., 2007
	norfloxacin, ciprofloxacin, lomefloxacin, and enrofloxacin	Up to 679.7	Tap water of Guangzhou and Macao	Wang et al., 2010
	Sulfonamides,	Up to 6800	Bohai Bay	Zou et al.,

	Fluoroquinolones Macrolides and Tetracyclines			2011
	dehydration erythromycin, sulfamethoxazole and trimethoprim	0.10-16.6	Bohai Sea and the Yellow Sea	Zhang et al., 2013b
	Sulfapyridine, etc	Up to 219	Yangtze Estuary	Yan et al., 2013
	Sulfadimidine, etc	Up to 475.8	East River (Dongjiang)	Zhang et al., 2012b
	Roxithromycin, etc	Up to 2260	Pearl River System	Yang et al., 2011
	Sulfonamides, etc	24-385 ng/L	Haihe River Basin	Luo et al., 2011

4.4. Elimination

Since antibiotics are often complex molecules which may possess different functionalities, under different pH conditions antibiotics can be neutral, cationic, anionic or zwitterionic (Kümmerer, 2009). Antibiotics can be degraded by biotic processes - biodegradation by bacteria and fungi. Depending on their physico-chemical properties, sorption, hydrolysis, photolysis, oxidation and reduction can play a role in antibiotics elimination as well. These processes have been applied in removal of the antibiotics from water in industry and scientific research.

Clay minerals are widely considered as an active component of soils for the adsorption of polar xenobiotics (Boyd et al., 2001). Studying the adsorption of antibiotics onto clay minerals can help to understand the environmental fate of those antibiotics in soils, subsoils, aquifers and sediments. On the other hand, clay minerals can be used as low-cost materials as the removal reagent for treating water with antibiotic contaminants. The adsorption behavior of enrofloxacin onto smectite clay and mechanisms of adsorption has been discussed (Yan et al., 2012). The study of adorption of tetracycline on illite has also been reported (Chang et al., 2012). In the next chapter, montmorillonite, a member of the smectite family, was used to uptake gentamicin from water. The mechanism was studied and the solid waste produced in the adsorption process (gentamicin-loaded montmorillonite) was recycled and reused to fabricate an antimicrobial film which is potentially usable as a skin wound dressing for burn patients.

Chapter 5

Gentamicin adsorption on Na^+-montmorillonite and preparation of gentamicin-montmorillonite-HPMC films as a burn wound dressing

Jing He, Pilar Aranda, Margarita Darder, Laurent Charlet and Eduardo Ruiz-Hitzky

5.1. Introduction

The presence of antibiotics in natural waters is of concern for many reasons. First, antibiotic resistance can develop in bacteria with exposure to sub-inhibitory concentrations (Ash et al., 2002). Second, aquatic organisms such as algae, nitrifying bacteria and zooplankton, can be adversely affected by mixtures of antibiotics even at low concentrations (Flaherty and Dodson, 2005; Yang et al., 2008; Ghosh et al., 2009). And lastly, although the human health effects of sustained exposure to antibiotics at sub-therapeutic doses are currently unclear, there is increasing public awareness about the presence of antibiotics and other pharmaceutical compounds in drinking water supplies (Benotti et al., 2009). Thus there is interest in procedures to remove antibiotics and other pharmaceutical compounds from water supplies (Wunder et al., 2011). Antibiotics are not effectively removed via conventional water treatment (i.e. coagulation/flocculation/sedimentation/filtration) or lime softening ($\leq$33%, Adams et al., 2002; Westerhoff et al., 2005; Wunder et al., 2011).

Gentamicin (Gt.), an aminoglycoside antibiotic produced by fermentation of *Micromonospura purpurea*, is a mixture of basic, water soluble compounds containing the aminocyclitol 2-deoxystreptamine and 2 additional amino sugars (MacNeil and Cuerpo, 1995). Its formula is shown in Figure 5.1 and the pKa of various functional groups are shown in Table 5.1. Gt. shares many structural and functional features with other antibiotics containing streptamin or its derivatives, such as streptomycin, meomycin and kanamycin (Butko et al., 1990). Gentamicin is used to treat many types of bacterial infections, particularly those caused by Gram-negative organisms (Moulds and Jeyasingham, 2010). The main toxic effects of the aminoglycoside antibiotics are nephrotoxicity and ototoxicity. Furthermore, fetotoxicity was observed for gentamicin (Gehring et al., 2005). Although application of Gt. in human

medicine has declined, its use in veterinary and agriculture is still intense. Gentamicin can enter the environment via pharmaceutical factories, hospital waste water and animal droppings.

Adsorption of Gt. onto Na^+-montmorillonite was investigated as a method to remove gentamicin-like positive charged antibiotics from water. Gentamicin-loaded montmorillonite, as the solid waste of the sorption process, can be recycled and reused in burn wound treatment.

Burn wound infections are among the most important and potentially serious complications that occur during the acute period following injury. Systemic treatment against infection is limited by inadequate wound perfusion, which restricts migration of host immune cells and the delivery of antimicrobial agents to the wound. In this case, the local concentration of the antibiotics may be insufficient and may lead to bacterial resistance (Elsner et al., 2011). The widespread application of a topical antimicrobial agent on the open burn wound surface can substantially reduce the microbial load and risk of infection (Murphy et al., 2003). The typical burn wound is initially colonized predominantly with Gram-positive organisms, which are replaced by antibiotic-susceptible Gram-negative organisms within 1 week after the burn injury. Gentamicin is accordingly used to treat many types of bacterial infections, particularly those caused by Gram-negative organisms and it can protect the recovering tissue from potential infection or re-infection, therefore gentamicin has been used for cure burn wounds (Moulds and Jeyasingham, 2010). Gentamicin-eluting collagen sponges have been found useful in both partial-thickness and full-thickness burn wounds (Elsner et al., 2011). A new concept of wound dressing, which is based on **a** polyglyconate mesh coated with a porous poly-($_{DL}$-lactic-*co*-glycolic acid) matrix loaded with gentamicin, are applied in burn wounds (Aviv el al., 2007; Elsner et al., 2011).

This study developed a gentamicin-loaded montmorillonite based on a hydroxypropyl methycellulose bionanocomposite, and which can be potentially used as a burn wound dressing. Hydroxypropyl methycellulose (HPMC, Figure 5.2) is the most important hydrophilic carrier material used for the preparation of oral controlled drug delivery systems (Doelker, 1987; Colombo, 1993). The reinforcing clay mineral and HPMC afford the necessary mechanical strength to the dressing, and the combined binding matrix is aimed to provide adequate moisture control and release of antibiotics to protect the wound bed from infection and to promote healing. Gt-Mt-HPMC films with different ratios of Gt-Mt to HPMC were synthesized and the mechanical properties and moisture adsorption behavior of several composite films examined. Antimicrobial effects against skin infection-causing bacteria *Staphylococcus aureus* of Gt-Mt-HPMC were also determined..

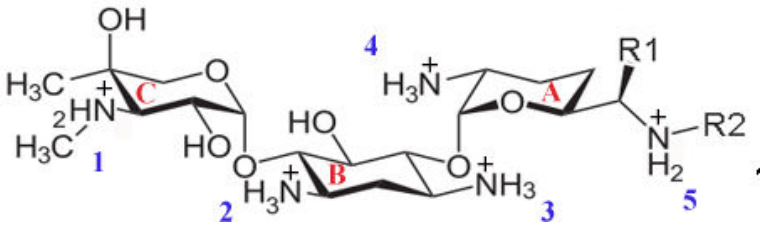

Figure 5.1: Gentamicin structures (Gentamicin C1: R1=R2=CH_3; Gentamicin C2: R1=CH_3, R2=H; Gentamicin C1a: R1=R2=H).

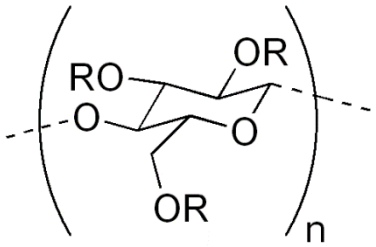

Figure 5.2: molecule structure of hydroxypropyl methycellulose (HPMC), R=H or CH_3 or $CH_2CH(OH)CH_3$.

5.2. Experimental section

5.2.1. Materials

Gentamincin sulfate (48760) was supplied by Sigma-Aldrich. Montmorillonite, Cloisite® Na+ Nanoclay, with a cationic exchange capacity of 92.6 meq/100 g was obtained from Southern Clay Products (Rockwood Additives). Deionized water (resistance of 18.2 MΩ. cm) was obtained with a Maxima Ultra Pure Water system from Elga.

5.2.2. Methods

5.2.2.1. Isotherm study

The Cloisite® Na^+ Nanoclay obtained for this study was used without any purification. A series of gentamincin sulfate solutions were prepared by dissolving known weights of gentamicin sulfate directly into deionized water. Clay and gentamicin mixtures in air-tight bottles covered by aluminum film were shaken for 7 days at constant temperature (294 K). In the batch experiment, the clay weight/ gentamicin solution volume ratio was 10 g/L.

Table 5.1: pKa values of gentamicin C1a, C2, C1 (Lesniak et al., 2003).

Amino group number (Fig. 5.1)	Gt-C1a	Gt-C2	Gt-C1
1	8.86	8.793	8.817
2	8.181	8.211	8.121
3	5.768	5.83	5.686
4	7.389	7.421	7.317
5	9.491	9.593	9.86

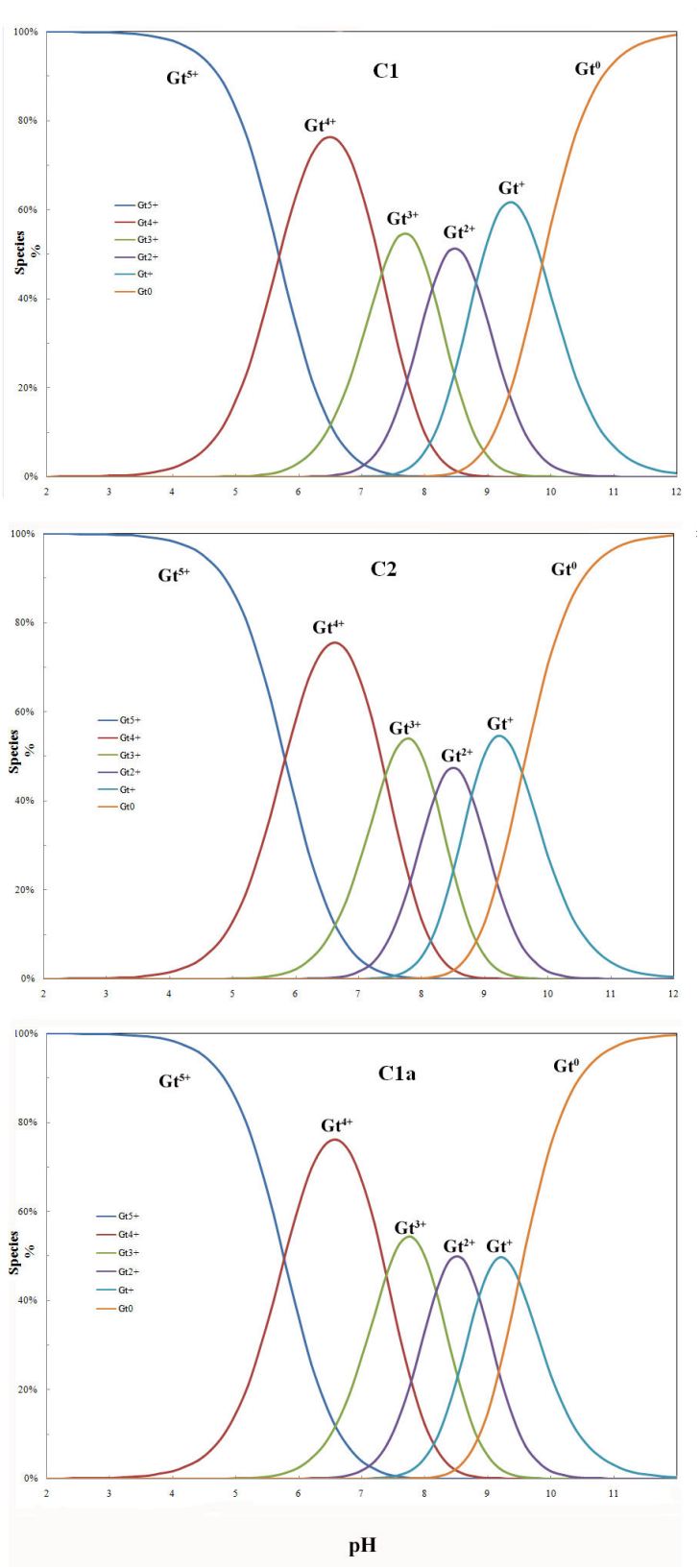

Figure 5.3: Ionization scheme of gentamicin C1, C2, C1a.

Table 5.2: Sample information for Isotherm experiments of gentamicin adsorption on Na^+-montmorillonite.

Sample No.	C_0 (gentamincin sulfate)-mg/L
b	250
c	500
d	2000
e	5000
f	5974
g	7316

All the mixtures were centrifuged at the end of adsorption process and the supernatants were removed. The centrifuged precipitates (labeled as b, c, d, e, f, g, corresponding to the solution numbers) were air-dried at 40℃ in the dark.

5.2.2.2. Characterization

The resulting gentamicin-clay samples were characterized by chemical analysis: the amount of organic matter in the samples was determined by C, H and N elemental chemical microanalysis with a Perkin–Elmer 2400 analyzer; X-ray diffraction (XRD) patterns of clay and drug-loaded clay were obtained on a Bruker D8 Advance powder diffractometer using CuK_α radiation with energy-discriminator and a scan speed of 0.02°/s; The thermal behavior of the different materials (montmorillonite, gentamicin and gentamicin-loaded montmorillonite) were determined from simultaneously recorded thermogravimetric analysis

(TGA) and differential thermal analysis (DTA) curves with a Seiko SSC/5200 instrument in experiments carried out under an air atmosphere (gas flow rate of 100 mL min^{-1}) from room temperature to 990 °C at a heating rate of 10 °C min^{-1}; FTIR spectra were measured in transmission absorption mode over the 4000-250 cm^{-1} region on a Bruker IFS 66v/S spectrophotometer, with the samples prepared in KBr pellets,.

5.2.2.3. Photo-stability studies

Gentamicin sulfate and Gentamicin-Montmorillonite (sample d) were exposed under ultraviolet radiation for 24 hours (continuous 254-nm UV lamp), at ambient temperature (25 ±4°C). About 5 mg of each sample was collected and analyzed by ATR-IR (GladiATR 10, SHIMADZU) after 3h, 6h, 12h, 18h and 24h of UV exposure.

5.2.2.4. In vitro Gt. release from Gt-Mt.

Several tubes which were wrapped by alumimum film were prepared. Twenty milligrams of gentamicin-clay (sample d) and 2 ml of PBS (phosphate buffer solution pH 7) were added into these tubes. They were shaken in reciprocatory water bath (37°C) at 75 rpm. At given time intervals, one tube was taken out of bath and the mixture was filtered by filtration film. All the precipitation was collected was treated as those samples in isotherm study. After 24h of drying, they were characterized by chemical analysis.

5.2.2.5. Preparation of Gt-Mt-HPMC films.

Gentamicin-montmorillonite nanocomposites were prepared by the method we used to prepare sample f in the isotherm experiments. After 5 days of the adsorption process, the final mixture was centrifuged at 294 K at 4000 rpm for 20 min.

The HPMC solution (control film) was obtained by dissolving 2 g of HPMC in 100 mL distilled water under magnetic stirring for 12 h. A 2% (w/v) HPMC solution was used in film formulations. To study the effect of Gt-Mt hybrid concentration in the HPMC film matrix, different concentrations of Gt-Mt nanohybrid were mixed with the 2 % HPMC solution to obtain different film compositions. The wet precipitation hybrids (freshly synthesized) which contained 220, 250, 300, 350 mg of dry hybrid were relatively added into four separated 10 ml HPMC solution. Each mixture was stirred in an oil bath at 40 °C at 400 rpm for 4 hours. The suspensions were then dropped on plastic plates (10×10 cm) at room temperature for film preparation. Those plastic plates were placed in a ventilation box with a UV lamp. The box and the samples were sterilized by UV lamp for the first 15 min. The films were formed by evaporation of water from the samples in the ventilation box for 4 days. Obverse side and reverse side (contacting the plastic plates) of the film were named as the O side and R side respectively. Resulting films formed by the four different initial mixtures containing increasing amount of Gt-Mt hybrid are named as film a, b, c, d, respectively.

5.2.2.6. Film characterization

Field Emission - Scanning Electron Microscopy (FE-SEM)

A Field Emission - Scanning Electron Microscopy (FEI Nova^{TM} NanoSEM 230) was used to study the morphology of the films. All the samples were deposited onto aluminum specimen

stubs using double-stick carbon tabs, and the morphology of both the O side and the R side of each sample were investigated. All samples were examined using an accelerating beam at a voltage of 7 kV. Magnifications of 3000× were used.

Moisture-Adsorption Isotherms

Moisture sorption was investigated by an Aquadyne DVS dynamic water-vapor sorption instrument from Quantachrome. Moisture-sorption isotherms were recorded at 25 ± 0.3 °C in the range of relative humidity from 0 to 95% by using amounts of samples of around 7 mg.

Mechanical Properties

Films used for tensile tests were conditioned at about 65% RH at 15 °C during the measurements. The sample films which were cut to have a rectangular shape (ca. 60 mm x 15 mm) were mounted between the grips with an initial separation of 50 mm. A Model 3345 Instron Universal Testing Machine (Instron Engineering Corporation Canton, MA, USA) was used to determine the maximum percentage (%) elongation at break, and elastic modulus E (or Young's modulus) according to the ASTM standard method D 882-88. The cross-head speed was set at 5 mm min^{-1}. Three replicates were run for each film sample. The elastic modulus E was obtained as the ratio of stress to strain at the initial linear portion of the stress-strain curve. The percentage elongation at thebreaking point was calculated by dividing the extension at rupture of the films by the initial length of the specimen and multiplying by 100.

5.2.2.7. Antimicrobial activity of Gt-Mt-HPMC film

Antimicrobial effectiveness was examined according to ASTM E2149 (Standard test Method for determining the antimicrobial activity of immobilized antimicrobial agents under dynamic contact conditions). 0.05 g film-c (3%) was introduced in test tubes containing 5 mL peptone

water. Pure montmorillonite and HPMC samples without gentamicin were used as controls. The samples were neutralized when required. Each tube was inoculated with 105 cells/mL of *Staphylococcus aureus* (CECT 86, ATCC 12600) in mid-exponential phase and incubated in a wrist action shaker (160 rpm) at 25ºC for 24h. For different samples and controls, bacterial counts were enumerated by sub-cultivation on TSA plates.

5.3. Result and Discussion

5.3.1. Preparation of Gt-Mt. nanohybrid and Isotherm study

The amino groups of the sugar rings of gentamicin exhibit variable pKa values which range from 5.6 to 9.8 as shown in Table 5.1. Thus, gentamicin carries a net positive charge under the experimental acidic conditions when all or parts of amino groups are protonated. All the initial pH values of gentamicin sulfate solutions for adsorption experiment were around 5.5, which made it possible that gentamicin intercalation in Na^+-montmorillonite by means of cationic exchange processes. Figure 5.4 shows the adsorption isotherm at 294 K from gentamicin sulfate solutions on Na^+-montmorillonite. The adsorbed amount of gentamicin was deduced from the CHN chemical analyses.

In order to investigate the adsorption isotherm, three equilibrium isotherm models were applied: the Langmuir, the Freundlich, and the Redlich-Peterson isotherms. The Langmuir adsorption isotherm is perhaps the best known of all isotherms describing adsorption (Langmuir, 1918). The theoretical Langmuir isotherm is often used to describe adsorption of a solute from a liquid solution as (Langmuir, 1918; Ho et al., 2002)

$$q_e = \frac{q_m K_a C_e}{1 + K_a C_e} \tag{5.1}$$

Where q_e is the equilibrium adsorption capacity, (mg/g), C_e is the equilibrium liquid phase concentration, (mg/L), q_m is the maximum adsorption capacity, (mg/g), K_a is adsorption equilibrium constant, (L/mg).

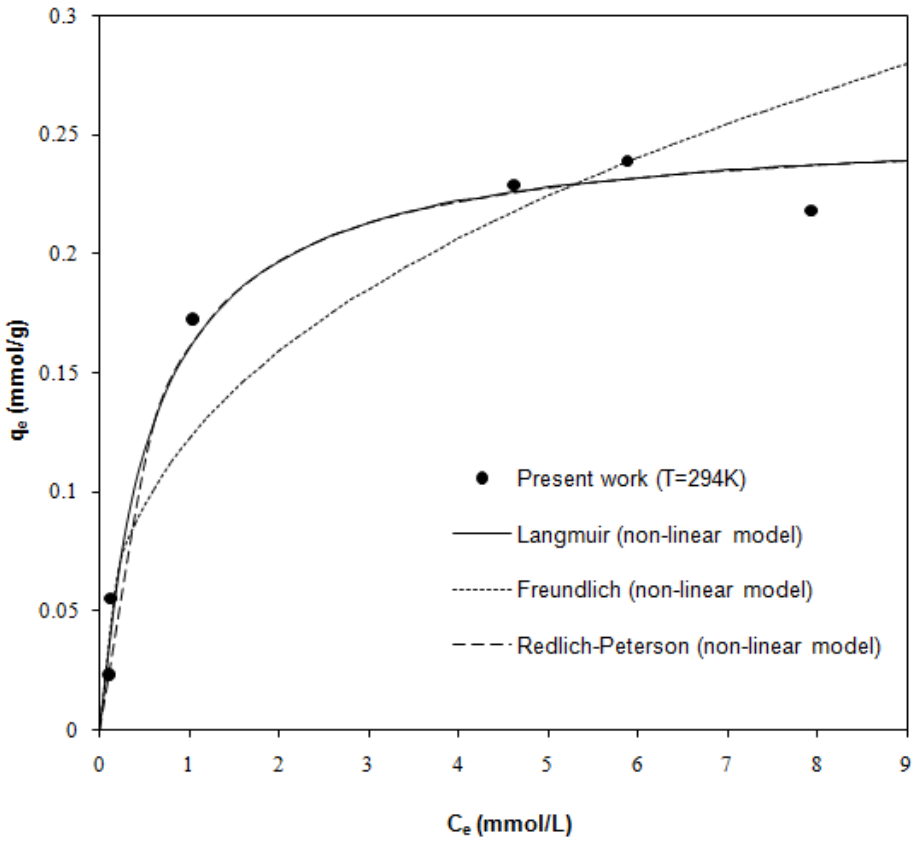

Figure 5.4: Isotherm of gentamicin adsorption onto Na^+-montmorillonite.

The Freundlich isotherm is the earliest known relationship describing the adsorption isotherm (Freundlich, 1906). This fairly satisfactory empirical isotherm can be used in adsorption from dilute solutions. The ordinary adsorption isotherm is expressed by the following equation:

$$q_e = K_F C_e^{1/n} \tag{5.2}$$

whereC_e is the equilibrium concentration in the solution, (mg/L), q_e is the equilibrium adsorption capacity, (mg/g), K_F and $1/n$ are empirical constants. K_F is the adsorption value, the

amount adsorbed at unit concentration, that is, at 1 mg/L. It is characteristic for the adsorbent and the adsobate adsorbed, and denotes multiple sorption site with varying Ka value (Sposito, 1984).

The Redlich-Peterson isotherm contains three parameters and incorporates the features of the Langmuir and the Freundlich isotherms (Redlich and Peterson, 1959). It can be described as follows:

$$q_e = \frac{AC_e}{1 + BC_e^g} \tag{5.3}$$

It has three isotherm constants, namely *A*, *B*, and *g* ($0 < g < 1$).

Due to the inherent bias resulting from linearisation, alternative isotherm parameter sets were determined by non-linear regression. This provides a mathematically rigorous method for determining isotherm parameters using the original form of the isotherm equation (Seidel and Gelbin, 1988; Ho, 2004). To compare the three isotherms, a trial-and-error procedure, wasapplied to obtain the isotherm parameters.The method is using an optimization routine to maximize the coefficient of determination r^2, between the experimental data and isotherms in the *solver* add-in with Microsoft's spreadsheet, Microsoft Excel (Ho and Ofomaja, 2005, Ho, 2006).

The coefficient of determination r^2 was

$$r^2 = \frac{\sum \left(q_m - \overline{q_e}\right)^2}{\sum \left(q_m - \overline{q_e}\right)^2 + \sum \left(q_m - q_e\right)^2}; \tag{5.4}$$

Where q_m is the equilibrium capacity obtained from the isotherm model, q_e is the equilibrium capacity obtained from experiment, and $\overline{q_e}$ is the average of q_e.

The Langmuir and the Redlich-Peterson isotherms have best fitted for the adsorption of gentamicin on Na^+-montmorillonite at 294 K.

Thermodynamic considerations of an adsorption process are necessary to conclude whether the process is spontaneous or not. Gibb's free energy change, $\Delta G°$, is the fundamental criterion of spontaneity. Reactions occur spontaneously at a given temperature if $\Delta G°$ is a negative value. Adsorption processes are calculated using the following equations:

$$\Delta G^o = -RT \ln K_a ; \qquad (5.5)$$

where R is universal gas constant (8.314 J/mol K) and T is the absolute temperature in K.

The thermodynamic parameters Gibb's free energy change, $\Delta G°$, are calculated using K_a which in obtained from Langmuir Eq. (5.1) and is shown in Table 5.3.

The Gibbs energy of adsorption was -1.119 kJ mol^{-1}. The negative values of Gibbs energy confirms the feasibility of the process and the spontaneous nature of adsorption of gentamicin on Na^+-montmorillonite

It is assumed that the cationic exchange sites in the clay, 92.6 meq/100 g, can adsorb certain amout of charged gentamicin due to protonation of $–NH_3^+$ and $–NH_2^+–$.The total charge depends on protonation state of hydroxyl group and amines at given pH. In the present work, the pH value in isotherm experiment was around 5.5. According to the study of Ganchev et al. (1973) and Lesniak et al. (2003), the ionic forms (Fig. 5.3) of gentamicin at our experimental pH should mainly be $Gentamicin^{5+}$, with small amout of $Gentamicin^{4+}$. The interlayer space

of smectites are known to be strongly acidic, thus it could be predicted that gentamicin were present only as Gentamicin^{5+} in the interlayer of montmorillonite in strong acidic environment. As a result, the total amount of gentamicin could be retained by the clay we used was around 0.232 mmol/g, deduced by CEC of the clay. In the sorption isotherm study, it was considered that sample e, f and g have reached maximum adsorption, and the amounts of gentamicin adsorbed by them were in the range of 0.22~0.24 mmol/g. The value proved that Gt^{5+} was the only ionic species of gentamicin intercalated into the clay interlayer.

Table 5.3: Isotherm parameters obtained using the non-linear method for the adsorption of gentamicin on Na^+-montmorillonite at 294 K.

Isotherm	T (K)	294
Langmuir	q_m, mg/g	184.2
	K_a, L/mg	0.0022
	r^2	0.978
Freundlich	$1/n$	0.375
	K_F, (mg/g)(L/mg)$^{1/n}$	7.51
	r^2	0.884
Redlich-Peterson	g	1.000
	B, (L/mg)^g	0.0024
	A, L/g	0.435
	r^2	0.978

We performed EDX measurement on starting montmorillonite (labeled as sample a), sample c, d and g. The EDX results indicate a decreasing Na^+ ratio and increasing carbon ratio with the increasing amout of gentamicin adsorbed on the clay Wt(Na^+) a > c > d > g (Table 5.4).

Table 5.4: EDX result of sodium weight percentage in the clay and Gt-Mt samples.

Sample No.	Wt(%) of Na to clay sample (EDX)	Wt(%) of C to clay sample	Gt. Uptake of the clay mmol/g	Wt(%) of Na to clay sample (estimated)
a	2.94	2.6	0	2.94 (EDX)
c	1.34	12.3	0.056	2.2
d	0.55	6.8	0.141	1.2
g	0.41	14.5	0.219	0.37

If we assume that all the exchangeable cations are Na^+, the weight percentage of Na^+ to Gt-Mt clay samples could be estimated by the amount of Gt. adsorbed on different clay samples. One gentamicin^{5+} molecule can exchange five Na^+ cations equivalently. Thus, the weight percentage of sodium of sample c, d and g can be estimated by:

$$w_t(\%) = \frac{m_{Na\,(i)} - m_{Na\,(e)}}{m_{clay} - m_{Na\,(e)} + m_{Gt}} \times 100\% = \frac{m_{Na\,(i)} - 5 \times n_{Gt} \times M_{Na}}{m_{clay} - 5 \times n_{Gt} \times M_{Na} + n_{Gt} \times M_{Gt}} \times 100\% \qquad (5.6)$$

$m_{Na(i)}$, $n_{Na(i)}$: initial mass and amount of substance of sodium in the clay (g);

$m_{Na(e)}$, mass lost of sodium due to exchange of gentamicin (g);

m_{clay}, initial mass of pure Na^+-montmorillonite (g);

m_{Gt}, n_{Gt}: mass and amount of substance of gentamicin intercalated in the clay (mol);

M_{Na}, M_{Gt}: molecular weight of sodium and gentamicin (g/mol),

The calculation results are shown in Table 5.4. The estimation shows the same trend of decreasing sodium ratio to Gt-Mt samples and the values are similar to EDX results. In this way, the predominance of ion-exchange mechanisms driving the intercalation of the gentamicin into the phyllosilicate substrate is experimentally confirmed.

5.3.2. Characterization, degradation and in vitro release experiment of Gt-Mt composites.

XRD characterization.

Figure 5.5 shows the XRD patterns of clay and gentamicin-clay nanocomposites. The intercalation of the gentamicin in the clay interlayers was confirmed by the decrease of 2θ values while the gentamicin/clay ratio increases. Sample e, f and g were obtained when gentamicin adsorption on clay reached saturation, which means these samples should have the same d_{001} spacing value. As shown in XRD results, the d_{001} spacing reaches 1.4 nm when the adsorption reaches equilibrium. However, sample d, which contains less gentamicin compared to e, f, g has same d_{001} spacing as those full cation-exchanged samples. In a study by Darder et al. (2003), the intercalation of chitosan in montmorillonite increases clay basal spacing to 1.4 nm when there's mono-layer of chitosan was uptaken by the clay. Because gentamicin molecule has similar structure as chitosan (both contain modified sugar rings), we believe that gentamicin intercalation has similar pattern as chitosan intercalation into clay shown in Scheme 4.1. The increase of clay d_{001} spacing was due to the thickness of gentamicin molecule sheet.

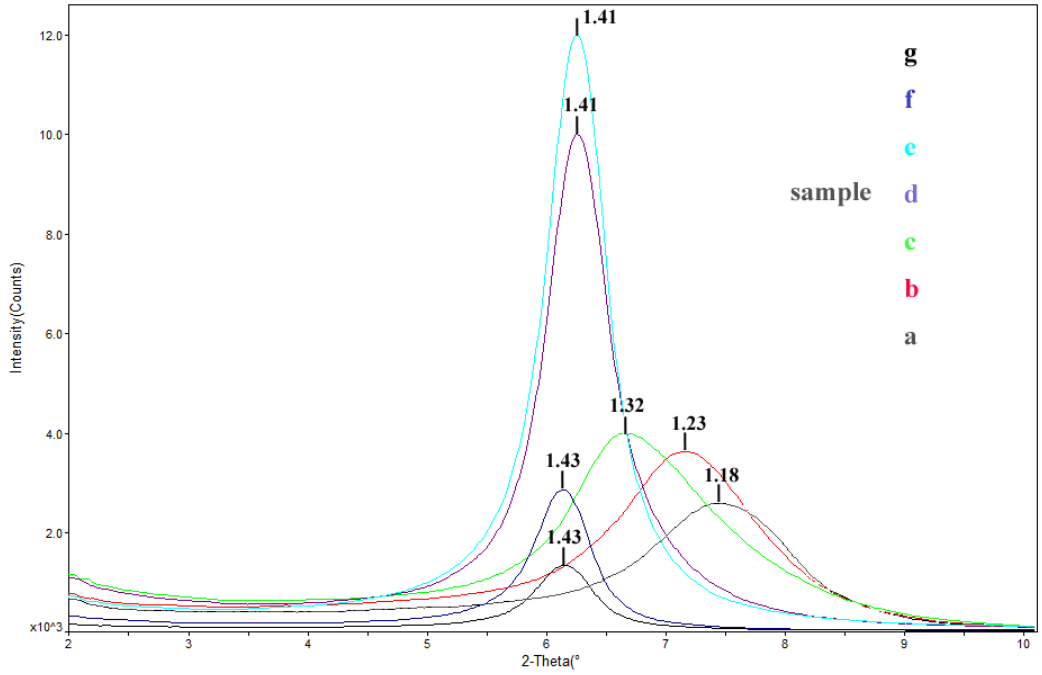

Figure 5.5: XRD patterns of a: starting montmorillonite; b, c, d e, f and g, samples obtained in isotherm study, d_{001} basal space unit: nm.

Scheme 5.1: Intercalation of gentamicin into Na^{+}-Montmorillonite.

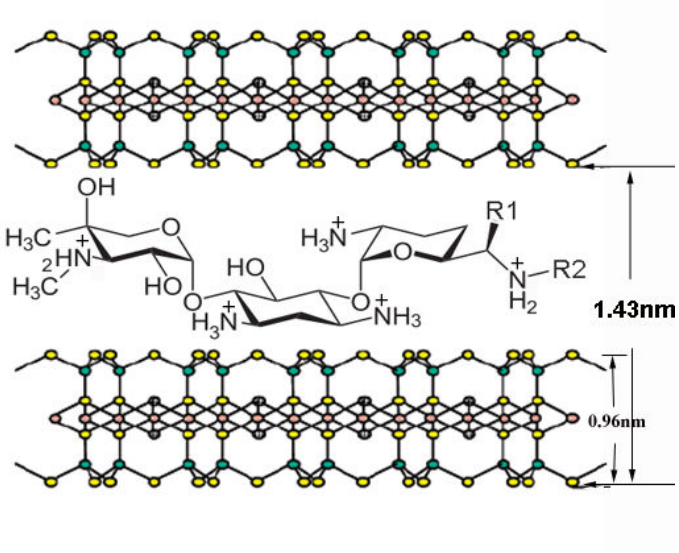

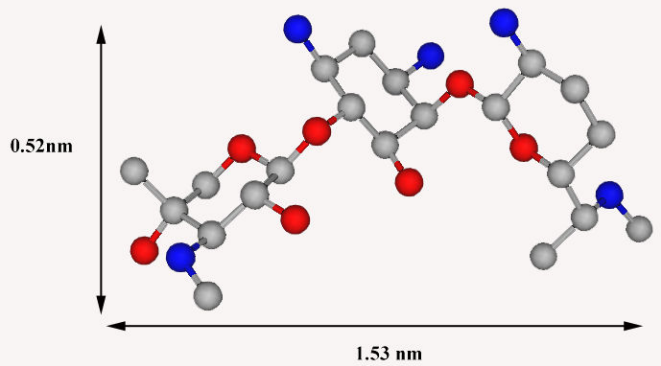

Figure 5.6: 3D gentamicin molecule (blue: N; red: O; grey: C, H atom was omitted).

Doadrio et al. (2004) reported the lower energy configuration of gentamicin (Fig. 5.6), with two-dimension size of a gentamicin molecular was around 0.52 × 1.53 nm^2. For sample e, f, g, distance between two consecutive smectite layers was about 0.47 nm, similar to the size of gentamicin molecule in one dimention (Scheme 4.1). The result showed that gentamicin molecule was intercalated as the configuration shown in Scheme 5.1, with the three ring chain of gentamicin molecule was positioned roughly paralled to the smectite layers.

In order to provide experimental confirmation of the optiomal layer spacing, the fwhm profile as a function of d_{001} of Gt-Mt samples was examined (Figure 5.7). Changes in fwhm have been attributed previously to the evolution of different configurations of the intercalated molecules, whereby, in a profile of fwhm values as a function of d_{001}, an increase in fwhm typically indicateds interstratifications of different layer types. Similar to the hypothesis put forth in the case of the adsorption of lysine on montmorillonite, a minimun in fwhm would be reached when the clay interlayers are saturated with adsorbed gentamicin, and the corresponding layer spacing would be considered optimal for the binding of gentamicin in the interlayer (Parbhakar et al., 2007; Wang et al., 2009; Aristilde et al., 2013). With the increasing amount of gentamicin intercalated in the clay, the FWHM was decreasing. When

the clay was saturated with gentamcin, the FWHM value reached the minimum level, which was proposed to be due a gradual change in the interlayer configuration occurring homogeneously within all layers, wherein the molecules would change position or orientation, for instance, from being stretched to a relatively flat chain molecure with high energy to being stable molecule chains less distorted.

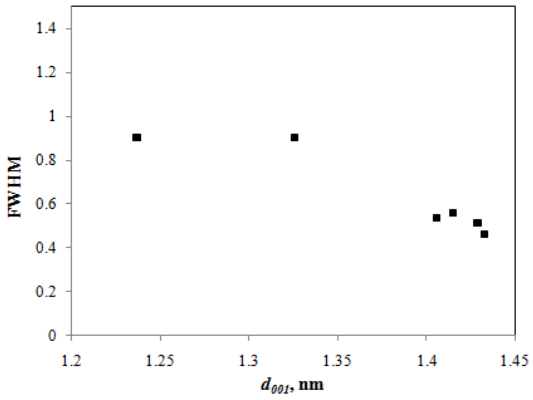

Figure 5.7: Changes in full-fixed width at half-maximum intensity (FWHM) as a function of d_{001} for Gt-Mt samples.

IR Spectroscopy

Besides the vibrational band characteristics of the silicate (νOH of Al, Mg(OH) 3633 cm^{-1}; νOH of H_2O 3451 and 3249 cm^{-1}; δHOH 1637 cm^{-1}; and νSiO of Si-O-Si 1045 cm^{-1}), the bands attributed to the intercalated gentamicin are also observed in the spectrum of gentamicin-clay composite (Figure 5.8). Also, vibrational bands (N-H in-plane deformation vibration of unprotonated amine group) of gentamicin overlap the bands (δHOH) of the silicate and a combination band is formed at 1632 cm^{-1} in gentamicin-clay composite. The frequency of vibrational bands at 1530 cm^{-1} in the gentamicin, which corresponds to symmetric deformation vibration (δNH_3^+) of the protonated primary amine group, is shifted to

1526 cm^{-1} after it is intercalated in clay. At about 1048 cm^{-1} of spectrum of gentamicin-clay sample, the vibration band for C-O-C of gentamicin overlaps band of Si-O-Si of the clay.

Thermal Stability

Thermal stability was investigated from DTA and TG curves recorded in the 30-990 °C range, under air flow conditions (Figure 5.9). Weight loss respected to water molecule desorption is completed at 87 °C and 160 °C for starting silicate and gentamicin-clay, respectively. Such a weight loss is about 4.6% in the starting silicate, while the gentamicin-clay composites show a slightly higher value 5.4%. This fact indicates the high water-retention capacity of gentamicin. A significant increase in thermal stability was observed by TG analysis for the gentamicin-clay nanocomposite respect to the starting gentamicin. The DTA curve of gentamicin-clay shows endothermic process of intercalated gentamicin started from around 237°C (melting point of gentamicin) and ended with an exothermic peak at ~600 °C when the combustion of gentamicin completed.

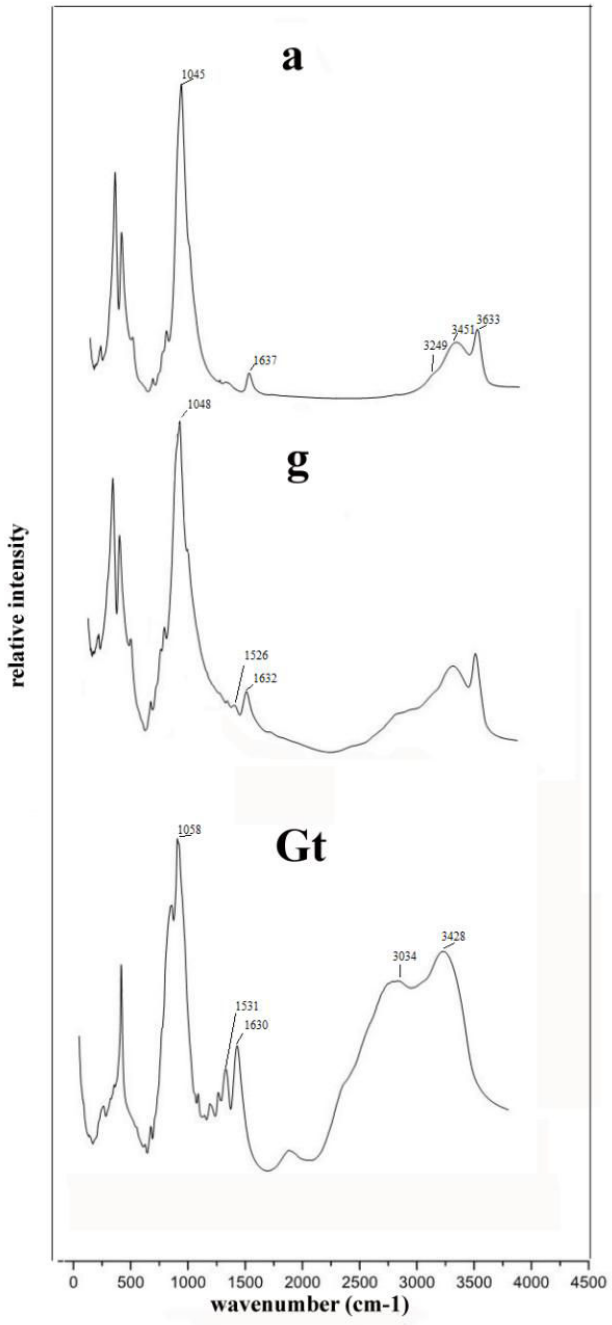

Figure 5.8: IR spectra (4000-350 cm^{-1} region) of the starting Na^{+}-montmorillonite (a), Gentamicin-Clay composite (sample g) (g), and starting gentamicin sulfate (Gt. sulfate)

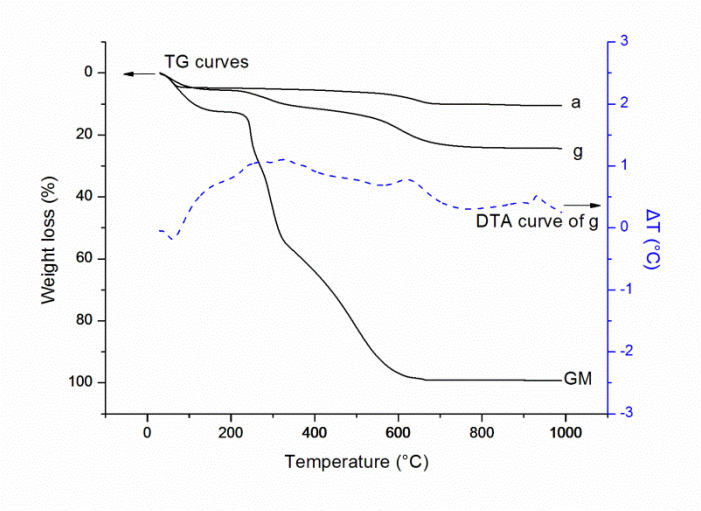

Figure 5.9: TG curves in the 30-990 °C temperature range (obtained under an air atmosphere) of Na^+-montmorillonite (a), gentamicin-clay nanocomposite (sample g) (g) and starting gentamicin sulfate (Gt.). The DTA curve corresponds to gentamicin-clay nanocomposite (sample g).

Photo Stability

The spectra of gentamicin-clay are shown in Figure 5.10. In 24 hours, there's no significant change on infrared spectrum. We can still see the same peaks that are assigned to vibration bands N-H and δNH_3^+ near 1600-1500 cm^{-1}. No new peak appears due to decomposition reaction. Kühn et al. (2008) studied stability of gentamicin in different antibiotic carriers. They indicated that the impurities and degradation products of gentamicin are garamin, 2-deoxy-streptamine and sisomicin with a background electrolyte containing 20 mM deoxycholic acid, 15 mM β-cyclodextrin and 100 mM tetraborate (pH 10.0). We presume that the photodegradation products in our study are the same as those considering no oxidation sign found in the infrared spectra. Another possibility is that degradation hadn't occurred in

24h UV-light decomposition test, because clay shows its protective effect on drug stability in other studies.

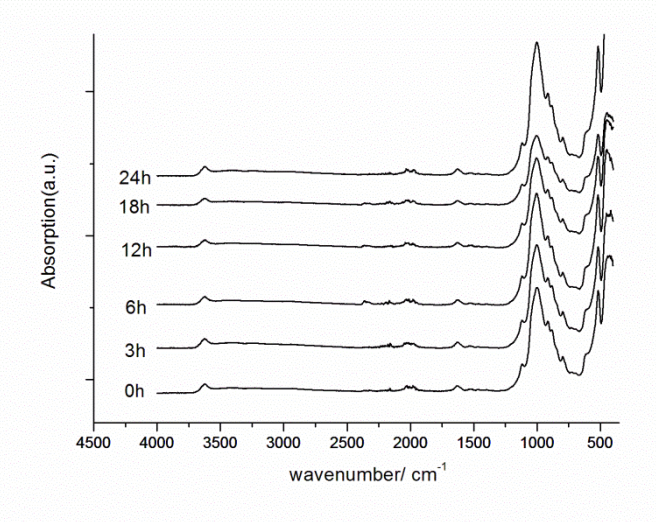

Figure 5.10: ATR-IR spectra (4000-350 cm^{-1} region) of gentamicin-clay nanocomposites (sample d) after continuous photodegradation test (under 254 nm UV light).

In vitro drug release

Results from chemical analysis show that there's no large amount of gentamicin had released from gentamicin-clay composite under our experimental condition in 72h. Gentamicin quantity adsorbed on clay slightly decreased from initial 0.17 mmol/g to 0.16 mmol/g 18 hours after the release experiment and gentamicin quantity of adsorption recovered to 0.17mmol/g. It can be considered that re-adsorption occurred. At pH 7, gentamicin is protonated as mixture of gentamicin^{3+}, gentamicin^{4+} and gentamicin^{5+}, which makes gentamicin compounds be steadily trapped in the interlayer of montmorillonite because of high electrostatic attraction.

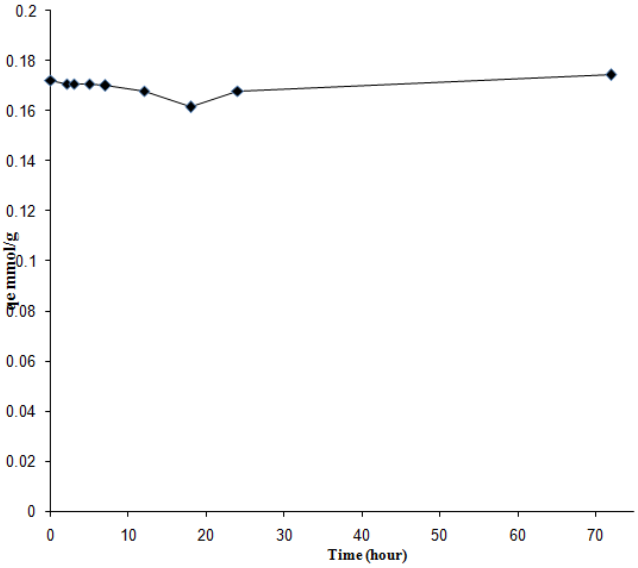

Figure 5.11: Release profile of gentamicin from gentamicin-clay (sample d) containing 50 mM PBS (pH=7) at 37 °C.

5.3.3. Gt-Mt-HPMC film

Morphology:

The morphology of the Gt-Mt-HPMC films containing nanocomposites was analyzed by FE-SEM. As shown in Fig 5.12, the morphologies of the films removed from the evaporation plastic plate are different on the two sides. Compared with the reverse R sides (toward the plates), Gt-Mt comopostites distribute more homogeneously in the obverse O sides of the films. Because the contents of Gt-Mt added to HPMC solution in film preparation vary from 2.2% to 3.5% (w/v), the void density of R sides of films decreases with increasing ratio of Gt-Mt to HPMC. The R sides contain more rough aggregated composites particles since larger particles having more mass than smaller particles (assuming that their density is the same) settle faster because of gravity. Through micrographs, we found the O sides of films have homogeneously distributed particles, as the matter of fact the O sides have clay-like coarse

touch while the R sides have plastic-like smooth touch since the HPMC component were formed against the plate. For the same reason, the R sides of the films are glossy while the O sides of films are dull by naked eyes observation.

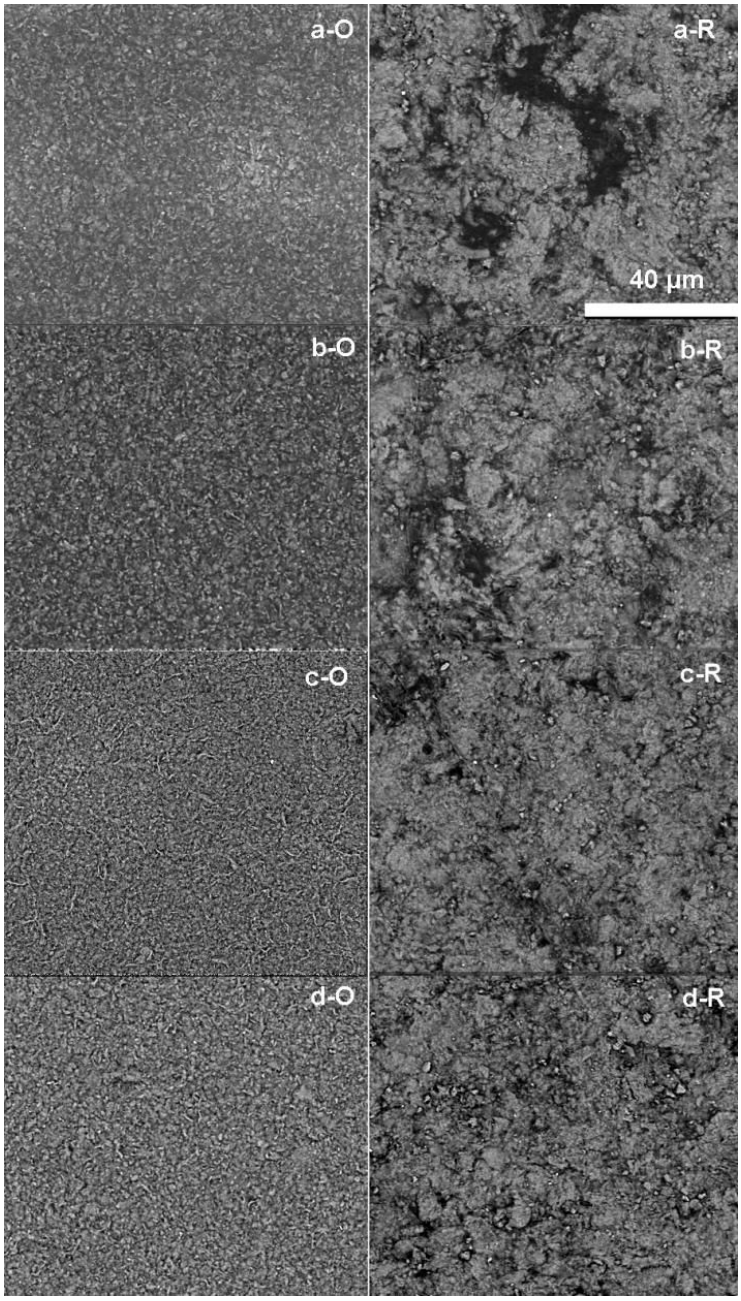

Figure 5.12: FE-SEM graphs of film samples (R: reverse side, O: observe side).

Table 5.5: Effect of Gt-Mt amount added in to 2% HPMC solution (w/v) on elastic modulus, and percent elongation of Gt-Mt-HPMC films produced by evaporation process.

Film No.	Gt-Mt porpotion in starting HPMC solution (w/v %)	Elastic modulus of films (GPa)	Elongation of films (%)
a	2.2	1.97 ± 0.14	1.62 ± 0.81
b	2.5	1.93 ± 0.52	1.25 ± 0.43
c	3.0	2.46 ± 0.29	1.53 ± 0.40
d	3.5	2.27 ± 1.01	2.11 ± 0.36

Mechanical Properties

The suitable use of antibiotics-loaded film is also strongly dependent on its favorable mechanical properties. Elastic modulus and elongation are parameters that are related with mechanical properties of films and their chemical structures (Dufresne and Vignon; 1998). Elastic modulus indicates the stiffness of the material, whereas elongation represents the capacity of the film for stretching (Alcântara et al., 2012). The pure HPMC film (2% w/v) has an elastic modulus of 1.2 GPa and percentage of elongation of break of 7.5% approximately. Table 5.5 shows the effects of Gt-Mt contents on elastic modulus and elongation at break values of the obtained Gt-Mt-HPMC films. The incorporating of Gt-Mt in the HPMC matrix gives an increase in the elastic modulus values to pure HPMC film but decrease in the value of elongation at break. Elastic modulus and elongation at break values of film sample c and d are slight higher than sample a and b, which is consistent with the morphology results showing Gt-Mt nanocomposites distribute more homogeneously in sample c and d than in

sample a and b. The voids exist in the R sides of sample a and b could contribute to their weaker mechanical properties and become the point from where the Gt-Mt-HPMC films start to crack.

Water uptake under moisture

Given that a balanced moist wound bed plays a key role for promoting wound healing, the composites can be designed to have an optimum recipe according to the patient wound. We studied water-absorption tendency of film a and d which contain highest and lowest portion of Gt-Mt based on HPMC. Figure 5.13 shows the weight increase due to water uptake expressed as grams of water incorporated per 100 gram of dry sample of BNC-HPMC with Gt-Mt as a function of the relative humidity (%). Before relative humidity reaches 80%, the water uptake capability of film a and film d differ little, while film a starts to adsorb more water vapor than film d at 80% or higher RH. The result shows that incorporation of Gt-Mt decreases slightly the water uptake capability of HPMC. Because of the amounts of Gt-Mt embed in HPMC film a and d don't vary largely, the difference of water uptake capability of two films is insignificant.

Antimicrobial activity of Gt-Mt-HPMC

Gt-Mt-HPMC and Gt-HPMC showed high antimicrobial properties compared with the control tube with peptone water. The samples HPMC or/and montmorillonite which were free of gentamicin showed no detectable antimicrobial effect. The result showed Gt-Mt-HPMC retained the antimicrobial capability of gentamicin. The efficiency of antimicrobial effect of the bionanocomposites was not weakened by the supporting material montmorillonite and HPMC.

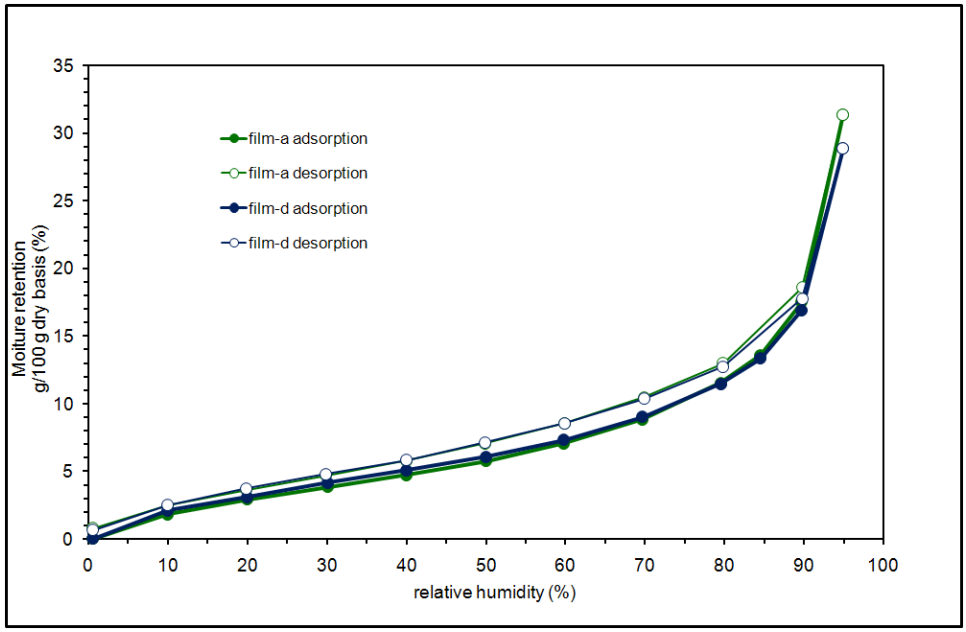

Figure 5.13: Effect of water uptake on two Gt-Mt-HPMC films(film-a and film-d).

Table 5.6: Antimicrobial effectiveness of Gt-Mt-HPMC film.

Sample description	**CFU/mL**	**CFU/mL**	**Mean**	**% reduction**
Control PW	9.40×10^6	9.80×10^6	9.60×10^6	-
Mt	1.20×10^7	1.06×10^7	1.13×10^7	-17.71%
HPMC	4.00×10^6	9.60×10^6	6.80×10^6	29.17%
Gt-HPMC	n.d.	n.d.	n.d,	100.00%
Gt-Mt-HPMC (3.0%)	n.d.	n.d	n.d.	100.00%

***% reduction: (CFU/mL control-CFU/mL sample)/CFU/mL control *100**

n.d. - not detectable

Related experiments are ongoing.

5.4. Conclusion

The adsorption of gentamicin onto Na^+-montmorillonite through cationic exchange mechanism is feasible, so montmorillonite can be used as removal reagent for decontaminating of high-gentamicin containing water in water treatment. The techniques employed in the characterization of the Gt-Mt (CHN chemical analysis, XRD, FTIR spectroscopy, EDX and thermal analysis) confirm the high affinity between the clay substrate and the gentamicin. The maximum d_{001} spacing of gentamicin-clay nanocomposite is 1.43 nm, which indicates that gentamicin orientation with the charged octahedral sheet is parallel to the basal surface and gentamicin molecules are not able to lap over each other but monolayer intercalation. The solid waste of the treatment – gentamicin loaded montmorillonite can be further incorporated with HPMC to form a bionanocomposites hybrid film for treating burn wound. Montmorillonite/HPMC offered better thermal stability and mechanical property for Gt-Mt (HPMC) nanocomposites than pure drug. Gt-Mt-HPMC and Gt-HPMC showed high antimicrobial properties compared with the control samples. The efficiency of antimicrobial effect of the bionanocomposites against *Staphylococcus aureus* was not weakened by the supporting material montmorillonite and HPMC. The releasing test of gentamicin from Gt-Mt preliminarily proved that clay mineral can counteract rapid release of antibiotics upon water uptake, which was one of the disadvantages of antibiotics-loaded natural polymer. The potential controlled-release mechanism of Gt-Mt-HPMC and anti-photodegradation behavior of Gt-Mt-HPMC will need to be further studied.

Chapter 6

Conclusions and perspectives

6.1. Conclusions

The importance of As removal from drinking water system

Drinking water contamination by arsenic in China is alarming. The problem is widespread throughout China - 19 provinces had been found to have As concentration in drinking water exceeding the standard level (0.05 mg/L) up to 2012.

A large population has been exposed to drinking water with high level of geogenic As which occurs mainly in the arid or semi-arid north of China. High-As spring or groundwaters are frequently found high pH value (≈8.5), reducing and located in low-lying areas. The climate, geochemical and hydrological conditions are favorable for As-rich water formation. Low precipitation-to-evaporation ratio leads to As-containing water becoming concentrated. High pH favors As being released and exchanged from minerals or rocks. In reducing conditions, As(III), which is more toxic and mobile than As(V), typically dominates. Low-lying closed basins make it hard for As to be flushed away. Because of surface water shortage, use of groundwater as water supply is more common in the North, where As-rich groundwaters are more likely to be discovered, than in the South.

As the same time, an increasing number of sudden and accidental As pollution events is taking place due to human activities. Those accidents usually happen in subtropical or tropical south of China where there are plenty of As-rich ores. Intensive chemical plants, smelting and mining activities increase the likelihood of pollution accidents. Contamination cases are usually triggered by heavy rains or floods which flushed the highly concentrated As-containing waste water/sluge directly into natural waters.

The synthesis and application of CGB in As removal

No matter for chronic endemic arsenicosis or for acute As poisoning cases, effective actions should be taken. High-As water need to be well treated according to water standard or guideline till its concentration reach the safe level. Adsorption - one of water treatment techniques - is used for excess arsenic contaminants removal from aqueous solution in our study. The most well-known adsorbents used in adsorption is activated carbon in modern times. However, its widespread use is restricted due to high cost. As such, numerous alternative materials have been investigated.

The novel material was synthesized in our study for removing arsenic from contaminated water: chitosan goethite bionanocomposite (CGB) bead.

CGB can adsorb both As(III) and As(V) efficiently. With initial arsenite and arsenate concentrations of 5.6 mmol/L and 7 mmol/L, the adsorbed quantities of the arsenate-adsorbed beads were 0.113 mmol/g, at pH=5 and 0.052 mmol/g, at pH=9, and that of the arsenite-adsorbed beads were 0.151 mmol/g, at pH=5 and 0.156 mmol/g, at pH=9. Isotherm study and pH effect on arsenic adsorption onto CGB reveal that pH value change is more significant for arsenate adsorption than arsenite, which could affect the surface charge of chitosan as well as goethite so that the electrical attraction between arsenate and material were weaken sharply while it has less effect on neutral arsenite molecule. Hence, manipulation of pre-oxidation of As(III)-contained water for enhancing As removal rate is not necessary. The kinetics study indicated As(V) was adsorbed faster than As(III), and pseudo-equilibrium to be reached in both cases within 2000 min. Diffusion of As(V) within the CGB beads was, according to

micro X-ray fluorescence, faster for As(V) than for As(III), and the later was partly oxidized, according to micro-XANES investigation. CGB beads are suitable to be used in rural areas for people don't have tap water and advanced water treatment plants. The material is safe, easy and practical to use in daily life. The results of leaching test prove CGB doesn't pose potential health risk by releasing nano-particle or toxic element in application. The mechanical property test shows that the material is very rigid and stable so that it's easy for storage, transport and daily use. The size and density of CGB allow users to obtain decontaminated water without need of complicated or energy-consuming separation procedure, since the large-size CGB applied in remediation process would precipitate at the bottom of the water container or could be kept in permeable porous textile or plastic bags. These possibilities highly reduce the cost and complexity of As water treatment process especially for underdeveloped areas.

Antibiotics pollution in China waters

Antibiotics presence has become a focus of research efforts due to different advert effects it causes, especially the contribution to antibiotic resistant bacteria in the environment. Such resistant bacteria can cause an infection both in humans and animals and may not respond to regular antibiotic treatments. Human and animal faeces, hospital effluents, pharmaceutical industries and municipal sewage influent that contain antibiotics result in antibiotic residue in surface water and ground water.

As China is the largest producer and consumer of antibiotics in the world, antibiotics have been found widespread in WWTPs and environment frequently. Densely populated areas are prone to antibiotics contamination. The review of antibiotic presence in WWTPs and natural

waters in China shows the diversity of antibiotics in the water cycles with high concentration. In some water bodies, the levels of antibiotics are in the same range of that in WWTPs. Presence of antibiotics in tap water of two cities in China (concentration up to 697 ng/L) reflects the fact that public is exposed to potential risk by long-term intake of antibiotics via drinking water (Wang et al., 2010).

Removal of gentamicin by clay mineral and the synthesis of hybrid film by resulting composites

The adsorption of gentamicin onto Na^+-montmorillonite through cationic exchange mechanism is feasible. Gentamicin molecule can be intercalated into clay. The techniques employed in the characterization of the nanocomposites, CHN chemical analysis, XRD, FTIR spectroscopy, EDX, and thermal analysis, confirm the high affinity between the clay substrate and the gentamicin. Gentamicin-clay nanocomposites have better thermal stability than pure drug. The maximum d001 spacing of gentamicin-clay nanocomposite is 1.43 nm, which indicates that gentamicin orientation with the charged octahedral sheet is parallel to the basal surface and gentamicin molecules are not able to lap over each other but monolayer intercalation. In 24-hour photodecomposition test, nanocomposites had no distinct changes on structures of functional groups. In vitro release experiment confirmed the strong affinity between the clay and gentamicin also. Gentamicin rarely released from nanocomposite under neutral pH in 3 days.

Gt-Mt-HPMC (gentamicin-loaded montmorillonite based on hydroxypropyl methycellulose) hybrid film was prepared for the possible use of skin wound treatment. Fe-SEM results reveal

that obverse (O) and reverse (R) sides of the films show different morphology. Gt-Mt comopostites distribute more homogeneously in the obverse O side of the films than the other side. The R sides contain more roughly aggregated composites particles. The void density of R sides of films decreases with increasing ratio of Gt-Mt to HPMC.

Mechanical property tests show that the incorporating of Gt-Mt in the HPMC matrix gives an increase in the elastic modulus values to pure HPMC film but decrease in the value of elongation at break. Elastic modulus and elongation at break values of film sample c and d (3% and 3.5% Gt-Mt in HPMC solution) are slight higher than sample a and b (2.2% and 2.5% Gt-Mt in HPMC solution), which is consistent with the morphology results showing Gt-Mt nanocomposites distribute more homogeneously in sample c and d than in sample a and b. The voids exist in the R sides of sample a and b could contribute to their weaker mechanical properties and become the point where the Gt-Mt-HPMC films start to crack.

Result of water absorption tests indicates that this hybrid film shows water retention property. Since the concentrations of Gt-Mt in 4 different samples don't vary largely, and both of HPMC and montmorillonite have water retention, the water absorption quantities of sample a and d are close, having a 30% mass change under 100% of RH at 25 ℃ without big difference for two samples.

Gt-Mt-HPMC and Gt-HPMC showed high antimicrobial properties compared with the control samples. The efficiency of antimicrobial effect of the bionanocomposites against *Staphylococcus aureus* was not weakened by the supporting material montmorillonite and HPMC.

6.2. Further work

As presence in China

Previous investigations of a number of affected sites in China have given people a better understanding of the As-contamination problem. However, most information are mainly about heavily contaminated water bodies with water As concentrations above 0.05 mg/L. Future research should attach importance to contaminated water with As concentration of 0.01 mg/L-0.05 mg/L according to the WHO guideline for drinking water. Low concentration of arsenic could be dangerous if there's a high ratio of As(III) to total As, thus knowledge on the speciation of arsenic is gaining increasing importance because toxicological effects of arsenic are connected to its chemical form and oxidation states. Arsenic speciation is important and necessary to be investigated for coming studies.

Besides, more researches should focus on understanding the occurrence, origin and distribution of arsenic. Government should pay more attention to industrial and agricultural activities which lead to As pollution, giving more technical supports to mining or chemical plants and managing supervision departments to carry out sampling and analyzing of the discharge from industrial plants.

Chitosan-geothite bionanocomposites (CGB) for arsenic removal

As contaminated groundwater which usually contains Ca, Mg, bicarbonate, phosphate, DOC and other components will need to be used in arsenic adsorption experiments in order to study the effect of these components on the As removal by CGB.

The recycling of As-loaded CGB will be studied. Two possible methods could be taken into consideration: i) regeneration of As-loaded by chemical reagents like NaOH; ii) possible means to transform As-loaded CGB into other phase or form to be reused into other industrial domains.

Since CGB beads, in our study, are designed for cleaning drinking water which is supposed to contain not very high concentration of As, after-use CGB beads might have not reached saturation and have capability to adsorb more contaminants in heavy polluted water, e.g. industrial waste waters. The regeneration of used CGB could be carried out after CGB material having been completely used and reached saturation. The sorption efficiency of regenerated CGB should be studied compared with primary CGB beads.

As a polymer-containing material with elasticity properties, there is possibility to apply CGB into road construction material. To be used as Solid Roads Polymer Soil Stabilizers, the incorporation of a polymer allows for a long lasting sub-base and wearing course while decreasing roll resistance and increasing performance. Increased surface elasticity will prohibit the formation of potholes, cracking and swelling due to traffic load or temperature change.

Different starting ratio of $FeCl_3$ reagent to chitosan could be tested to form beads with different composition. The ratio effect on resulting material will be studied. Magnetic field could be introduced into the fabrication process and the effect of the magnetic field could be interesting to investigate because goethite or other Fe-containing magnetic materials might be formed in the fabrication.

Antibiotics removal and medical film

The present study has demonstrated that gentamicin, as one kind of widely used antibiotics for the treatment of human and veterinary infectious diseases as well as animal feed additives, can be adsorbed by low-cost clay material montmorillonite. However, the gentamicin-containing solutions were prepared in the chemistry lab. To investigate the real-life application of montmorillonite in removing gentamicin, water samples from disposal of sewage, hosipital wastewater, animal wastewater, etc. should be used in the future study. Besides wastewaters, antibiotic residues in natural waters with relative low concentration (less than 1000 ng/L) also draw public concerns since they can pose potential threats to public health and environment. Research related to gentamicin-containing water with low concentration should be carried out. This would require more sensitive instrument such as LC-MS/MS to be used for the examination of low concentration gentamicin. Futhermore, studies on application of montmorillonite in removing other kinds of antibiotic could be carried out, especially positive charged antibiotics due to probable electrostatic attraction between antibiotic and clay.

The Gt-Mt-HPMC film hybrid material can also be used as wound dressing. Besides *Staphylococcus aureus*, resistance or inhibition behavior of this film with other common bacteria, which cause skin infection such as *Pseudomonas aeruginosa*, etc. will be investigated. Clinical trials on this new drug could be carried out to assess its effect on skin wounds based on exudate amounts, wound tissue color and whether the wound become infected. The potential controlled-release mechanism of Gt-Mt-HPMC and anti-photodegradation behaviour of Gt-Mt-HPMC will need to be further studied.

Reference

Acharyya, S., 2005. Arsenic levels in groundwater from quaternary alluvium in the ganga plain and the bengal basin, indian subcontinent: Insights into influence of stratigraphy. Gondwana Res., 8(1), 55-66.

Adams, C., Wang, Y., Loftin, K., Meyer, M., 2002. Removal of antibiotics from surface and distilled water in conventional water treatment processes. Journal of environmental engineering, 128(3), 253-260.

Aksoy, N., Simsek, C., Gunduz, O., 2009. Groundwater contamination mechanism in a geothermal field: A case study of Balcova, Turkey. J. Contam. Hydrol. 103, 13-28.

Akter, F., Amin, M.R., Osman, K.T., Anwar, M.N., Karim, M.M., Hossain, M.A., 2012. Ciprofloxacin-resistant escherichia coli in hospital wastewater of bangladesh and prediction of its mechanism of resistance. World J. Microb. Biot., 28(3), 827-834.

Amini, M., Abbaspour, K.C., Berg, M., Winkel, L., Hug, S.J., Hoehn, E., Yang, H., Johnson, C.A., 2008. Statistical modeling of global geogenic arsenic contamination in groundwater. Environ. Sci. Technol., 42(10), 3669-3675.

Angelone, M., Cremisini, C., Piscopo, V., Proposito, M., Spaziani, F., 2009. Influence of hydrostratigraphy and structural setting on the arsenic occurrence in groundwater of the cimino-vico volcanic area (central italy). Hydrogeol. J., 17(4), 901-914.

Ankudinov, A.L., Ravel, B., Rehr, J.J., Conradson, S.D., 1998. Real-space multiple-scattering calculation and interpretation of x-ray-absorption near-edge structure. Phys. Rev. B, 58(12), 7565-7576.

Appelo, C.A.J., Van der Weiden, M.J.J., Tournassat, C., Charlet, L., 2002. Surface complexation of ferrous iron and carbonate on ferrihydrite and the mobilization of arsenic. Environ. Sci. Technol. 36, 3096-3103.

Aristilde, L., Lanson, B., Charlet, L., 2013. Interstratification patterns from the ph-dependent intercalation of a tetracycline antibiotic within montmorillonite layers. Langmuir., 29(14), 4492-4501.

Ash, R.J., Mauck, B., Morgan, M., 2002. Antibiotic resistance of gram-negative bacteria in rivers, united states. Emerg. Infect. Dis., 8(7), 713-716.

Auffan, M., Rose, J., Bottero, J.-Y., Lowry, G.V., Jolivet, J.-P., Wiesner, M.R., 2009. Towards a definition of inorganic nanoparticles from an environmental, health and safety perspective. Nature nanotechnology, 4(10), 634-641.

Aureli, A., 2006. Preface. In: Appelo, T. (Ed.), Arsenic in Groundwater- A World Problem. NNC-IAH Publication, Utrecht, pp. ii.

Aviv, M., Berdicevsky, I., Zilberman, M., 2007. Gentamicin‐loaded bioresorbable films for prevention of bacterial infections associated with orthopedic implants. Journal of Biomedical Materials Research Part A, 83(1), 10-19.

Ballantyne, J.M., Moore, J.N. 1988. Arsenic geochemistry in geothermal systems. Geochim. Cosmochim. Acta. 52, 475-483.

Bardelli, F., Benvenuti, M., Costagliola, P., Di Benedetto, F., Lattanzi, P., Meneghini, C., Romanelli, M., Valenzano, L., 2011. Arsenic uptake by natural calcite: An XAS study. Geochim Cosmochim Acta. 75, 3011-3023.

Barkovskii, A.L., Bridges, C., 2012. Persistence and profiles of tetracycline resistance genes in swine farms and impact of operational practices on their occurrence in farms' vicinities. Water Air. Soil Poll., 223(1), 49-62.

Bates, M.N., Smith, A.H., Hopenhaynrich C., 1992. Arsenic ingestion and internal cancers - a review, Am. J. Epidemiol. 135 (5), 462-476.

Benotti, M.J., Trenholm, R.A., Vanderford, B.J., Holady, J.C., Stanford, B.D., Snyder, S.A., 2008. Pharmaceuticals and endocrine disrupting compounds in us drinking water. Environ. Sci. Technol., 43(3), 597-603.

Berkowitz, A.E., Rodriguez, G.F., Hong, J.I., An, K., Hyeon, T., Agarwal, N., Smith, D.J., Fullerton, E.E., 2008. Antiferromagnetic mno nanoparticles with ferrimagnetic mn(3)o(4) shells: Doubly inverted core-shell system. Phys. Rev. B, 77(2).

Bhattacharya, P., Claesson, M., Bundschuh, J., Sracek, O., Fagerberg, J., Jacks, G., Martin, R.A., Storniolo, A.D., Thir, J.M., 2006. Distribution and mobility of arsenic in the Rio Dulce alluvial aquifers in Santiago del Estero Province, Argentina. Science of the Total Environment, 358 (1-3), 97-120.

Bhattacharya, P., Jacks, G., Ahmed, K.M., Routh, J., Khan, A.A., 2002. Arsenic in groundwater of the bengal delta plain aquifers in bangladesh. B. Environ. Contam. Tox, 69(4), 538-545.

Bocquet, S., Pollard, R.J., Cashion, J.D., 1995. Shape anisotropy in antiferromagnetic superparamagnetic particles. J. Appl. Phys., 77(6), 2809-2810.

Boyd, S.A., Sheng, G., Teppen, B.J., Johnston, C.T., 2001. Mechanisms for the adsorption of substituted nitrobenzenes by smectite clays. Environ. Sci. Technol., 35(21), 4227-4234.

Boyle, R.W., Jonasson, I.R., 1973. The geochemistry of As and its us as an indicator element in geochemical prospecting. J. Geochem. Explor. 2, 251-296.

Breit, G., Guo, H.M., 2012. Geochemistry of arsenic during low-temperature water-rock interaction Preface. Applied Geochemistry, 27(11), 2157-2159.

Butko, P., Salamon, Z., Tien, H., 1990. Adsorption of gentamicin onto a bilayer lipid membrane. Journal of electroanalytical chemistry and interfacial electrochemistry, 298(2), 153-160.

Chang, P.-H., Li, Z., Jean, J.-S., Jiang, W.-T., Wang, C.-J., Lin, K.-H., 2012. Adsorption of tetracycline on 2: 1 layered non-swelling clay mineral illite. Appl. Clay. Sci., 67, 158-163.

Charlet, L., 1994. Reactions at the mineral-water interface. In: Bidoglio, G., Stumm, W. (Eds.), Chemistry of aquatic systems: Local and global perspectives. Kluwer Academic, Dordrecht, pp. 290-293.

Charlet, L., Morin, G., Rose, J., Wang, Y.H., Auffan, M., Burnol, A., Fernandez-Martinez, A., 2011. Reactivity at (nano)particle-water interfaces, redox processes, and arsenic transport in the environment. C. R. Geosci. 343, 123-139.

Charlet, L., Polya, D.A., 2006. Arsenic in shallow, reducing groundwaters in southern asia: An environmental health disaster. Elements, 2(2), 91-96.

Chassary, P., Vincent, T., Guibal, E., 2004. Metal anion sorption on chitosan and derivative materials: A strategy for polymer modification and optimum use. React. Funct. Polym., 60, 137-149.

Chatterjee, S., Lee, M.W., Woo, S.H., 2009. Enhanced mechanical strength of chitosan hydrogel beads by impregnation with carbon nanotubes. Carbon, 47(12), 2933-2936.

Chen, C.J., 1990. Black foot disease. Lancet. 336 (8712). 442-442.

Chen, C.J., Hsueh, Y.M., Lai, M.S., Shyu, M.P., Chen, S.Y., Wu, M.M., Kuo, T.L., Tai, T.Y., 1995. Increased prevalence of hypertension and long-term arsenic exposure. Hypertension. 25, 53-60.

Chen, J.B., Zhou, X.F., Zhang, Y.L., Gao, H.P., 2012. Potential toxicity of sulfanilamide antibiotic: Binding of sulfamethazine to human serum albumin. Sci. Total. Environ., 432, 269-274.

Chen, M., Wang, D.S., Zhang, B.Z., 2010. Analysis of sudden incidents of secondary arsenic pollution. Chin. Emerg. Manage. 4, 40-50.

Coleman, B.L., Louie, M., Salvadori, M.I., McEwen, S.A., Neumann, N., Sibley, K., Irwin, R.J., Jamieson, F.B., Daignault, D., Majury, A., Braithwaite, S., Crago, B., McGeer, A.J., 2013. Contamination of canadian private drinking water sources with antimicrobial resistant escherichia coli. Water Res., 47(9), 3026-3036.

Colombo, P., 1993. Swelling-controlled release in hydrogel matrices for oral route. Adv. Drug Deliver. Rev, 11(1), 37-57.

Conversation, T., 2013. China's farms pose growing antibiotic resistance risk.

Courrier International, 2009. Quand la Chine mourra de soif. No. 987, 01 Oct, 2009, pp, 38-45. http://www.courrierinternational.com/magazine/2009/987-quand-la-chine-mourra-de-soif

CWRC 2005-2013. The General to the Yangtze River Basin. From http://eng.cjw.gov.cn/eng-about.asp

Darder, M., Aranda, P., Ruiz-Hitzky, E., 2007. Bionanocomposites: A new concept of ecological, bioinspired, and functional hybrid materials. Adv. Mater., 19(10), 1309-1319.

Darder, M., Colilla, M., Ruiz-Hitzky, E., 2003. Biopolymer-clay nanocomposites based on chitosan intercalated in montmorillonite. Chem. Mater., 15(20), 3774-3780.

Deng, Y.M., 2008. Geochemical processes of high arsenic groundwater system at western Hetao Basin. China University of Geosciences (Wuhan).

Deng, Y.M., Wang, Y.X., Ma, T., Gan, Y.Q., 2009. Speciation and enrichment of arsenic in strongly reducing shallow aquifers at western Hetao Plain, northern China. Environ. Geol. 56, 1467-1477.

Dias, A., Hussain, A., Marcos, A.S., Roque, A.C.A., 2011. A biotechnological perspective on the application of iron oxide magnetic colloids modified with polysaccharides. Biotechnol. Adv., 29(1), 142-155.

Dixit, S., Hering, J.G., 2003. Comparison of arsenic(v) and arsenic(iii) sorption onto iron oxide minerals: Implications for arsenic mobility. Environ. Sci. Technol., 37(18), 4182-4189.

Doadrio, A., Sousa, E., Doadrio, J., Pérez Pariente, J., Izquierdo-Barba, I., Vallet-Regı, M., 2004. Mesoporous sba-15 hplc evaluation for controlled gentamicin drug delivery. Journal of Controlled Release, 97(1), 125-132.

Doelker, E., 1987. Water-swollen cellulose derivatives in pharmacy. Hydrogels in medicine and pharmacy, 2, 115-160.

Dufresne, A., Vignon, M.R., 1998. Improvement of starch film performances using cellulose microfibrils. Macromolecules., 31(8), 2693-2696.

Dzombak, D.A., Morel, F.M.M. 1990. Surface Complexation Modeling: Hydrous Ferric Oxide, Wiley-Interscience, New York.

Elmanama, A.A., Elaiwa, N.M., El-Ottol, A.E.Y., Abu-Elamreen, F.H., 2006. Antibiotic resistance of uropathogens isolated from al-shifa hospital in gaza strip in 2002. J. Chemotherapy., 18(3), 298-302.

Elsner, J.J., Egozi, D., Ullmann, Y., Berdicevsky, I., Shefy-Peleg, A., Zilberman, M., 2011. Novel biodegradable composite wound dressings with controlled release of antibiotics: Results in a guinea pig burn model. Burns, 37(5), 896-904.

Emsley, J., 2001. Nature's building blocks:An a-z guide to the elements, 43. Oxford University Press, Oxford.

Engel, R.R., Hopenhaynrich, C., Receveur, O., Smith, A.H., 1994. Vascular eects of chronic arsenic exposure - a review. Epidemiol. Rev. 16, 184-209.

Environmental Protection Agency of Yunnan, 2008-2010. Highland Lake Water Quality Report.From:http://www.ynepb.gov.cn/color/default.aspx

EPA, U.S., 2000. Technologies and costs for removal of arsenic from drinking water. In: Water, O.o. (Ed.).

Fan, H., Su, C., Wang, Y., Yao, J., Zhao, K., Wang, Y., Wang, G., 2008. Sedimentary arsenite-oxidizing and arsenate-reducing bacteria associated with high arsenic groundwater from Shanyin, Northwestern China. J. Appl. Microbiol. 105 (2), 529-539.

Fendorf, S., Michael, H.A., van Geen, A., 2010. Spatial and temporal variations of groundwater arsenic in south and southeast asia. Science, 328(5982), 1123-1127.

Fernandez-Martinez, A., Roman-Ross, G., Cuello, G.J., Turrillas, X., Charlet, L., Johnson, M.R., Bardelli, F., 2006. Arsenic uptake by gypsum and calcite: Modelling and probing by neutron and X-ray scattering. Phys. B Condens. Matter. 385-86, 935-937

Freundlich, H.M.F., 1906. ber die adsorption in lösungen. Z. Phys. Chem., 57A, 385-470.

Gao, L.H., Shi, Y.L., Li, W.H., Niu, H.Y., Liu, J.M., Cai, Y.Q., 2012. Occurrence of antibiotics in eight sewage treatment plants in beijing, china. Chemosphere, 86(6), 665-671.

Garcia, S., Wade, B., Bauer, C., Craig, C., Nakaoka, K., Lorowitz, W., 2007. Effect of wastewater treatment on antibiotic resistance in escherichia coli and enterococcus sp. Water Environ. Res., 79(12), 2387-2395.

Gehring, R., Haskell, S.R., Payne, M.A., Craigmill, A.L., Webb, A.I., Riviere, J.E., 2005. Aminoglycoside residues in food of animal origin. J. Am. Vet. Med. Assoc., 227(1), 63-66.

Ghosh, G., Okuda, T., Yamashita, N., Tanaka, H., 2009. Occurrence and elimination of antibiotics at four sewage treatment plants in japan and their effects on bacterial ammonia oxidation.

Gonzalez-Pleiter, M., Gonzalo, S., Rodea-Palomares, I., Leganes, F., Rosal, R., Boltes, K., Marco, E., Fernandez-Pinas, F., 2013. Toxicity of five antibiotics and their mixtures towards photosynthetic aquatic organisms: Implications for environmental risk assessment. Water Res., 47(6), 2050-2064.

Gros, M., Rodriguez-Mozaz, S., Barcelo, D., 2013. Rapid analysis of multiclass antibiotic residues and some of their metabolites in hospital, urban wastewater and river water by ultra-high-performance liquid chromatography coupled to quadrupole-linear ion trap tandem mass spectrometry. Journal of Chromatography A, 1292, 173-188.

Guardabassi, L., Wong, D., Dalsgaard, A., 2002. The effects of tertiary wastewater treatment on the prevalence of antimicrobial resistant bacteria. Water Res., 36(8), 1955-1964.

Guibal, E., Milot, C., Tobin, J.M., 1998. Metal-anion sorption by chitosan beads: Equilibrium and kinetic studies. Ind. Eng. Chem. Res., 37(4), 1454-1463.

Gulkowska, A., Leung, H.W., So, M.K., Taniyasu, S., Yamashita, N., Yeunq, L.W.Y., Richardson, B.J., Lei, A.P., Giesy, J.P., Lam, P.K.S., 2008. Removal of antibiotics from wastewater by sewage treatment facilities in hong kong and shenzhen, china. Water Res., 42(1-2), 395-403.

Guo, H.M., Wang, Y.X., 2005. Geochemical characteristics of shallow groundwater in Datong basin, northwestern China. J. Geochem. Explor. 87, 109-120.

Guo, H.M., Wang, Y.X., Li, H.M., 2003. Analysis of factors resulting in anomalous arsenic concentration in groundwaters of Shanyin, Shanxi Province. Environ. Sci. 24(4), 60-67.

Guo, X.J., Chen, F.H., 2005. Removal of arsenic by bead cellulose loaded with iron oxyhydroxide from groundwater. Environ. Sci. Technol., 39(17), 6808-6818.

Han, S. B., Zhang, F.C., Zhang, H., Jia, X.F., He, J., Li, X.F., 2010. An analysis of the distribution and formation of high arsenic groundwater in northern China. Geol. Chin. 37, 747-753.

Health Surveillance, A.H.a.W., 2000. Arsenic in groundwater from domestic wells in three areas of northern alberta, Health Surveillance-Alberta Health and Wellness, Edmonton, Alberta.

Ho, Y.S., 2004. Selection of optimum sorption isotherm. Carbon, 42(10), 2115-2116.

Ho, Y.S., 2006. Isotherms for the sorption of lead onto peat: Comparison of linear and non-linear methods. Pol. J. Environ. Stud., 15(1), 81-86.

Ho, Y.S., Huang, C.T., Huang, H.W., 2002. Equilibrium sorption isotherm for metal ions on tree fern. Process Biochem., 37, 1421-1430.

Ho, Y.S., McKay, G., 1999. Pseudo-second order model for sorption processes. Process. Biochem., 34(5), 451-465.

Ho, Y.S., McKay, G., 2000. The kinetics of sorption of divalent metal ions onto sphagnum moss peat. Water Res., 34(3), 735-742.

Ho, Y.S., Ofomaja, A.E., 2005. Kinetics and thermodynamics of lead ion sorption on palm kernel fibre from aqueous solution. Process. Biochem., 40(11), 3455-3461.

Holmstrom, K., Graslund, S., Wahlstrom, A., Poungshompoo, S., Bengtsson, B.E., Kautsky, N., 2003. Antibiotic use in shrimp farming and implications for environmental impacts and human health. Int. J. Food Sci. Tech., 38(3), 255-266.

Hopenhayn-Rich, C., Biggs, M.L., Smith, A.H., 1998. Lung and kidney cancer mortality associated with arsenic in drinking water in cordoba, argentina. Int. J. Epidemiol., 27(4), 561-569.

Hopenhayn-Rich, C., Browning, S.R., Hertz-Picciotto, I., Ferreccio, C., Peralta, C., Gibb, H., 2000. Chronic arsenic exposure and risk of infant mortality in two areas of Chile. Environ. Health. Perspect. 108, 667-673.

Huang, H., Lee, S.C., Cao, J.J., Zou, C.W., Chen, X.G., Fan, S.J., 2007. Characteristics of indoor/outdoor PM2.5 and elemental components in generic urban, roadside and industrial plant areas of Guangzhou City, China. J. Environ. Sci.-Chin. 19, 35-43.

Huang, J.J., Hu, H.Y., Lu, S.Q., Li, Y., Tang, F., Lu, Y., Wei, B., 2012. Monitoring and evaluation of antibiotic-resistant bacteria at a municipal wastewater treatment plant in china. Environ. Int., 42, 31-36.

James, F., Roos, M., 1975. Minuit - system for function minimization and analysis of parameter errors and correlations. Comput. Phys. Commun., 10(6), 343-367.

Jiang, L., Hu, X.L., Yin, D.Q., Zhang, H.C., Yu, Z.Y., 2011. Occurrence, distribution and seasonal variation of antibiotics in the huangpu river, shanghai, china. Chemosphere, 82(6), 822-828.

Jin, L., Bai, R.B., 2002. Mechanisms of lead adsorption on chitosan/pva hydrogel beads. Langmuir., 18(25), 9765-9770.

Karci, A., Balcioglu, I.A., 2009. Investigation of the tetracycline, sulfonamide, and fluoroquinolone antimicrobial compounds in animal manure and agricultural soils in turkey. Sci. Total. Environ., 407(16), 4652-4664.

Khan, G.A., Berglund, B., Khan, K.M., Lindgren, P.E., Fick, J., 2013. Occurrence and abundance of antibiotics and resistance genes in rivers, canal and near drug formulation facilities - a study in pakistan. Plos One, 8(6).

Kim, S., Aga, D.S., 2007. Potential ecological and human health impacts of antibiotics and antibiotic-resistant bacteria from wastewater treatment plants. Journal of Toxicology and Environmental Health, Part B, 10(8), 559-573.

Kolodziejska, M., Maszkowska, J., Bialk-Bielinska, A., Steudte, S., Kumirska, J., Stepnowski, P., Stolte, S., 2013. Aquatic toxicity of four veterinary drugs commonly applied in fish farming and animal husbandry. Chemosphere, 92(9), 1253-1259.

Korzeniewska, E., Korzeniewska, A., Harnisz, M., 2013. Antibiotic resistant escherichia coli in hospital and municipal sewage and their emission to the environment. Ecotox. Environ. Safe., 91, 96-102.

Kühn, K.-D., Weber, C., Kreis, S., Holzgrabe, U., 2008. Evaluation of the stability of gentamicin in different antibiotic carriers using a validated mekc method. J. Pharmaceut. Biomed., 48(3), 612-618.

Kummerer, K., 2003. Significance of antibiotics in the environment. J. Antimicrob. Chemoth, 52(1), 5-7.

Kummerer, K., 2009. Antibiotics in the aquatic environment - a review - part i. Chemosphere, 75(4), 417-434.

Lado, L.R., Polya, D., Winkel, L., Berg, M., Hegan, A., 2008. Modelling arsenic hazard in cambodia: A geostatistical approach using ancillary data. Applied Geochemistry, 23(11), 3010-3018.

Langmuir, I., 1918. The adsorption of gases on plane surfaces of glass, mica and platinum. J. Am. Chem. Soc., 40, 1361-1403.

Larsson, D.G.J., de Pedro, C., Paxeus, N., 2007. Effluent from drug manufactures contains extremely high levels of pharmaceuticals. J. Hazard. Mater., 148(3), 751-755.

Le Corre, K.S., Ort, C., Kateley, D., Allen, B., Escher, B.I., Keller, J., 2012. Consumption-based approach for assessing the contribution of hospitals towards the load of pharmaceutical residues in municipal wastewater. Environ. Int., 45, 99-111.

Le, T.X., Munekage, Y., 2004. Residues of selected antibiotics in water and mud from shrimp ponds in mangrove areas in viet nam. Mar. Pollut. Bull., 49(11-12), 922-929.

Lee, J.-J., Jang, C.-S., Liu, C.-W., Liang, C.-P., Wang, S.-W., 2009. Determining the probability of arsenic in groundwater using a parsimonious model. Environ. Sci. Technol., 43(17), 6662-6668.

Lee, P.A., Citrin, P.H., Eisenberger, P., Kincaid, B.M., 1981. Extended x-ray absorption fine-structure - its strengths and limitations as a structural tool. Rev. Mod. Phys., 53(4), 769-806.

Leung, H.W., Minh, T.B., Murphy, M.B., Lam, J.C.W., So, M.K., Martin, M., Lam, P.K.S., Richardson, B.J., 2012. Distribution, fate and risk assessment of antibiotics in sewage treatment plants in hong kong, south china. Environ. Int., 42, 1-9.

Levy, S.B., 2008. Genome size and antibiotic resistance. Antimicrob. Agents. Ch, 52(7), 2696-2696.

Levy, S.B., The antibiotic paradox: How miracle drugs are destroying the miracle. Plenum Press, New York.

Li, T., Ni, S.B., 1997. Element abundances of the continental lithosphere in China. Geol. Prospect. 33 (1), 31-37.

Li, W.D., Zou, Z., Zhao, L.S., Zhang, J.Q., Wang, X., Wang, Y.D., 2006. Investigation of endemic arsenism in areas Anhui Province of China. Anhui J. Prev. Med. 12 (4), 193-196.

Li, W.H., Shi, Y.L., Gao, L.H., Liu, J.M., Cai, Y.Q., 2012. Occurrence of antibiotics in water, sediments, aquatic plants, and animals from baiyangdian lake in north china. Chemosphere, 89(11), 1307-1315.

Li, W.H., Shi, Y.L., Gao, L.H., Liu, J.M., Cai, Y.Q., 2013. Occurrence and removal of antibiotics in a municipal wastewater reclamation plant in beijing, china. Chemosphere, 92(4), 435-444.

Liang, X.M., Chen, B.W., Nie, X.P., Shi, Z., Huang, X.P., Li, X.D., 2013. The distribution and partitioning of common antibiotics in water and sediment of the pearl river estuary, south china. Chemosphere, 92(11), 1410-1416.

Lin, N.F., Tang, J., 1999. The study on environmental characteristicsinarseniasis areas in China. Sci. Geogr. Sinica. 19(2), 135-139.

Ling, J.H., Lin, K., Su, W.M., 2009. Jiangsu was exposed to arsenic contamination again, Economic Information, Beijing.

Liu, H., Zhang, G.P., Jin, Z.S., Liu, C.Q., Han, G.L., Li, L., 2009. Geochemical characteristics of geothermal fluid in Tengchong Area, Yunnan Province, China. Acta Miner. Sinica. 29(4), 496-501.

Liu, Y., 2009. Joking remarks of Yangzonghai: Review of contamination accident. Water & Wastewater Inf. 2, 39-41.

Luo, B., Liu, L., Zhang, J.L., Tan, F. Z., Meng, W., Zhen, B.H., Zhao, X.G. Zhang, Y.S., 2010. Levels and Distribution Characteristics of Heavy Metals in Sediments in Main Stream of Huaihe River. J. Environ. Health. 12, 1122 - 1127.

Luo, Y., Xu, L., Rysz, M., Wang, Y.Q., Zhang, H., Alvarez, P.J.J., 2011. Occurrence and transport of tetracycline, sulfonamide, quinolone, and macrolide antibiotics in the haihe river basin, china. Environ. Sci. Technol., 45(5), 1827-1833.

Luo, Y.L., Jiang, P.G., Yu, Y.H., Zheng, C.X., Wu, H.Q., Zhang, G.B., 2007. Arsenic pollution of soil in Kuitun No. 123 state farm, Xinjiang. Chin. J. Soil Sci. 38, 558-561.

MacNeil, J.D., Cuerpo, L., 1995. Gentamicin, Residues of some veterinary drugs in animals and foods fao food and nutrition paper 41/7. Food and Agriculture Organization, Rome, pp. 45-55.

Mamindy-Pajany, Y., Hurel, C., Marmier, N., Romeo, M., 2011. Arsenic (V) adsorption from aqueous solution onto goethite, hematite, magnetite and zero-valent iron: Effects of pH, concentration and reversibility. Desalination. 281, 93-99.

Mamindy-Pajany, Y., Hurel, C., Marmier, N., Romeo, M., 2011. Arsenic (v) adsorption from aqueous solution onto goethite, hematite, magnetite and zero-valent iron: Effects of ph, concentration and reversibility. Desalination., 281, 93-99.

Martin, J.M., Whitfield, M., 1983. The significance of the river input of chemical elements to the ocean. In: Wong, C.S., Boyle, E., Bruland, K.W., Burton, J.D., Goldberg, E.D. (Eds.), Trace Metals in Seawater. Plenum Press, New York, pp. 265–296.

Masscheleyn, P.H., Delaune, R.D., Patrick, W., 1991. Arsenic and selenium chemistry as affected by sediment redox potential and ph. J. Environ. Qual., 20(3), 522-527.

McNeill, L.S., Edwards, M., 1995. Soluble arsenic removal at water treatment plants. Journal of the American Water Works Association, 87(4).

Mellon, M., Benbrook, C., Benbrook, K.L., 2001. Hogging it. Estimates of antimicrobial abuse in livestock. UCS Publications, Cambridge, MA.

Meneghini, C., Bardelli, F., Mobilio, S., 2012. Estra-fitexa: A software package for exafs data analysis. Nucl. Instrum. Meth. B, 285, 153-157.

Millman, A., Tang, D.L., Perera, F.P., 2008. Air pollution threatens the health of children in China. Pediatr. 122, 620-628.

Ministry of Health of China, Standardization Administration of China, 2006. Standards of drinking water quality (GB 5749-2006). National Standard of the People's Republic of China.

Ministry of Health of Inner Mongolia, 2009. Discovery and confirmation of endemic areas. In: Prevention and treatment of endemic arsenism. Ministry of Health of Inner Mongolia.From:http://www.nmwst.gov.cn/html/tslm/nmgzwsz/d3pdfbfz/d8zdfxfzdfz/200904/17-13342.html

Ministry of Health PRC, National Development, Reform Comission, Ministry of Finance PRC, 2012. "12th five-year plan" on control of national endemic diseases. Ministry of Health PRC.

Ministry of Water Resources PRC, 2011. 2010 Statistic Bulletin on China Water Activities, first ed. Ministry of Water Resources, RPC, Beijing.

Miranda, J.M., Mondragon, A.C., Martinez, B., Guarddon, M., Rodriguez, J.A., 2009. Prevalence and antimicrobial resistance patterns of salmonella from different raw foods in mexico. J. Food Protect., 72(5), 966-971.

Mohan, D., Pittman, C.U., 2007. Arsenic removal from water/wastewater using adsorbents - a critical review. J. Hazard. Mater., 142(1-2), 1-53.

Monesi, C., Meneghini, C., Bardelli, F., Benfatto, M., Mobilio, S., Manju, U., Sarma, D.D., 2005. Local structure in lamno3 and camno3 perovskites: A quantitative structural refinement of mn k-edge xanes data. Phys. Rev. B, 72(17), 158-164.

Mørup, S., Topsøe, H., Lipka, J., 1976. Modified theory for mössbauer spectra of superparamagnetic particles: Application to fe3o4. Le Journal de Physique Colloques, 37(C6), C6-287.

Moulds, R.F., Jeyasingham, M.S., 2010. Gentamicin: A great way to start. Australian Prescriber, 33, 134-135.

Mukherjee, A., Fryar, A.E., O'Shea, B.M., 2009. Major occurrences of elevated arsenic in groundwater and other natural waters. Arsenic: Environmental Chemistry, Health Threats and Waste Treatment, 303-350.

Murad, E., 1982. The characterization of goethite by mossbauer-spectroscopy. Am. Mineral., 67(9-10), 1007-1011.

Murphy, K.D., Lee, J.O., Herndon, D.N., 2003. Current pharmacotherapy for the treatment of severe burns. Expert opinion on pharmacotherapy, 4(3), 369-384.

Na, G.S., Fang, X.D., Cai, Y.Q., Ge, L.K., Zong, H.M., Yuan, X.T., Yao, Z.W., Zhang, Z.F., 2013. Occurrence, distribution, and bioaccumulation of antibiotics in coastal environment of dalian, china. Mar. Pollut. Bull., 69(1-2), 233-237.

Nedelko, N., Slawska-Waniewska, A., Kazmierczak, J., Rodrigues, C.A., Bordini, C., 2006. Magnetic studies of fe(iii)-crosslinked chitosan. In: Kisielewski, M. (Ed.), Physica status solidi c - current topics in solid state physics, vol 3, no1. Physica status solidi c-current topics in solid state physics. Wiley-V C H Verlag Gmbh, Weinheim, pp. 126-129.

Ngah, W.S.W., Teong, L.C., Hanafiah, M., 2011. Adsorption of dyes and heavy metal ions by chitosan composites: A review. Carbohyd. Polym., 83(4), 1446-1456.

Nordstrom, D.K., 2002. Public health - worldwide occurrences of arsenic in ground water. Science, 296(5576), 2143-2145.

Nordstrom, D.K., 2002. Public health - Worldwide occurrences of arsenic in ground water. Science. 296, 2143-2145.

Novo, A., Andre, S., Viana, P., Nunes, O.C., Manaia, C.M., 2013. Antibiotic resistance, antimicrobial residues and bacterial community composition in urban wastewater. Water Res., 47(5), 1875-1887.

Parbhakar, A., Cuadros, J., Sephton, M.A., Dubbin, W., Coles, B.J., Weiss, D., 2007. Adsorption of l-lysine on montmorillonite. Colloids and Surfaces A: Physicochemical and Engineering Aspects, 307(1), 142-149.

Peng, X.Z., Huang, Q.X., Zhang, K., Yu, Y.Y., Wang, Z.F., Wang, C.W., 2012. Distribution, behavior and fate of azole antifungals during mechanical, biological, and chemical treatments in sewage treatment plants in china. Sci. Total. Environ., 426, 311-317.

Peng, X.Z., Wang, Z.D., Kuang, W.X., Tan, J.H., Li, K., 2006. A preliminary study on the occurrence and behavior of sulfonamides, ofloxacin and chloramphenicol antimicrobials in wastewaters of two sewage treatment plants in guangzhou, china. Sci. Total. Environ., 371(1-3), 314-322.

Peoples Court of Minquan County, 2010. Criminal judgment and civil judgment, Min xing chu zi, No. 76.

Phan, T.P.H., Managaki, S., Nakada, N., Takada, H., Shimizu, A., Anh, D.H., Viet, P.H., Suzuki, S., 2011. Antibiotic contamination and occurrence of antibiotic-resistant bacteria in aquatic environments of northern vietnam. Sci. Total. Environ., 409(15), 2894-2901.

Pomati, F., Castiglioni, S., Zuccato, E., Fanelli, R., Vigetti, D., Rossetti, C., Calamari, D., 2006. Effects of a complex mixture of therapeutic drugs at environmental levels on human embryonic cells. Environ. Sci. Technol., 40(7), 2442-2447.

Proux, O., Biquard, X., Lahera, E., Menthonnex, J.J., Prat, A., Ulrich, O., Soldo, Y., Trevisson, P., Kapoujyan, G., Perroux, G., Taunier, P., Grand, D., Jeantet, P., Deleglise, M., Roux, J.P., Hazemann, J.L., 2005. Fame: A new beamline for x-ray absorption investigations of very-diluted systems of environmental, material and biological interests. Phys. Scripta., T115, 970-973.

Proux, O., Nassif, V., Prat, A., Ulrich, O., Lahera, E., Biquard, X., Menthonnex, J.J., Hazemann, J.L., 2006. Feedback system of a liquid-nitrogen-cooled double-crystal monochromator: Design and performances. J. Synchrotron. Radiat, 13, 59-68.

Qiu, H., Zhang, S.J., Pan, B.C., Zhang, W.M., Lv, L., 2012. Effect of sulfate on cu(ii) sorption to polymer-supported nano-iron oxides: Behavior and xps study. J. Colloid Interf. Sci, 366(1), 37-43.

Ratnaike, R.N., 2003. Acute and chronic arsenic toxicity. Postgrad. Med. J. 79, 391-396.

Ravel, B., 2001. Atoms: Crystallography for the x-ray absorption spectroscopist. J. Synchrotron. Radiat, 8, 314-316.

Ravel, B., Newville, M., 2005. Athena, artemis, hephaestus: Data analysis for x-ray absorption spectroscopy using ifeffit. J. Synchrotron. Radiat, 12, 537-541.

Ravenscroft, P., Brammer, H., Richards, K., 2009. Arsenic pollution: A global synthesis. Wiley-Blackwell, Chichester.

Redlich, O., Peterson, D.L., 1959. A useful adsorption isotherm. J. Phys. Chem., 63(6), 1024-1024.

Regassa, T.H., Koelsch, R.K., Wortmann, C.S., Randle, R.F., Abunyewa, A.A., 2008. Antibiotic use in animal production: Environmental concerns, University of Nebraska-Lincoln.

Reinthaler, F.F., Posch, J., Feierl, G., Wust, G., Haas, D., Ruckenbauer, G., Mascher, F., Marth, E., 2003. Antibiotic resistance of e-coli in sewage and sludge. Water Res., 37(8), 1685-1690.

Ren, D.Y., Zhao, F.H., Wang, Y.Q., Yang, S.J., 1999. Distributions of minor and trace elements in Chinese coals. Int. J. Coal Geol.. 40, 109 – 118.

Rodríguez-Lado, L., Polya, D., Winkel, L., Berg, M., Hegan, A., 2008. Modelling arsenic hazard in Cambodia: a geostatistical approach using ancillary data. Appl. Geochem. 23, 3010-3018.

Roman-Ross, G., Cuello, G.J., Turrillas, X., Fernandez-Martinez, A., Charlet, L., 2006. Arsenite sorption and co-precipitation with calcite. Chem. Geol. 233, 328-336.

Rorrer, G.L., Hsien, T.Y., Way, J.D., 1993. Synthesis of porous-magnetic chitosan beads for removal of cadmium ions from waste-water. Ind. Eng. Chem. Res., 32(9), 2170-2178.

Sarmah, A.K., Meyer, M.T., Boxall, A.B.A., 2006. A global perspective on the use, sales, exposure pathways, occurrence, fate and effects of veterinary antibiotics (vas) in the environment. Chemosphere, 65(5), 725-759.

Schreiber, M., Gotkowitz, M., Simo, J., Freiberg, P., 2003. Mechanisms of arsenic release to ground water from naturally occurring sources, eastern wisconsin, Arsenic in ground water. Springer, pp. 259-280.

Schwarzenbach, R.P., Gschwend, P.M., Imboden, D.M., 2005. Environmental organic chemistry. Wiley.

Seidel, A., Gelbin, D., 1988. On applying the ideal adsorbed solution theory to multicomponent adsorption equilibria of dissolved organic-components on activated carbon. Chem. Eng. Sci., 43(1), 79-89.

Sheldon, L., Clayton, A., Keever, J., Perritt, R., Whitaker, D., 1992. PTEA: Monitoring of Phthalates and PAHs in Indoor and Outdoor Air Samples in Riverside, California. Sacramento, CA: California Environmental Protection Agency, Air Resources Board Research Division.

Shen, Y.F., Sun, D.J., Zhao, X.H., Yu, G.Q., 2005. Screening report in areas of endemic arsenism and high content of arsenic in China. Chin. J. Endemiol. 24 (2), 172-175.

Shi, W.D., Guo, J.Q., Zhang, S.Q., Ye, C.M., Li, J., Ma, X.H., 2010. The distribution and geochemistry of geothermal groundwater bearing F and as in the Guide Basin. Hydrogeol. Eng. Geol. 37(2), 36-41.

Skariyachan, S., Lokesh, P., Rao, R., Kumar, A.U., Vasist, K.S., Narayanappa, R., 2013. A pilot study on water pollution and characterization of multidrug-resistant superbugs from byramangala tank, ramanagara district, karnataka, india. Environ. Monit. Assess, 185(7), 5483-5495.

Smedley, P.L., Kinniburgh, D.G., 2002. A review of the source, behaviour and distribution of arsenic in natural waters. Applied Geochemistry, 17(5), 517-568.

Smedley, P.L., Zhang, M., Zhang, G., Luo, Z., 2003. Mobilisation of arsenic and other trace elements in fluviolacustrine aquifers of the Huhhot Basin, Inner Mongolia. Appl. Geochem. 18, 1453-1477.

Smith, A.H., Marshall, G., Yuan, Y., Ferreccio, C., Liaw, J., von Ehrenstein O, et al., 2006. Increased mortality from lung cancer and bronchiectasis in young adults after exposure to arsenic in utero and in early childhood. Environ. Health. Perspect. 114, 1293-1296.

Smith, D.L., Harris, A.D., Johnson, J.A., Silbergeld, E.K., Morris, J.G., 2002. Animal antibiotic use has an early but important impact on the emergence of antibiotic resistance in human commensal bacteria. Proceedings of the National Academy of Sciences of the United States of America, 99(9), 6434-6439.

Sole, V.A., Papillon, E., Cotte, M., Walter, P., Susini, J., 2007. A multiplatform code for the analysis of energy-dispersive x-ray fluorescence spectra. Spectrochim. Acta B, 62(1), 63-68.

Sposito, G., 1984. The surface chemistry of soils. Oxford University Press, New York.

Sun, D.J., 2011. The study of fluoride and arsenic contents in drinking water of rural areas of China. From: www.crwstc.org/uploads/soft/110520/3-110520145030.pdf

Sun, G.F., 2004. Arsenic contamination and arsenicosis in China. Toxicol. Appl. Pharmacol. 198, 268-271.

Symposium, C.F., 2008. Antibiotic resistance: Origins, evolution, selection and spread. Wiley.

Theron, J., Walker, J., Cloete, T., 2008. Nanotechnology and water treatment: Applications and emerging opportunities. Crit. Rev. Microbiol., 34(1), 43-69.

Thibaut, R., Schnell, S., Porte, C., 2006. The interference of pharmaceuticals with endogenous and xenobiotic metabolizing enzymes in carp liver: An in-vitro study. Environ. Sci. Technol., 40(16), 5154-5160.

Thirunavukkarasu, O.S., Viraraghavan, T., Subramanian, K.S., 2003. Arsenic removal from drinking water using iron oxide-coated sand. Water Air. Soil Poll., 142(1-4), 95-111.

Tian, H.Z., Qu, Y.P., 2009. Inventories of atmospheric arsenic emissions from coal combustion in China, 2005. Environ. Sci. 30 (4), 956-962.

Tondel, M., Rahman, M., Magnuson, A., Chowdhury, I. A., Faruquee, M. H., Ahmad, S. A., 1999. The relationship of arsenic levels in drinking water and the prevalence rate of skin lesions in Bangladesh. Environ. Health. Perspect. 107, 727-729.

Tong, L., Li, P., Wang, Y.X., Zhu, K.Z., 2009. Analysis of veterinary antibiotic residues in swine wastewater and environmental water samples using optimized spe-lc/ms/ms. Chemosphere, 74(8), 1090-1097.

Turekian, K.K., Wedepohl, K.H., 1961. Distribution of the Elements in some major units of the Earth's crust. Geol. Soc. Amer. Bull. 72, 175-192.

Twarakavi, N.K.C., Kaluarachchi, J.J., 2006. Arsenic in the shallow ground waters of conterminous united states: Assessment, health risks, and costs for mcl compliance1. JAWRA Journal of the American Water Resources Association, 42(2), 275-294.

U.S. Geological Survey, 2012, Arsenic, in: Brooks, W.E. (Eds.), Mineral commodity summaries 2012: U.S. Geological Survey, Reston, pp. 20-21.

Vandenberghe, R.E., Degrave, E., Degeyter, G., Landuydt, C., 1986. Characterization of goethite and hematite in a tunisian soil-profile by mossbauer-spectroscopy. Clay. Clay. Miner., 34(3), 275-280.

Vega, L., Soto, G., Luna, A., Acosta, L., Conde, P., Cebrian, M., et al. 2008. Early signs of immunodepression induced by arsenic in children, in: Bundschuh, J., Bhattacharya, P. (Eds). Arsenic in the environment. CRC Press/Taylor and Francis, Boca Raton, London & New York, chapter 45, volume 1.

Wang, C., Ding, Y., Teppen, B.J., Boyd, S.A., Song, C., Li, H., 2009. Role of interlayer hydration in lincomycin sorption by smectite clays. Environ. Sci. Technol., 43(16), 6171-6176.

Wang, G., 1984. Arsenic poisoning from drinking water in Xinjiang. Chin. J. Prevent. Med. 18, 105–107.

Wang, G.Q., Zhen, Y.J., Yao, H., Hu, Y., Wei, L., Kang, L., Zhang, J.W., 2004. Study of intervention experiment and its long-term effects in endemic arsenism in Xinjiang. J. Xinjiang Med. Univ. 27(1), 12-14.

Wang, G.S., Sun, Y.W., Yue, J.M., 1985. Fuzzy Clustering Analysis for exploration of the source of Fluorine in Kuitun Area, Xinjiang. J. Xinjiang Med. Univ. 2, 143-148.

Wang, L., Huang, J., 1994. Chronic arsenism from drinking water in some areas of Xinjiang, China. In: Nriagu, J.O. (Ed.), Arsenic in the Environment, Part II: Human Health and Ecosystem Effects. John Wiley, New York, pp. 159–172.

Wang, M.S., Zheng, B.S., Hu, J., Li, S.H., Wang, B.B., 2005. Distribution of arsenic in southwest coals. J. Chin. Coal Soc. 30 (3), 344 - 348.

Wang, Y.L., Li, B.Q., Zhou, Y., Jia, D.C., 2009. In situ mineralization of magnetite nanoparticles in chitosan hydrogel. Nanoscale Res. Lett., 4(9), 1041-1046.

Wang, Z.H., He, B., Pan, X.J., Zhang, K.G., Wang, C., Sun, J., Yun, Z.J., Jiang, G.B., 2010. Levels, trends and risk assessment of arsenic pollution in Yangzonghai Lake, Yunnan Province, China. Sci. China-Chem. 53, 1809-1817.

Waychunas, G.A., Rea, B.A., Fuller, C.C., Davis, J.A., 1993. Surface-chemistry of ferrihydrite .1. Exafs studies of the geometry of coprecipitated and adsorbed arsenate. Geochimica Et Cosmochimica Acta, 57(10), 2251-2269.

Webster, J.G., Nordstrom, D.K., 2003. Geothermal Arsenic, In: Welch, A.H., and Stollenwerk, K.G. (Eds.), Arsenic in Ground Water: Geochemistry and Occurrence. Kluwer Academic Publishers, Boston, pp. 101-126.

Wehrli, B., Wieland, E., Furrer, G., 1990. Chemical mechanisms in the dissolution kinetics of minerals - the aspect of active-sites. Aquat. Sci., 52(1), 3-31.

Wei, F.S., Zheng, C.J., Chen, J.S., Wu, Y.Y., 1991. Study on the background contents on 61 elements of soils in China. Chin. J. Environ. Sci. 12(4), 12-19.

Wei, L.H., Zhou, W.G., 1992. Development of arsenic mineral resources and environment control. Hunan Geol. 11(3), 259-262.

Welch, A.H., Lico, M.S., Hughes, J.L. 1988. Arsenic in ground water of the western United States. Ground Water. 26(3), 333-347.

Weng, H.X., Zhang, H.Y., Zou, L.J., Zhang, X.M., Liu, G.S., 2000. Natural existence of arsenic in soil of China and its cause of formation. J. Zhejiang Univ. (Eng. Sci.). 34(1), 88-92.

Westerhoff, P., Yoon, Y., Snyder, S., Wert, E., 2005. Fate of endocrine-disruptor, pharmaceutical, and personal care product chemicals during simulated drinking water treatment processes. Environ. Sci. Technol., 39(17), 6649-6663.

Winkel, L., Berg, M., Amini, M., Hug, S.J., Johnson, C.A., 2008. Predicting groundwater arsenic contamination in southeast asia from surface parameters. Nature Geoscience, 1(8), 536-542.

Winkel, L., Casentini, B., Bardelli, F., Voegelin, A., Nikolaidis, N.P., Charlet, L. 2013. Speciation of arsenic in Greek travertines: Co-precipitation of arsenate with calcite. Geochim. Cosmochim. Acta. 106, 99-110.

Winkel, L.H.E., Pham, T.K.T., Vi, M.L., Stengel, C., Amini, M., Nguyen, T.H., Pham, H.V., Berg, M., 2011. Arsenic pollution of groundwater in vietnam exacerbated by deep aquifer exploitation for more than a century. Proceedings of the National Academy of Sciences of the United States of America, 108(4), 1246-1251.

Wu, S.C., Gschwend, P.M., 1988. Numerical modeling of sorption kinetics of organic-compounds to soil and sediment particles. Water Resour. Res., 24(8), 1373-1383.

Wu, W., He, Q.G., Jiang, C.Z., 2008. Magnetic iron oxide nanoparticles: Synthesis and surface functionalization strategies. Nanoscale Res. Lett., 3(11), 397-415.

Wunder, D.B., Bosscher, V.A., Cok, R.C., Hozalski, R.M., 2011. Sorption of antibiotics to biofilm. Water Res., 45(6), 2270-2280.

Xia, Y.J., Liu, J., 2004. An overview on chronic arsenicsm via drinking water in PR China. Toxicol. 198, 25-29.

Xiao, X.Y., Chen T.B., Liao, X.Y., Wu, B, Yan, X.L., Zhai, L.M., Xie, H., Wang, L.X., 2008. Regional distribution of arsenic contained minerals and arsenic pollution in China. Geogr. Res. 1, 201-212.

Xie, H., Mason, M.M., Wise, J.P., 2011. Genotoxicity of metal nanoparticles. Reviews on Environmental Health, 26(4), 251-268.

Xie, H., Nie, A.G., 2007. Metallogenetic factors of high As coal in southwestern Guizhou. Coal Geol. Explor. 35(6), 10-14.

Xie, R.K., Seip, H.M., Wibetoe, G., Nori, S., McLeod, C.W., 2006. Heavy coal combustion as the dominant source of particulate pollution in Taiyuan, China, corroborated by high concentrations of arsenic and selenium in PM10. Sci. Total Envir. 370, 409-415.

Xie, X.J., Wang, Y.X., Ellis, A., Su, C.L., Li, J.X., Li, M.D., 2011. The sources of geogenic arsenic in aquifers at Datong basin, northern China: Constraints from isotopic and geochemical data. J. Geochem. Explor. 110, 155-166.

Xu, W., Wang, H.J., Wu, K., Liu, R.P., Gong, W.X., Qu, J.H., 2012. Arsenic desorption from ferric and manganese binary oxide by competitive anions: Significance of ph. Water Environ. Res., 84(6), 521-528.

Xu, W.H., Zhang, G., Li, X.D., Zou, S.C., Li, P., Hu, Z.H., Li, J., 2007. Occurrence and elimination of antibiotics at four sewage treatment plants in the pearl river delta (prd), south china. Water Res., 41(19), 4526-4534.

Xue, B.M., Zhang, R.J., Wang, Y.H., Liu, X., Li, J., Zhang, G., 2013. Antibiotic contamination in a typical developing city in south china: Occurrence and ecological risks in the yongjiang river impacted by tributary discharge and anthropogenic activities. Ecotox. Environ. Safe., 92, 229-236.

Yan, C.X., Yang, Y., Zhou, J.L., Liu, M., Nie, M.H., Shi, H., Gu, L.J., 2013. Antibiotics in the surface water of the yangtze estuary: Occurrence, distribution and risk assessment. Environ. Pollut., 175, 22-29.

Yan, M.C., Chi, Q.H., Gu, T.X., Wang, C.S., 1997. Chemical compositions of continental crust and rocks in eastern China. Geophys. Geochem. Explor. 21 (6), 451- 459.

Yan, W., Hu, S., Jing, C., 2012. Enrofloxacin sorption on smectite clays: Effects of ph, cations, and humic acid. J. Colloid Interf. Sci, 372(1), 141-147.

Yanez, L., Garcia-Nieto, E., Rojas, E., Carrizales, L., Mejia, J., Calderon, J., et al., 2003. DNA damage in blood cells from children exposed to arsenic and lead in a mining area. Environ. Res. 93, 231-240.

Yang, G.S., Ma, L.L., Xu, D.D., Li, J., He, T.T., Liu, L.Y., Jia, H.L., Zhang, Y.B., Chen, Y., Chai, Z.F., 2012. Levels and speciation of arsenic in the atmosphere in Beijing, China. Chemosphere. 87, 845-850.

Yang, J. 1992. Pollution of arsenical mine spoil and its treatment. Ind. Saf. and Dust Prevent. 5, 2-7.

Yang, J.F., Ying, G.G., Zhao, J.L., Tao, R., Su, H.C., Liu, Y.S., 2011. Spatial and seasonal distribution of selected antibiotics in surface waters of the pearl rivers, china. Journal of Environmental Science and Health Part B-Pesticides Food Contaminants and Agricultural Wastes, 46(3), 272-280.

Yang, L.H., Ying, G.G., Su, H.C., Stauber, J.L., Adams, M.S., Binet, M.T., 2008. Growth - inhibiting effects of 12 antibacterial agents and their mixtures on the freshwater microalga pseudokirchneriella subcapitata. Environ. Toxicol. Chem, 27(5), 1201-1208.

Yang, S.Z., Guo, H.M., Tang, X.H., Shen, Z.L., 2008. Distribution of abnormal groundwater arsenic in Hetao Plain, Inner Mongolia. Earth Sci. Front. 15 (1), 242-249.

Ye, Z., Weinberg, H.S., Meyer, M.T., 2007. Occurrence of antibiotics in drinking water. Anal. Bioanal. Chem, 387, 1365-1377.

Yiruhan, Wang, Q.J., Mo, C.H., Li, Y.W., Gao, P., Tai, Y.P., Zhang, Y., Ruan, Z.L., Xu, J.W., 2010. Determination of four fluoroquinolone antibiotics in tap water in guangzhou and macao. Environ. Pollut., 158(7), 2350-2358.

Yu, G.Q., Sun, D.J., Zheng, Y., 2007. Health effects of exposure to natural arsenic in groundwater and coal in China: An overview of occurrence. Environ. Health. Perspect.115, 636-642.

Yuan, Y., Marshall, G., Ferreccio, C., Steinmaus, C., Selvin, S., Liaw, J., et al., 2007. Acute myocardial infarction mortality in comparison with lung and bladder cancer mortality in arsenic exposed region II of Chile from 1950 to 2000. Am. J. Epidemiol. 166, 1381-1391.

Zhang, C.S., Zhang, S., Zhang, L.C., Wang, L.J., 1995. Calculation of heavy metal contents in sediments of the Changjiang River system. Acta Sci. Circumstantiae. 15 (3), 257 – 264.

Zhang, F.C., Wen, D.G., Guo, J.Q., Zhang, E.Y., Hao, A.B., An, Y.H., 2010. Research progress and prospect of geological environment in main endemic disease area. Geol. Chin. 37(3), 551-562.

Zhang, M.Y., Zhang, Y.M., Zhang, G.Y. et al., 2002. Analysis of underground water quality in chronic endemic arsenic poisoning areas, Hohhot. J. Environ. Health. 19(3), 220-222.

Zhang, Q., Rodriguez-Lado, L., Johnson, C.A., Xue, H.B., Shi, J.B., Zheng, Q.M., Sun, G.F., 2012. Predicting the risk of arsenic contaminated groundwater in Shanxi Province, Northern Chin. Environ. Pollut. 165, 118-123.

Zhang, R.J., Tang, J.H., Li, J., Cheng, Z.N., Chaemfa, C., Liu, D.Y., Zheng, Q., Song, M.K., Luo, C.L., Zhang, G., 2013. Occurrence and risks of antibiotics in the coastal aquatic environment of the yellow sea, north china. Sci. Total. Environ., 450, 197-204.

Zhang, R.J., Tang, J.H., Li, J., Zheng, Q., Liu, D., Chen, Y.J., Zou, Y.D., Chen, X.X., Luo, C.L., Zhang, G., 2013b. Antibiotics in the offshore waters of the bohai sea and the yellow sea in china: Occurrence, distribution and ecological risks. Environ. Pollut., 174, 71-77.

Zhang, R.J., Zhang, G., Tang, J.H., Xu, W.H., Li, J., Liu, X., Zou, Y.D., Chen, X.X., Li, X.D., 2012b. Levels, spatial distribution and sources of selected antibiotics in the east river (dongjiang), south china. Aquatic Ecosystem Health & Management, 15(2), 210-218.

Zhang, R.J., Zhang, G., Zheng, Q., Tang, J.H., Chen, Y.J., Xu, W.H., Zou, Y.D., Chen, X.X., 2012. Occurrence and risks of antibiotics in the laizhou bay, china: Impacts of river discharge. Ecotox. Environ. Safe., 80, 208-215.

Zhang, T., Li, B., 2011. Occurrence, transformation, and fate of antibiotics in municipal wastewater treatment plants. Crit. Rev. Env. Sci. Tec, 41(11), 951-998.

Zhang, Y.L., Xiao, J.M., 1993. Study on environment pollution by arsenical pesticides. J. Convalescence Rehabil. 8(4), 165-166.

Zheng, Q., Zhang, R.J., Wang, Y.H., Pan, X.H., Tang, J.H., Zhang, G., 2012. Occurrence and distribution of antibiotics in the beibu gulf, china: Impacts of river discharge and aquaculture activities. Mar. Environ. Res., 78, 26-33.

Zhou, L.J., Ying, G.G., Liu, S., Zhang, R.Q., Lai, H.J., Chen, Z.F., Pan, C.G., 2013. Excretion masses and environmental occurrence of antibiotics in typical swine and dairy cattle farms in china. Sci. Total. Environ., 444, 183-195.

Zou, S.C., Xu, W.H., Zhang, R.J., Tang, J.H., Chen, Y.J., Zhang, G., 2011. Occurrence and distribution of antibiotics in coastal water of the bohai bay, china: Impacts of river discharge and aquaculture activities. Environ. Pollut., 159(10), 2913-2920.

Zou, W.W., Geng, H., Lin, M.F., Xiong, X.P., 2012. Facile one-pot preparation of superparamagnetic chitosan sphere and its derived hollow sphere. J. Appl. Polym. Sci., 123(6), 3587-3594.

Acknowlegements

Though only my name appears as the author on the cover of this dissertation, a great many people have contributed to its production. I owe my gratitude to all these people who have made this dissertation possible and because of whom my graduate experience has been one that I will cherish forever.

My deepest gratitude is to my advisor, Prof. Laurent Charlet at Université Joseph Fourier. I have been amazingly fortunate to have an advisor who gave me the freedom to explore on my own and at the same time the guidance to recover when my steps faltered. I am thankful to my supervisors Prof. Fuxing Gan, Prof. Dihua Wang and Prof. Song Hong at Wuhan University during my master-PhD program for their continued guidance, support and encouragement. I am grateful to Prof. Yuh-Shan Ho at Asia University, who has dedicated unselfish help and very enlightening guidance to my research. I would like to acknowledge Prof. Eduardo Ruiz-Hitzky, Prof. Pilar Aranda and Dr Margarita Darder at Instituto de Ciencia de Materiales de Madrid, who have advised me and given practical help on the research related to design and synthesis of gentamicin loaded film.

I am also thankful to my colleagues and friends, Dr Fabrizio Bardelli and Dr Antoine Gehin and Dr Yael Kirsch for their great contribution on my dissertation work, numerous discussions and lectures on related topics that helped me improve my knowledge in the area.

I am grateful to Delphine Tisserand and Lionel Rossetto at ISTerre; Denis Testemale at the FAME beamline of ESRF; Dominique Thiaudiere and Cristian Mocuta at the DIFFABS beamline of the French synchrotron source (SOLEIL); Dr Christophe Martin, Charles Josserond and Xavier Bataillon from SIMaP lab of Grenoble; Andrés Valera Bernal, Carlos

Sebastián Checa and Javier Perez Carvajal from ICMM lab of Madrid, Pedro Vázquez and Patricia Fernández at Nanobiomatters, SL (Paterna, Valencia, Spain) for their invaluable help given during different measurements of the work.

Many friends at ISTerre and IPAG have helped me stay sane through these difficult years far from my family. Their support and care helped me overcome setbacks and stay focused on my graduate study. I greatly value their friendship and I deeply appreciate their belief in me. I am also grateful to Dr-to- be Yann Berquin, who helped to prepare the French version of this dissertation summary.

Most importantly, none of this would have been possible without the love and patience of my family. My immediate family, to whom this dissertation is dedicated to, has been a constant source of love, concern, support and strength all these years. I would like to express my heart-felt gratitude to my family. My extended family has aided and encouraged me throughout this endeavor. I have to give a special mention for from my uncle, who passed away in October, 2013. He was my guarantee of my scholarship agreement with China Government. Without his support and love I wouldn't have made my PhD in France.

Finally, I would like to express my appreciation to China Government, who funded my PhD through State-Sponsored Study Abroad Program from Ministry of Education of the P.R. China. I would like to thank to Institut Universitaire de France and Rhône-Alpes Region of France who partly fund my research during the PhD research.

Curriculum Vitae

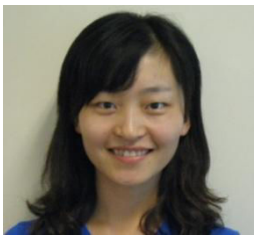

Date of Birth: 11th, July, 1985
Place of birth: Wuhan, China
Email: jhe0711@gmail.com

EDUCATION

PhD

Environmental Geochemistry

Université Joseph Fourier Grenoble I, France (Sep. 2010 – Dec. 2012)

Master

Environmental Science

Wuhan University, China (Sep. 2008 – Jun. 2010)

Bachelor

Material Chemistry

China University of Geosciences (Wuhan), China (Sep. 2003 – Jul. 2007)

RESEARCH INTERESTS

Waste/Drinking water treatment: Arsenic, fluoride, antibiotics and etc. removal from polluted water system.

(Bio)nanocomposites: Synthesis and modification of bionanocomposites and their application into water treatment and medical use.

RESEARCH EXPERIENCES

PhD Thesis:

(Bio)nanocomposites for water treatment of arsenic/gentamicin contaminated water or medicine use

Research Intern

Bionanocomposites synthesis and application in drug delivery systems

Instituto de Ciencia de Materiales de Madrid, Spain (Apr- Jun. 2012; Dec.- Feb. 2013)

***Master Period*:**

1. Adsorption equilibrium and thermodynamic study of fluoride onto mineral material from aqueous solution.
2. Adsorption thermodynamics study of dyes onto mineral material (Bentonite and Rectorite).
3. Surface-modification of mineral materials.

***Bachelor Thesis*:** Synthesis and infrared spectroscopy study of Schiff base coordination

TEACHING EXPERIENCE

Laboratory work for Master students at University of Grenoble I (2011 –2012)

1. Extraction of Pb^{2+} content from polluted soil
2. Geochemisty of soil: The Atomic Absorption Spectrophotometer AAS

WORKSHOP & CONFERENCE ATTENDENCE

2009 Sino-Japan International Conference on Resources & Environmental Sustainable Development, Wuhan China

2010 University Groups Conference on Yangtze River Water Environment, Shanghai, China

2011 The 21st Goldschmidt Geochemistry Conference, Prague, Czech Republic

2011 BIT's 1st Annual World Congress of Nano-S&T (NANO-S&T2011), Dalian, China (oral presentation)

2011 Second International Conference on Selenium inthe Environment and Human Health

2013 The 23rd Goldschmidt Geochemistry Conference, Florence, Italy (oral presentation)

AWARD AND HONORS

2011 Bourses de Mobilité Explora'Doc 2011, Région Rhône-Alpes

2010 State-Sponsored Scholarship from China Government

2006 Award Scholarships

2005 Award of Excellent Social Activities

2002 First Prize National Competition of Chemistry (in Wuhan)

SKILLS

Languages: Chinese (mother tongue), English (advanced); French (intermediate communication)

Computer: Windows, Microsoft WORD EXCEL POWERPOINT

Chemistry Instruments: Infrared Spectroscopy; X-ray Diffraction; ICP-OES; TC/TN; etc.

Referee of Basketball (1^{st}Category)

PUBLICATIONS

He, J., Charlet, L., 2013. A review of arsenic presence in china drinking water. J. Hydrol., 492(7), 79-88.

He, J., Hong, S., Zhang, L.A., Gan, F.X., Ho, Y.S., 2010. Equilibrium and thermodynamic parameters of adsorption of methylene blue onto rectorite. Fresenius Environmental Bulletin 19, 2651-2656.

Hong, S., Wen, C., He, J., Gan, F.X., Ho, Y.S., 2009. Adsorption thermodynamics of Methylene Blue onto bentonite. Journal of Hazardous Materials 167, 630-633.

Zhang, L.A., Hong, S., He, J., Gan, F.X., Ho, Y.S., 2010. Isotherm Study of Phosphorus Uptake from Aqueous Solution Using Aluminum Oxide. Clean-Soil Air Water 38, 831-836.

Zhang, L.A., Hong, S., He, J., Gan, F.X., Ho, Y.S., 2011. Adsorption characteristic studies of phosphorus onto laterite. Desalination and Water Treatment 25, 98-105.

Annex1: Calculation of site density: arsenic on goethite

The site density for As adsorption onto goethite is calculated as following method.

(i). We assume that goethite nano-particles in CGB have a cuboid geometry with size of 250×50×10 nm, as observed by FE-SEM.

(ii). The adsorption of As onto chitosan in CGB is neglected (As adsorption onto chitosan gel beads were tested. The sorption quantity was very small compared with the As sorption quantity onto CGB (q_e(As-chitosan)<70μg/g while q_e(As-CGB)>7000μg/g).

(iii). Because of (ii), the maximum amount of adsorbed As(V) and As(III) onto goethite, q_m(goethite)=q_m(CGB)/w

w: mass fraction of goethite in CGB, w=20.33%,

q_{m1} (goethite) =0.74 mmol/g for As(V) and , q_{m2} (goethite)=0.56 mmol/g for As(III).

For CGB material which contains 1g of goethite nanoparticles, the total volume of goethite NPs, V_{total} (nm^3) can be calculated:

$$V_{total} = \frac{m}{d} \times 10^{21} = \frac{1g}{4.27\,g/cm^3} \times 10^{21} \quad \text{(A1.1)}$$

Where,

m, mass of goethite (g), m=1g;

d, density of goethite (g/cm^3),

For each goethite NP,

$$S_{NP} = [(a \times b) + (b \times c) + (b \times c)] \times 2 \quad \text{(A1.2)}$$

$$V_{NP} = a \times b \times c \quad \text{(A1.3)}$$

Where

S_{NP}, surface area of each goethite NP (nm^2);

$V_{NP,}$ volume of each goethite NP (nm^3);

a, b and c are three side-lengths of goethite NP. a= 250nm, b=50nm, c=10 nm,

Therefore, the number of goethite NP, N, in CGB which contains 1 g of goethite can be calculated:

$$N = V_{total} \div V_{NP} \quad \text{(A1.4)}$$

So the total surface area, S_{total} (m^2), is:

$$S_{total} = N \times S_{NP} \times 10^{-18} \quad \text{(A1.5)}$$

The site density of As(V) and As(III), d_{ST} (μmol/g)are calculated by:

$$d_{ST} = \frac{q_m(\text{goethite}) \times m}{S_{total}} \times 1000 \quad \text{(A1.6)}$$